CHAPTER 3

SYNTHESIS AND DESIGN OF SPARSE PLANAR ANTENNA (SPA) ARRAYS

3.1. Context and Background

Chapter 1 described the limitations and requirements of active antenna arrays for radar applications. In chapter 2, the author studied sparse linear antenna arrays and discussed the synthesis approaches developed for linear arrays. Chapter 3 extends these approaches for the synthesis of sparse planar antenna arrays. This chapter deals with the synthesis of TPA and NUSPA arrays utilizing GA, PSO optimization algorithms and their variants considering various objectives.

3.2. Thinned Planar Antenna (TPA) Arrays

3.2.1. Introduction

The research work on TPA arrays is broadly divided into the following four categories:

- Reduction in PSLL and Maximization of Number of 'OFF' Elements in 10×20-element TPA Array Using MBC-GA
- PSLL Optimization with Minimum Number of Turn 'ON' Elements in 10×10- and 14×14-element TPA Arrays over ± 40° Scan Volume Using IBc-GA
- Optimization of Peak, Average and RMS SLLs in 10×20-element TPA Array Using PSO
- Optimization of PSLL by Jointly Determining Thinned Configuration and Amplitude Weights in 10×20- and 8×8-element TPA Arrays Using MBC-GA
- EM Simulation and Experimental Validation of 8×8-element AW-TPA Array

Details of each category are described subsequently in different Sub-sections.

3.2.1.1 Reduction of PSLL and Maximization of Number of 'OFF' Elements in 10×20-Element TPA Array Using MBC-GA

In this research work, an innovative approach for the synthesis of uniformly excited thinned planar antenna arrays is proposed. This approach results in better reduction in peak side lobe level (PSLL) at less computational cost. In addition, the design performance is achieved with less number of turn 'ON' elements in order to reduce the cost as well as weight of the antenna array. Towards achieving this objective, an innovative variant of genetic algorithm (GA) designated as modified binary coded genetic algorithm (MBC-GA) is proposed. Novel techniques for crossover and mutation operations are investigated to make proposed MBC-GA optimizer a more efficient synthesis tool as compared to classical GA and other methods reported in literature. The potentiality of the proposed approach is exemplified by numerically analyzing 10 × 20-element thinned planar antenna (TPA) arrays. Results obtained using the proposed synthesis strategy for the array under consideration demonstrate the significant improvement in design performance in terms of PSLL reduction with less number of turn 'ON' elements at less computational complexity over the existing state-of-the-art methods.

The process of thinning of an antenna array makes some of the antenna elements 'inactive' in order to achieve the desired elements' density related to reduced PSLL while maintaining other characteristics of antenna array nearly the same as for a fully filled array of identical size [Oliveri *et al.* (2010)]. The advantage gained through array thinning is that the total number of radiating elements is substantially reduced which scales down the array cost, weight and power consumption. Further, it results in simple realization of feed network as all elements across the array would have equal amplitude excitations [Leeper (1999)], [Pocca (2010)].

Various global optimization techniques such as genetic algorithm (GA) [Goldberg *et al.* (1991), Haupt (1994), Tang *et al.* (1996), Weile and Michielssen (1997), Yan and Lu (1997), and Man *et al.* (1999)], and its variants [Donelli (2004), Kadri *et al.* (2010), Zhang *et al.* (2012), Cheng *et al.* (2016), and Ha *et al.* (2016)], improved binary invasive weed optimization (IBIWO) [Liu and Wu (2014)], boolean differential evolution (BDE) [Zhang *et al.* (2010)], particle swarm optimization (PSO) and its variants [Deligkaris *et al.* (2009), Donelli *et al.* (2009), Zhang *et al.* (2009), Wang *et al.* (2012), and Gangwar *et al.* (2016)], ant colony optimization (ACO) [Teruel and Iglesias (2006)], and others [Oliveri and Massa (2011a)], [Oliveri *et al.* (2011b)] have been successfully employed and proven to be suitable for the synthesis of thinned arrays. In general, capability of optimization algorithms is determined by their solution quality in terms of design performance, computational complexity and stability in solving the problem at hand. Although various techniques including [Goldberg *et al.* (1991), Haupt (1994), Tang *et al.* (1996), Weile and Michielssen (1997), Yan and Lu (1997), Man *et al.* (1999), Teruel and Iglesias (2006), Zhang *et al.* (2010), Wang *et al.* (2012), and Liu and Wu (2014)] have been employed successfully, but the solution quality obtained through them may not be efficacious and might have ended up with sub-optimum solution.

To improve the solution quality, several researchers suggested some novel processions in their GA based synthesis techniques including those reported in [Donelli (2004), Chen *et al.* (2006), Mahanti *et al.* (2007), Kadri *et al.* (2010), Cen *et al.* (2012), Zhang *et al.* (2012), Cheng *et al.* (2016), and Ha *et al.* (2016)]. Ha *et al.* [Ha *et al.* (2016)] proposed modified compact genetic algorithm (M-cGA), which is derived from compact genetic algorithm (cGA) by implementing more than one probability vector.

Mahanti *et al.* [Mahanti *et al.* (2007)] used real coded genetic algorithm with elitist strategy. In [Cheng *et al.* (2016)], Cheng *et al.* brought in an improved multi-objective optimization algorithm based on non-dominated sorting GA II (NSGA-II) to meet the thinning requirements of a large planar array with a given filling factor and lowest possible PSLL. In this synthesis technique, GA is combined with iterative fast Fourier transform (IFFT) technique to improve the solution quality. Kadri *et al.* [Kadri *et al.* (2010)] introduced fuzzy genetic algorithms (FGAs) in which the control parameters, like crossover and mutation probabilities of a standard version of genetic algorithm (SGA) are adjusted using a fuzzy controller (FLC) to achieve good improvement in the thinned array performance. In [Zhang *et al.* (2012)] Zhang *et al.* proposed an orthogonal genetic algorithm (OGA) to optimize the planar thinned array for minimum peak side lobe level in which crossover operator formed by the orthogonal array and the factor analysis is employed to enhance its performance. In addition, many techniques other than GA including those reported in [Donelli *et al.* (2009), Zhang *et al.* (2009), and Liu and Wu (2014)] have also shown some furtherance for such purpose. Liu and Wu [Liu and Wu (2014)] utilized the adaptive dispersion mechanism to improve the search ability of binary IWO. Donelli *et al.* [Donelli *et al.* (2009)] devised a hybrid approach, which exploits and combines the most attractive feature of PSO and those of a combinatorial method based on the noncyclic difference sets of Hadamard type. Zhang *et al.* [Zhang *et al.* (2009)] proposed a modified PSO where the code resetting of optimal variables was introduced during optimization process while Oliveri and Massa [Oliveri and Massa (2011a)] proposed a hybrid approach based on genetic algorithm (GA)-enhanced almost difference set (ADS) to improve the performance. Although

advancements in aforesaid state–of-the-art synthesis methods have improved the solution quality but still the solution achieved through them may not be optimum.

In this research work, towards the objective to enhance the solution quality, a modified binary coded genetic algorithm (MBC-GA) is proposed. Particularly, the MBC-GA is investigated to accomplish the following improvements, which would make it a more efficient synthesis tool compared to state-of-the-art thinning techniques:

- An innovative robust randomization strategy for crossover operation, which ameliorates convergence rate by allowing for adequate amount of randomization and diversity to the solution space
- An unexampled systematic mutation strategy that leads the MBC-GA much dynamism, soundness and rapidity in attaining desired solution
- Higher computational efficiency.

The innovative contents and motivations for the present study differ from the state-of-the-art thinning techniques available in the literature in terms of two main aspects: The first one refers to achieving maximum possible reduction in PSLL with less number of turn 'ON' antenna elements. The second aspect refers to development of MBC-GA technique for the synthesis of thinned arrays, which yields good quality and stable solution i.e. best PSLL in a computationally efficient manner. The distinguishing competency of the proposed method is demonstrated by numerically examining 10×20-element TPA array. Results obtained through the proposed technique are compared with those obtained through the techniques available in literature [Teruel and Iglesias (2006), Zhang *et al.* (2010), Wang *et al.* (2012), and Liu and Wu (2014)]. These results show the superiority of proposed MBC-GA technique. Further, the stability of solution is examined by running several independent trials for the array under consideration.

3.2.1.2 PSLL Optimization with Minimum Number of Turn 'ON' Elements in 10×10- and 14×14-Elements TPA Arrays over ± 40^0 Scan Volume Using IBc-GA

In this study, a novel strategy for the synthesis of uniformly excited thinned planar antenna (UE-TPA) arrays which renders maximum possible reduction in the peak side lobe level (PSLL) with minimum number of turn 'ON' elements over wide steering angles is proposed. The main objective of this work is to investigate an efficient variant of genetic algorithm (GA) which yields good quality solution at affordable computational complexity. The author has attempted to develop a powerful synthesis tool denoted as improved binary coded GA (IBc-GA) by investigating novel chromosome arrangements and ameliorated process techniques for crossover and mutation operations to improve the flexibility as well as the global search ability in achieving the best possible reduction in PSLL without increasing computational burden. In order to corroborate the effectiveness and superiority of the proposed synthesis technique, two examples consisting of 10×10-and 14×14-elements UE-TPA arrays are numerically examined at antenna boresight as well as at steering angles up to $\pm 40^0$ with respect to antenna boresight in both azimuth and elevation planes. The numerical results of 10×10-element UE-TPA obtained through the proposed synthesis method at antenna boresight are compared with those determined at 20^0 and 40^0 scan angles and with those of same size arrays reported in the literature. In addition, results at antenna boresight achieved by proposed method for the case of 14×14-element UE-TPA array are compared with those determined at 20^0 and 40^0 scan angles. It is inferred from the investigation that wide angle scanning with lowest possible PSLL without appearance of grating lobes is achieved at comparable computational cost.

The synthesis of thinned array involves random removal of some of the radiating elements from the array aperture. This process not only reduces the total number of radiating elements in the array but also has advantages in terms of reduction in cost as well as weight of the array and ease in the design of power divider to feed each array element. The removal process involves switching off of array elements by feeding them with excitation amplitude equal to '0'. The thinned antenna arrays without any amplitude tapering i.e. having uniform amplitude excitations contribute to an optimum radiation pattern with reduced PSLL [Haupt (2010)]. In the recent past, many techniques have been used to address the challenges of array thinning, such as ant colony optimization (ACO) [Teruel and Iglesias (2006)], boolean differential evolution (BDE) [Zhang *et al.* (2010)], improved binary invasive weed optimization (IBIWO) [Liu and Wu (2014)], teaching learning based optimization (TLBO) [Nihad (2014)], particle swarm optimization (PSO) and its variants [Donelli *et al.* (2009), Deligkaris *et al.* (2009), Wang *et al.* (2011), Dev *et al.* (2012), Wang *et al.* (2012), Gangwar *et al.* (2015), and Gangwar *et al.* (2016)], and genetic algorithm (GA) [Haupt (1994), Weile and Michielssen (1997), Bray *et al.* (2002), and Jain and Mani (2011)]. Researchers in most of the techniques including those reported in [Teruel and Iglesias (2006), Deligkaris *et al.* (2009), Donelli *et al.* (2009), Zhang *et al.* (2010), Dev *et al.* (2012), Wang *et al.* (2012), Liu and Wu (2014), Nihad (2014), and Gangwar *et al.* (2016)] considered the optimization of PSLL only at boresight. However, determining the optimum combination of 'ON' and 'OFF' antenna elements corresponding to lowest PSLL when the array is scanned at angles away from boresight is even more challenging. Synthesis techniques reported in [Haupt (1994), Bray *et al.* (2002), and Gangwar *et al.* (2015a)] have been used to optimize the arrays when they are steered to the maximum scan angle, but the PSLL achieved is still high, although much better than

earlier reported values.

In the present study, it is aimed to synthesize a planar thinned array, which offers maximum possible reduction in the PSLL at affordable computational burden and also ascertains the absence of grating lobe when the beam is steered to maximum scan angle of 40^0 in both azimuth and elevation planes with respect to antenna boresight. It is intended to achieve such design performance with less number of 'ON' elements in order to reduce the cost as well as weight of the array. To achieve this objective, an improved genetic algorithm based optimization technique designated as IBc-GA is investigated in which following advancements are introduced to make it more efficient synthesis tool as compared to standard GA and other synthesis techniques available in literature:

- A novel multi-segment chromosome arrangement which enables the IBc-GA with more degrees of freedom and less complexity during optimization through the reduced number of variables for optimization
- A new robust randomization approach for crossover operation, which improves the offspring production and convergence rate of maximization process by rendering sufficient amount of randomization and diversity to the population
- A novel systematic mutation approach that makes the IBc-GA more vigorous, efficacious, and rapid in attaining good quality solution

In order to examine the synthesis capability in terms of reduction in PSLL and involved computational burden and to support the novelty of proposed approach, 10×10-and 14×14-elements UE-TPA arrays are numerically analysed at boresight as well as over the specified scan volume. The results obtained for 10×10-element UE-TPA array at antenna boresight are compared with those determined at 20^0 and 40^0 scan angles and with those for similar configuration arrays reported in [Zhang *et al.* (2010),

Deb *et al.* (2012), and Nihad (2014)] which would demonstrate the superiority of the proposed approach in achieving PSLL reduction. In addition, the total number of functional evaluations required till the convergence in the proposed method is almost comparable to those obtained using the techniques reported in [Zhang *et al.* (2010), Deb *et al.* (2012), and Nihad (2014)], with significant improvement in PSLL. Further, results at antenna boresight achieved by proposed method for the case of 14×14-element UE-TPA array are compared with those determined at 20^0 and 40^0 scan angles. It is expressed that the achieved thinned array configuration in this case yields better PSLL with much less number of 'ON' elements as compared to previous example of 10×10-element UE-TPA array.

3.2.1.3 Optimization of Peak, Average and RMS SLLs in 10×20-element TPA Array Using PSO

In this study, an optimistic design of thinned planar antenna (TPA) array that provides radiation pattern with reduced peak, RMS and average side lobe levels (SLLs) required for radar operating scenario is proposed. The main design objective is to inactivate some elements of the fully dense array while keeping the half power beam width (HPBW) and directivity unaffected and ensuring the maximum reduction in peak side level (PSLL), RMS SLL (RSLL) as well as average side lobe level (ASLL). Particle swarm optimization (PSO) is applied to find out optimum arrangement of 'active' and 'inactive' elements in TPA array which results in maximum possible reduction in SLLs. Thinning of a planar array comprising of 10×20 elements is considered in the present study and the computed results obtained through application of proposed technique are compared with those recently reported in the literature for similar design examples and those for fully dense array of equal size. The results show satisfying improvements

pertaining to reduction in peak, RMS and average side lobe levels using the proposed technique for the design of thinned array.

The major design objectives for radar antenna array include achieving the narrow beam in desired direction for better angular resolution, low peak, RMS and average side lobe levels to minimize clutter during detection of targets, and higher gain or directivity to obtain longer range of operation [Skolnik (1990)]. In order to obtain aforementioned radiation characteristics from an antenna array system, interest in the design of thinned antenna array has arisen in the recent past. In an effort to meet the design objectives, number of antenna elements is made inactive to obtain appropriate current distribution on the antenna aperture which results in the necessitated far-field radiation pattern. The aforesaid procedure permits to attain almost the same half power beam width (HPBW) and directivity of a fully dense array of equal size and at the same time suppresses the side lobe levels, bringing down cost and weight and ameliorating thermal management of the active antenna system. Furthermore, it makes realization of feed network for passive antenna easy [Haupt (2010)].

There are many evolutionary or stochastic optimization techniques, such as particle swarm optimization (PSO) [Donelli *et al.* (2009), Hooker and Arora (2010), Wang *et al.* (2012), and Gangwar *et al.* (2015a)], genetic algorithm (GA) [Haupt (1994), Haupt (2005), Mahanti *et al.* (2007), and Cen *et al.* (2012)], improved binary invasive weed optimization (IBIWO) [Liu and Wu (2014)], simulated annealing (SA) [Trucco (1999)], ant colony optimization (ACO) [Teruel and Iglesias (2006)], and boolean differential evolution algorithm (BDE) [Zhang *et al.* (2010)], which turn out to be very efficacious to synthesize thinned antenna arrays. In most of the algorithms reported in aforementioned literature, the authors have focused on reducing PSLL in the principal planes only. However, it is desirable for radar applications to suppress RMS

and average SLLs as well.

In the present study, an attempt is made to synthesize uniformly-excited thinned planar antenna (TPA) array with reduced peak, RMS and average SLLs by maintaining almost the same HPBW and directivity of a fully dense array of equal size. The optimum combination of 'active' and 'inactive' elements corresponding to lowest attainable side lobe levels of TPA array is estimated using particle swarm optimization (PSO) technique. The synthesized TPA array is modelled in X-band with the objective of assessing the performance of proposed algorithm in reducing peak, RMS and average side lobe levels and the results are compared with those obtained using recently reported methods.

3.2.1.4 Optimization of PSLL by Jointly Determining Thinned Configuration and Amplitude Weights in 10×20- and 8×8-elements TPA Array Using MBC-GA

In this study, a novel synthesis technique, which deals with jointly optimizing amplitude weight and thinned configuration of planar arrays to achieve best possible reduction in peak side lobe level (PSLL) is proposed. It is primarily aimed at the synthesis of uniformly excited thinned planar antenna (UE-TPA) arrays to get PSLL as low as possible, and went ahead to concurrently optimize both amplitude weight and configuration of thinned planar antenna (AW-TPA) array for further reduction in PSLL without altering HPBW. A modified binary coded genetic algorithm (MBC-GA) is utilized in which meliorated techniques for crossover and mutation operators are investigated to improve the radiation characteristics of arrays under consideration. A 10×20-element TPA array is numerically analysed to verify the effectiveness and examine the distinguishable differences of the proposed technique. The numerical

results obtained through the synthesis of this array show that the present technique outmatches those available in the literature. In order to further ascertain and validate the performance of present study as well as to understand the implications and operations in practical scenario, an 8×8-element AW-TPA array is realized and evaluated through numerical computation, EM simulation and experimentally. The experimental results obtained for the array are found nearly in agreement with numerically computed and electromagnetically simulated ones.

Synthesis of thinned planar antenna (TPA) arrays was first studied by Willey [Willey (1962)] and since then various advancements including those described in [Haupt (1994), Teruel and Iglesias (2006), Mahanti *et al.* (2007), Zhang *et al.* (2010), Wang *et al.* (2012), Goudos *et al.* (2013), Bhargav and Gupta (2013), Liu and Wu (2014), and Ha *et al.* (2016)] have been reported in the literature. This field has attracted substantial attention of researchers owing to the advantages of TPA array including considerably reduced number of radiating elements which brings down the cost and weight of the array for a given aperture size while at the same time allowing the investigators to attain almost same HPBW as that of a fully populated array of equal size [Haupt (1994]. The synthesis of thinned array is an optimization problem related to determination of the optimum combination of 'ON' and 'OFF' array elements corresponding to minimum possible PSLL. Many techniques including those described in [Haupt (1994), Teruel and Iglesias (2006), Zhang *et al.* (2010), Wang *et al.* (2012) and Liu and Wu (2014)] have been appropriately employed to solve such problems and achieve substantial reduction in PSLL by determining appropriate thinned arrangement for the arrays. However, the achieved HPBW may not be the narrowest one.

Present day radar systems require array antennas with low PSLL and narrow HPBW to avoid clutter and achieve better target signature accuracy. Achieving both

reduced PSLL and narrow HPBW are contradictory in nature as lowering of side lobe level results in broadening of HPBW. It is an ambitious problem involving multi-parameter optimization. In the recent past, few synthesis techniques [Mahanti *et al.* (2007), Bhargav and Gupta (2013), and Goudos *et al.* (2013)] have employed multi-objective optimization to cope up with aforesaid problem. In [Mahanti *et al.* (2007)], Mahanti *et al.* have optimized thinned arrangement to achieve low PSLL and maximize the thinning percentage. Goudos *et al.* [Goudos *et al.* (2013)] used multi-objective modified differential algorithm to optimize directivity and PSLL. Furthermore, multi-objective GA optimization technique is reported in [Bhargav and Gupta (2013)] to reduce PSLL and beamwidth.

In this work, optimization of only thinned array configuration is done to achieve low PSLL. Next, joint optimization of both amplitude weight and thinned arrangement is done to achieve further reduction in PSLL, while maintaining almost same HPBW in both cases. A modified binary coded genetic algorithm (MBC-GA) is utilized to solve both the aforesaid problems. Novel meliorated techniques for crossover and mutation genetic operators are investigated to enhance the potentialities in terms of design efficiency and performance of the proposed synthesis method. A 10×20-element UE-TPA array is considered to examine the effectiveness of the proposed method and distinguishable differences between the proposed synthesis technique and other techniques reported in literature for design of similar array configurations. Numerical results obtained through the proposed MBC-GA based synthesis technique for the array under consideration demonstrate the superiority of present technique over other methods reported in [Teruel and Iglesias (2006), Zhang *et al.* (2010), Liu and Wu (2014), and Wang *et al.* (2012)].

In order to further ascertain and validate the potentialities of present study as well as to understand implications and functioning in practical scenario, an 8x8-element AW-TPA array is designed, fabricated and tested experimentally. The experimental results are found nearly in agreement with computed and simulated ones. Hence, the proposed MBC-GA based synthesis technique is expected to be very effective in designing the TPA arrays for practical applications.

3.2.2 Geometrical Configuration and Problem Statement for TPA Arrays

3.2.2.1 Reduction of PSLL and Maximization of Number of 'OFF' Elements in 10×20-element TPA Array Using MBC-GA

Figure 3-1 shows general configuration of a planar array with 2N × 2M elements located symmetrically about the origin in X-Y plane. The total field radiated by this array is given as [Wang *et al.* (2012), Gangwar *et al.* (2016)]

$$\vec{E}_{total}(\theta,\phi)) = \left[\vec{E}\left(\text{element at ref}(\theta,\phi)\right)\right] \times [\text{Array Factor (AF }(\theta,\phi))] \quad (3.1)$$

where the array factor in $(\theta,\phi))$ direction is expressed as

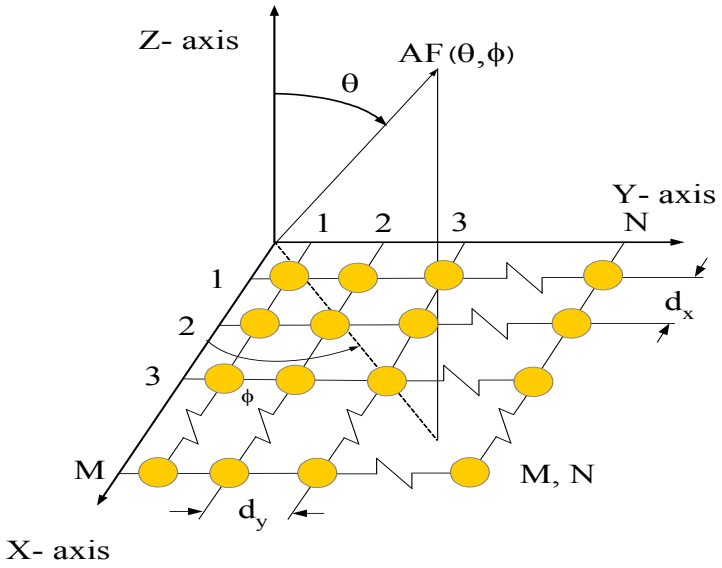

Fig. 3-1: General configuration of one quadrant of planar array with 2M×2N-elements.

$$AF(\theta,\phi) = \sum_{n=1}^{N}\sum_{m=1}^{M} A_{nm}\cos\left[\frac{(2n-1)}{2}\times kd_x\sin\theta\cos\phi\right] \times \cos\left[\frac{(2m-1)}{2}\times kd_y\sin\theta\sin\phi\right] \quad (3.2)$$

$\vec{E}\left(\text{element at ref}\,(\theta,\Phi)\right)$ is the radiated field vector of individual elements in the (θ,Φ) direction which is assumed as cos(θ) pattern, $A_{nm} \in \{1,0\}$ is the amplitude excitation coefficient of the element at (n, m)th position, where '1' implies an 'active' element and '0' an inactive element, d_x and d_y are the inter-element spacings along X-and Y-axes respectively (both are assumed to be same equal to 0.5 λ in the present study), θ is the elevation angle with respect to Z-axis and ϕ is the azimuth angle with respect to X-axis. The fitness function utilized in present study is to reduce the peak side lobe level (PSLL) in principal planes ($\phi = 0^0$ and $\phi = 90^0$ planes) of the radiation pattern while maintaining other radiation characteristics of the pattern. The normalized side lobe level ($F_{PSLL}\,(A_{nm},\theta,\Phi)$) of the array radiation pattern can be computed using Eq. (3.3) [Wang *et al.* (2012), Gangwar *et al.* (2016)]

$$F_{PSLL}(A_{nm},\theta,\Phi) = \max_{\forall\theta\in AC}\left[20\log\left|\frac{AF(A_{nm},\theta,\Phi)}{AF_{max}}\right|\right] \quad (3.3)$$

The thinning percentage (THP) in the thinned array geometry can be formulated as [Gangwar *et al.* (2015a)]

$$THP = \frac{N_{OFF}}{N_{ON}+N_{OFF}}\times 100 \quad (3.4)$$

where N_{OFF} is total number of 'OFF' elements and N_{ON} is total number of 'ON' elements in thinned array.

The fitness values in the individual planes are calculated using Eq. (3.3) and the function given below in Eq. (3.5) is used to reduce the total PSLL in both planes during optimization while keeping thinning percentage equal to or more than a fixed value.

$$f_{PSLL}(A_{nm},\theta) = \{F_{PSLL}(A_{nm},\theta)|_{\Phi=0^0} + F_{PSLL}(A_{nm},\theta)|_{\Phi=90^0}\} |$$

$$s.t.\ \ THP_a \geq THP_d \qquad (3.5)$$

3.2.2.2 PSLL Optimization with Minimum Number of Turn 'ON' Elements in 10×10-and 14×14-Elements TPA Arrays over ± 40° Scan Volume Using IBc-GA

In this study, as per the general structure of planar array shown in Fig. 3-1, the total field radiated by this planar array is given in Eq. (3.1). The fitness values in the individual planes are calculated using Eq. (3.3) and the function given below in Eq. (3.6) is used to reduce the total PSLL in both planes during optimization.

$$f(Amp_{nm},\theta) = F_{PSLL}(A_{nm},\theta,\Phi)|_{\phi=0^0} + F_{PSLL}(A_{nm},\theta,\Phi)|_{\phi=90^0} \qquad (3.6)$$

The thinning percentage (TP) can be formulated as:

$$TP = \frac{Ele_{OFF}}{Ele_{ON}+Ele_{OFF}} \times 100 \qquad (3.7)$$

where Ele_{OFF} is total number of 'OFF' elements and Ele_{ON} is total number of 'ON' elements in TPA array.

Thus, the problem is to minimize

$$\{f(Amp_{nm},\theta)\} \text{ in Eq.}(3.6) \ \text{ subject to } \ TP_a \geq TP_d \qquad (3.8)$$

where TP_a is the achieved thinned percentage and TP_d is the desired thinned percentage, $Amp_{nm} \in \{1, 0\}$, n = 1, 2, 3……. 2N, m=1, 2, 3….2M. In the present study, the values of both M and N are assumed to be the same.

3.2.2.3 Optimization of Peak, Average and RMS SLLs in 10×20-element TPA Array Using PSO

The geometrical configuration of planar array as shown in Fig. 3-1 is considered for this study. The array comprises of 2N×2M antenna elements symmetrically populated in X-

Y plane with no element located at the origin. The far-field radiation pattern of this array can be calculated using Eq. (3.1).

The fitness function considered in the present study is to minimize peak side lobe level (PSLL) of the radiation pattern in principal planes as well as in all other inter-coordinal planes while maintaining almost same HPBW and directivity of a fully dense array of equal size. The normalized peak side lobe level (F_{PSLL} (A_{nm}, θ, ϕ)) of the antenna array can be computed using Eq. (3.3). The optimization goal is to minimize function given below in Eq. (3.9) with the objective of achieving maximum possible reduction in side lobe level.

$$f(A_{nm}) = \mathrm{F_{PSLL}}(\mathrm{A_{nm}}, \theta, \Phi)|_{\phi=\in\{-180^0:1:180^0\}} \tag{3.9}$$

3.2.2.4 Optimization of PSLL by Jointly Determining Thinned Configuration and Amplitude Weights in 10×20- and 8×8-elements TPA Array Using MBC-GA

The geometrical configuration of a planar array with $2N \times 2M$ elements symmetrically distributed in X-Z plane as shown in Fig. 3-1 is assumed in this study. The total field radiated by this array can be computed using Eq. (3.1).

The objective is to minimize fitness function $f\,(A_{nm})_{UE-TPA}$ for UE-TPA array

$$f\,(\mathrm{A_{nm}})_{\mathrm{UE-TPA}} = \mathrm{F_{PSLL}}(\mathrm{A_{nm}}, \theta)|_{\phi=0^0} + \mathrm{F_{PSLL}}(\mathrm{A_{nm}}, \theta)|_{\phi=90^0} \tag{3.10}$$

Therefore synthesis problem is given by

$$\text{Minimize } \{f\,(\mathrm{A_{nm}})_{\mathrm{UE-TPA}}\},\ \text{s.t. } \mathrm{A_{nm}} \in \{1, 0\}, \tag{3.11}$$

where n=1, 2, 3…….N, m=1, 2, 3….M

In case of AW-TPA array, the fitness function $f(A_{nm})_{AW-TPA}$ is

$$f(A_{nm})_{Aw-TPA} = F_{PSLL}(A_{nm}, \theta)|_{\phi=0^0} + F_{PSLL}(A_{nm}, \theta)|_{\phi=90^0} \quad (3.12)$$

Hence the optimization problem is given by

$$\text{Minimize} \quad \{f(A_{nm})_{AW-TPA}\}, \quad \text{s.t.} \quad A_{nm} \in \begin{Bmatrix} 1, 0, \text{or any fractional} \\ \text{value } \not\in 0 \text{ and } 1 \end{Bmatrix} \quad (3.13)$$

where n = 1, 2, 3…….N, m = 1, 2, 3….M

3.2.3 Optimization Techniques for the Synthesis of TPA Arrays

3.2.3.1 Reduction of PSLL and Maximization of Number of 'OFF' Elements in 10×20-element TPA Array Using MBC-GA

In this study, MBC-GA described in section A1.2 (Appendix-A) is used to determine the best configuration of TPA array that would result in lowest possible value of PSLL and maximum number of 'OFF' elements. The commencing population of 50 chromosomes are randomly generated wherein each chromosome consists of 10×20-genes. MBC-GA minimizes the function given in Eq. (3.5) during optimization.

3.2.3.2 PSLL Optimization with Minimum Number of Turn 'ON' Elements in 10×10-and 14×14-elements TPA Arrays over ± 40^0 Scan Volume Using IBc-GA

In this study, IBc-GA as explained in section A1.3 (Appendix-A) is used to determine the best configuration of TPA arrays that would result in optimal values of PSLL over pre-specified scan volume. The algorithm is started with a population of 1000 chromosomes. The fitness function given in Eq. (3.8) is minimized using the IBc-GA algorithm in order to obtain best fitness value.

3.2.3.3 Optimization of Peak, Average and RMS SLL in 10×20-element TPA Array Using PSO

In this study PSO as explained in section A2.1 (Appendix–A) is used to determine the best configuration of TPA array corresponding to optimal values of peak, average and RMS SLLs. The fitness function given in Eq. (3.9) is minimized using the PSO algorithm in order to obtain best fitness value.

3.2.3.4 Optimization of PSLL by Jointly Determining Thinned Configuration and Amplitude Weights in 10×20- and 8×8-elements TPA Array Using MBC-GA

MBC-GA described in section A1.2 (Appendix-A) is utilized to determine the best configuration of TPA arrays that would result in lowest possible value of PSLL through the optimization of both thinned arrangement and amplitude excitations. MBC-GA minimizes the function given in Eqs. (3.11) and (3.13) during optimization.

3.2.4 Numerical Analysis, Results and Discussion

In this section, numerical studies of various examples under consideration which examine the effectiveness of the proposed synthesis methods are described.

3.2.4.1. Reduction of PSLL and Maximization of Number of 'OFF' Elements in 10×20-element TPA Array Using MBC-GA

In this section, thinned array configuration of a 10×20-element planar array symmetrically spaced 0.5λ apart along both the X- and Y-axes with its centre at the origin, is numerically examined. All the elements in the array were excited with equal amplitude and equal phase. During optimization process, the elements at the array boundary may be made inactive which would alter the array size in every iteration. Therefore to keep the array of fixed size, the boundary elements were always kept 'active'.

This section describes the numerical analysis of the thinned configuration of a 10×20-element uniformly excited planar array and comparison of results obtained through the proposed scheme and with those of arrays reported in literature are presented. Fitness function illustrated in Eq. (3.5) was applied to suppress PSLL in $\Phi = 0^0$ and $\Phi = 90^0$ planes by utilizing the proposed MCB-GA optimization technique. The variations of best fitness values measured by PSLL as functions of iteration number in single trial and average over 30 trials are depicted in Fig. 3-2. It can be noticed from Fig. 3-2 that the optimal solutions (Best PSLLs in single trial < -27.53 dB in $\Phi = 0^0$ plane, and < -29.05 dB in $\Phi = 90^0$ plane, PSLLs averaged over 30 trials < -26.56 dB in $\Phi = 0^0$ plane and < -28.5 dB in $\Phi = 90^0$ plane) occur after around 162 and 190 iterations for single and averaged over 30 trials respectively. The best combination of 'active' and 'inactive' elements obtained through the proposed algorithm is depicted in Fig. 3-3 and optimum distribution of antenna elements on the aperture of the proposed TPA array is shown in Fig. 3-4.

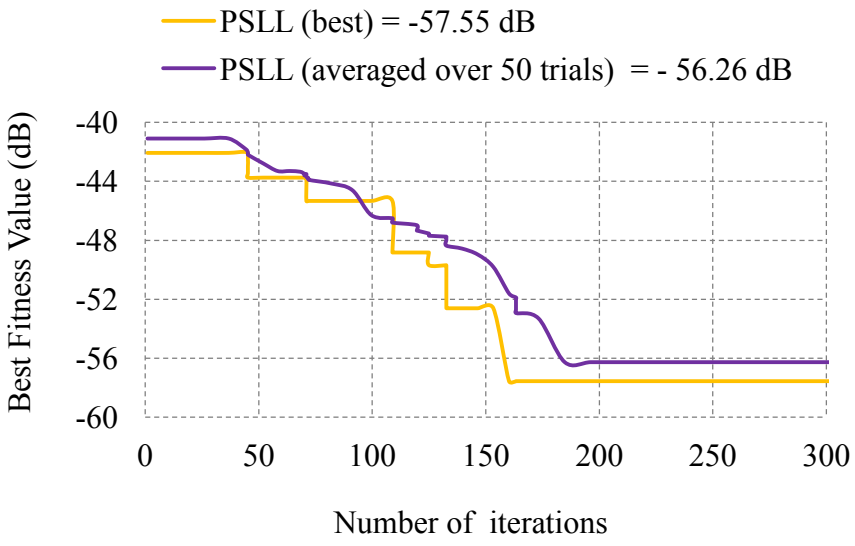

Fig. 3-2: Variations of overall best and averaged over 30 trials fitness value i.e. PSLL with number of iterations in the optimization of proposed 10×20-element TPA array.

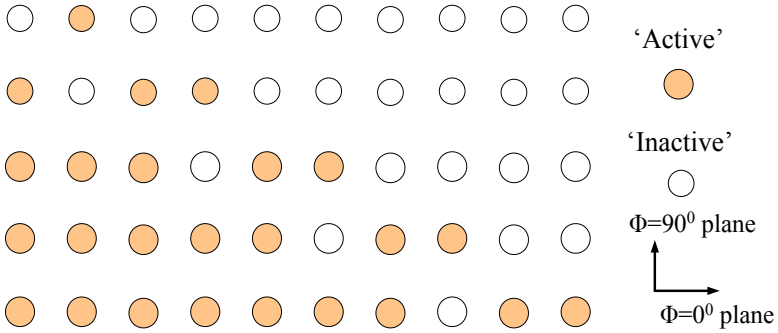

Fig. 3-3: Optimal sequence of 'active' and 'inactive' elements of one quadrant (X-positive and Y-positive planes) of the proposed 10×20-element TPA array.

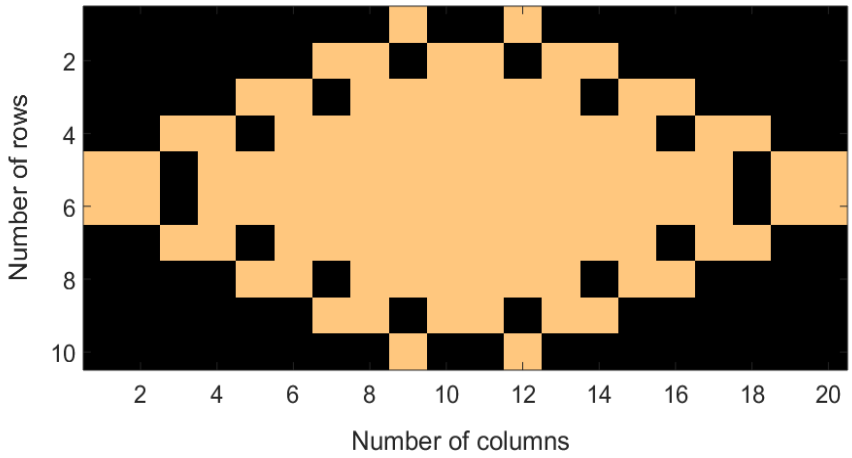

Fig. 3-4: Optimal distribution of 'active' (brown colour) and 'inactive' (black colour) antenna elements on the aperture of the proposed 10×20-element TPA array.

The numerically computed array patterns obtained through the proposed technique and those reported in literature using ACO [Teruel and Iglesias (2006)], BDE [Zhang *et al.* (2010)], BPSO [Wang *et al.* (2012)], and IBIWO [Liu and Wu (2014)] are depicted in Figs. 3-5 and 3-6 in $\Phi = 0^0$ and $\Phi = 90^0$ planes respectively. The 3D radiation pattern and intensity plot are depicted in Figs. 3-7 and 3-8 respectively. Radiation parameters evoked from Figs. 3-5 - 3-8 are indexed in Table 3-1. It can be noticed clearly from Table 3-1 that the lowest possible PSLL achieved by the proposed MBC-GA technique is -27.53 dB in $\Phi = 0^0$ plane, which is 1.77 dB lower than that attained using ACO in [Teruel and Iglesias (2006)], 2.45 dB lower than that attained through BDE in [Zhang *et al.* (2010)], 11.96 dB lower than that achieved using BPSO in [Wang *et al.* (2012)], and 3.89 dB lower than that achieved using IBIWO in [Liu and Wu (2014)]. In $\Phi = 90^0$ plane, best PSLL achieved through the proposed synthesis technique is -29.05 dB, which is at least 2.96 dB better than those reported in [Liu and Wu (2014), Zhang *et al.* (2010), Wang *et al.* (2012), and Teruel and Iglesias (2006)]. This is likely because of the reality that the innovative robust randomization strategy for crossover operation and unexampled systematic mutation strategy described in section A1.2.2 (Appendix-A) might have provided sufficient amount of randomization and diversity to the solution space. This has enabled MBC-GA with rapid convergence (fewer generations) in attaining good quality solution in terms of PSLL and computational load as confirmed by results depicted in Table 3-2. However, methods in [Teruel and Iglesias (2006), Zhang *et al.* (2010), Wang *et al.* (2012), and Liu and Wu (2014)] have taken more generations to converge and even got immobilized in local maxima and finally ended up with sub-optimal solution. The reason might be because their solution space would be having insufficient amount of randomization and diversity.

In addition, the HPBW and directivity obtained through the proposed MBC-GA synthesis method are comparable to those reported in previously mentioned literature, however 50 % of thinning is achieved which is greater than 32% in [Teruel and Iglesias (2006)], 46% in [Zhang *et al.* (2010)], 46% in [Wang *et al.* (2012)], and 48% acheived in [Liu and Wu (2014)]. Hence, the foregoing results and theoretical facts certified that MBC-GA is an efficacious synthesis tool in terms of reduction in PSLL with less number of turn 'ON' antenna elements.

In addition to solution quality, computational complexity is also compared which is generally measured in terms of number of fitness function evaluations associated with the problem at hand. The function evaluations involved till the convergence of algorithm can be calculated as [Haupt (1994)]

$$\text{Computational cost} = K \times N_p \times N_{opt} \times G_n \tag{3.14}$$

where K is number of angles at which array factor is being calculated, N_p is population size, N_{opt} is number of variables involved in optimization, and G_n is number of generations till convergence. Therefore, for a fixed precision (number of angles for array factor computation), the total number of functional evaluations involved till the convergence in the proposed method is compared with those obtained from techniques reported in [Wang *et al.* (2012), and [Liu and Wu (2014)] and the results are depicted in Table 3-2. It can be noticed from Table 3-2 that computational cost involved in proposed method is 1.63×10^6, which is 60.4% less than that of in [Liu and Wu (2014)], and 61.56% less than that in [Wang *et al.* (2012)]. This proves that MBC-GA is computationally more efficient than those techniques reported in [Liu and Wu (2014)], and [Wang *et al.* (2012)].

Apart from MBC-GA capability in terms of attaining best possible reduction in PSLL in a computationally efficient fashion, its reliability is also of great concern which is examined by running 30 independent trials. The final results are averaged over all the trials. It may be noticed that the best PSLL and the PSLL averaged over 30 trials are almost same (as confirmed by Fig. 3-8). This evidences the stability of proposed MBC-GA optimization algorithm.

The involved computational load and flexibility in attaining good quality solution support that MBC-GA based synthesis approach is more suitable to solve sparse linear and planar arrays having smaller sizes (number of antenna elements upto 100 or multiples of hundred) and is not effective for larger size arrays.

Therefore, it is corroborated that proposed MBC-GA is a stable optimization technique. Thus, it may be concluded that the thinned array synthesis approach based on MBC-GA optimization technique offers an efficient solution in terms of attaining best possible reduction in PSLL at less computational complexity and with great stability.

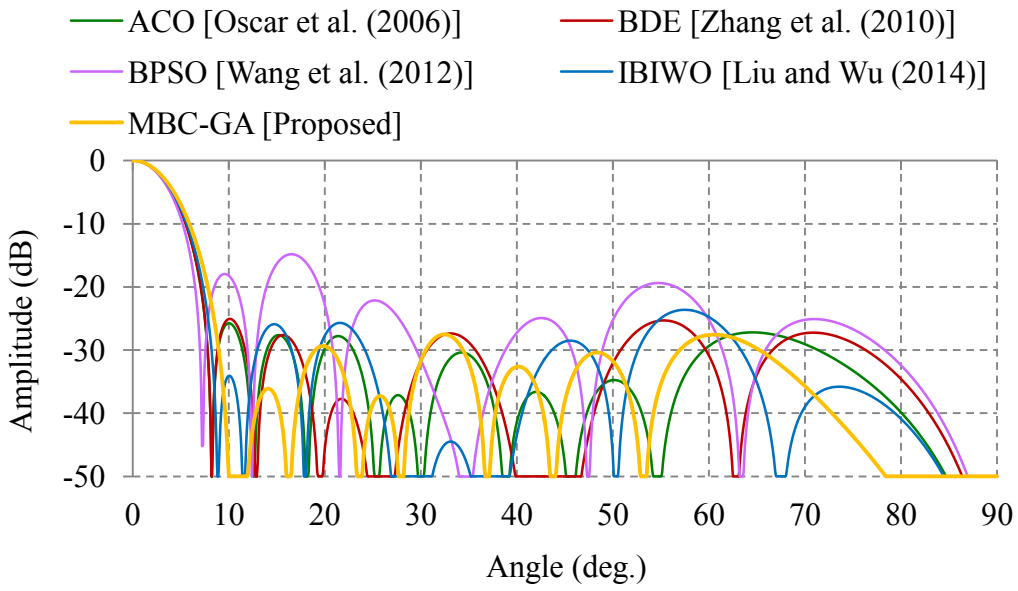

Fig. 3-5: Comparison of radiation patterns of the proposed 10×20-element TPA array with those of arrays reported in [Teruel and Iglesias (2006)], [Zhang *et al.* (2010)], [Wang *et al.* (2012)], and [Liu and Wu (2014)] in $\Phi = 0^0$ plane.

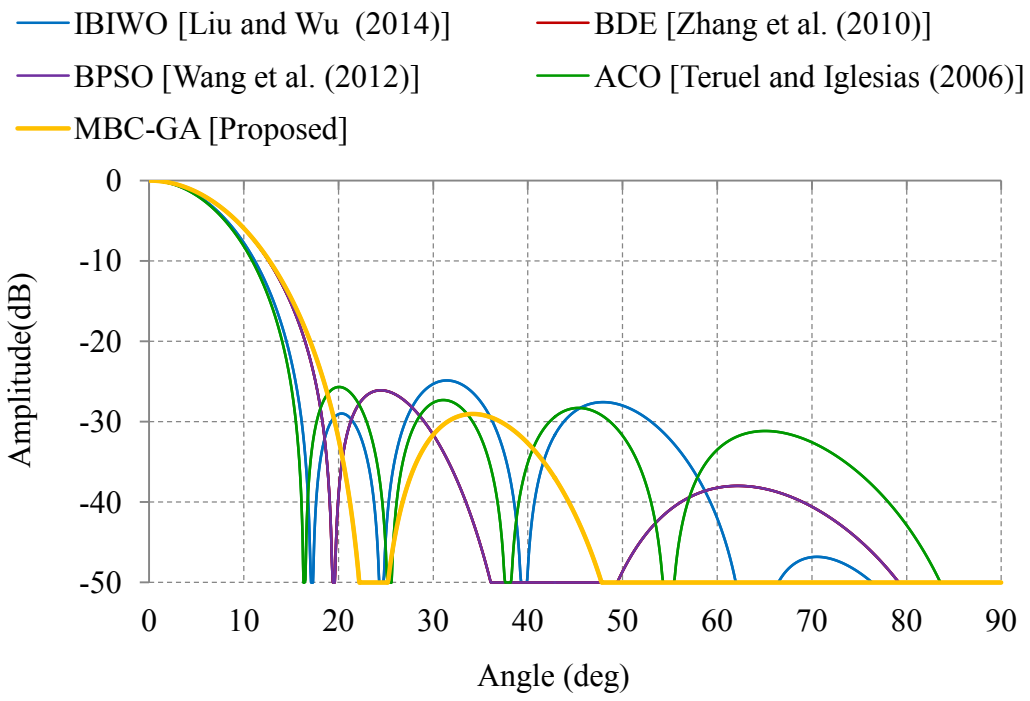

Fig. 3-6: Comparison of radiation patterns of the proposed 10×20-element TPA array with those of arrays reported in [Teruel and Iglesias (2006)], [Zhang *et al.* (2010)], [Wang *et al.* (2012)], and [Liu and Wu (2014)] in $\Phi = 90^0$ plane.

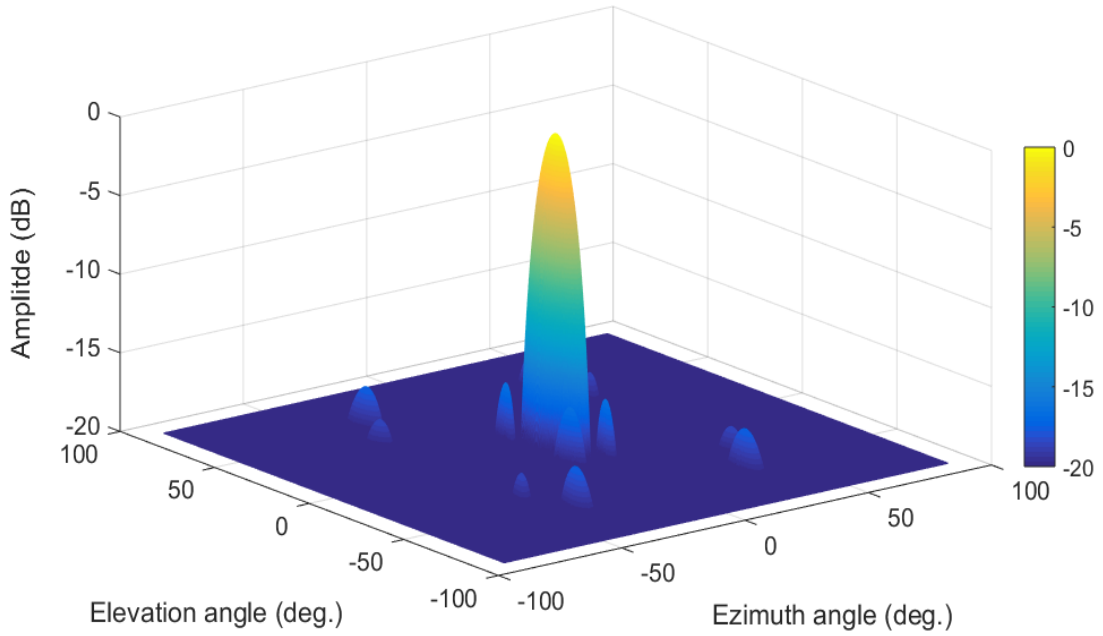

Fig. 3-7: 3D radiation pattern of the proposed 10×20-element TPA array

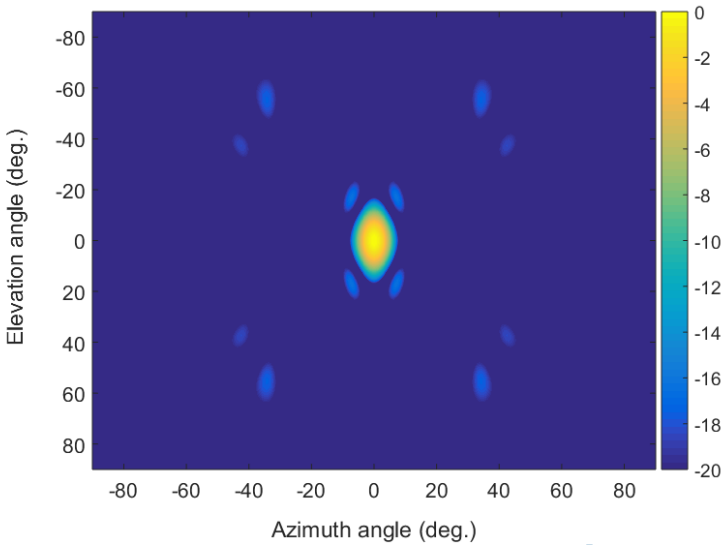

Fig. 3-8: Intensity plot of the proposed 10×20-element TPA array

Table 3-1: Comparison of numerically evaluated results for the proposed 10×20-element TPA array with those of the arrays reported in [Teruel and Iglesias (2006)], [Zhang *et al.* (2010)], [Wang *et al.* (2012)], and [Liu and Wu (2014)].

Design parameters	**ACO [Teruel and Iglesias (2006)]**	**BDE [Zhang et al. (2010)]**	**BPSO [Wang *et al.* (2012)]**	**IBIWO [Liu and Wu (2014)]**	**MBC-GA [Proposed]**
Thinning percentage	32	46	46	48	50
PSLL (dB) in $\Phi=0^0$ plane	-25.76	-25.09	-15.57	-23.64	-27.53
PSLL (dB) in $\Phi=90^0$ plane	-25.67	-26.09	-26.09	-24.87	-29.05
HPBW (deg.) in $\Phi=0^0$ plane	6.2	6.2	6.0	6.4	6.6
HPBW (deg.) in $\Phi=90^0$ plane	12.6	14.4	14.4	12.8	14.4
Directivity (dB)	27.2	26.64	26.78	27.05	26.98

Table 3-2: Comparison of computational cost of the proposed approach with that of the methods reported in [Wang *et al.* (2012)], and [Liu and Wu (2014)] for the synthesis of 10×20-element TPA array.

Parameters	**BPSO [Wang *et al.* (2012)]**	**IBIWO [Liu and Wu (2014)]**	**MBC-GA [Proposed]**
Population size	100	100	50
Number of iterations till the convergence	206	212	163
Computational cost	4.12×10^6	4.24×10^6	1.63×10^6

3.2.4.2. PSLL Optimization with Minimum Number of Turn 'ON' Elements in 10×10-and 14×14-elements TPA Arrays over ± 40^0 Scan Volume Using IBc-GA

The synthesis capability of proposed IBc-GA based approach is examined through the comparison of our results with those obtained by other approaches on the same size arrays reported in the literature. In Particular, IBc-GA performance is compared in terms of the potentiality to obtain quality solution i.e. lowest achievable peak side lobe level (PSLL) and computational complexity involved in solving the problem at hand [Haupt (1994), Donelli et al (2009), Zhang *et al.* (2010), and Wang *et al.* (2011)]. Larger population (1,000 chromosomes) was used by author to provide significant amount of flexibility in search for an optimum solution. If the population size is small, proposed algorithm may not have adequate tractability and it requires more number of generations till it arrives at the required solution. Further, even for more number of generations, the algorithm may not arrive at optimum solution and may end up with sub-optimum solution.

3.2.4.2.1 10×10-element UE-TPA Array

In this section, a 10×10-element TPA array with uniform amplitude excitation and inter-element spacing equal to 0.5λ is considered for optimization of thinned array configuration corresponding to lowest possible PSLL over the aforesaid scan volume. During optimization, the proposed IBc-GA reduces the fitness function expressed in Eq. (3.8). The variation of best fitness value with number of iterations taken from 50 trials is shown in Fig. 3-9, where most desired value occurs after around 42 iterations. The most suitable 'ON' and 'OFF' positions of array elements achieved through the aforementioned IBc-GA settings are indicated in Fig. 3-10 and corresponding distribution of antenna elements on the aperture of array is shown in Fig. 3-11. The radiation patterns of the proposed 10×10-element UE-TPA array obtained through IBc-GA and those obtained using boolean differential evolution algorithm (BDE) [Zhang *et al.* (2010)], particle swarm optimization (PSO) [Deb *et al.* (2012)], and teaching learning based optimization (TLBO) [Nihad (2014)] are shown in Fig. 3-12 at antenna boresight. 3D radiation pattern and intensity plot at antenna boresight are shown in Figs. 3-13 and 3-14 respectively. The radiation characteristics extracted from Figs. 3-12 - 3-14 are shown in Table 3-3. It can be seen from Figs. 3-12 - 3-14 and Table 3-3 that PSLL at boresight achieved through the proposed approach is -26.73 dB, which is 7.17 dB lower than that reported in [Zhang *et al.* (2010)], 3.69 dB lower than that obtained in [Deb *et al.* (2012)], and 7.09 dB lower than that attained in [Nihad (2014)]. This is probably because large population size (1,000 chromosomes) is considered in the proposed approach. The larger population (several solutions) and new robust randomization approach for crossover operation as well as a novel systematic mutation operation, has provided sufficient amount of randomization and diversity to the population and eventually proposed IBc-GA has got converged to an

optimum solution in fewer generations. However, smaller population sizes in [Zhang *et al.* (2010)], [Deb *et al.* (2012)], and [Nihad (2014)] have taken more generations to converge and probably might have got trapped in local maxima and eventually ended up with sub-optimal solution. Furthermore, the optimized thinned array configuration determined through the investigated IBc-GA has 40% 'OFF' elements, while same obtained through BDE in [Zhang *et al.* (2010)] has 24% 'OFF' element, and that obtained through TLBO in [Nihad (2014)] has 35% 'OFF' elements. The foregoing results and facts evidenced that IBc-GA significantly outperforms the BDE in [Zhang *et al.* (2010)] and TLBO in [Nihad (2014)] by achieving much better PSLL with less number of turn 'ON' elements.

It is well known that the computational complexity of global optimization techniques is measured in terms of number of fitness function evaluations, which increases rapidly with number of unknowns (number of array elements involved in optimization). The computational cost involved till the convergence can be calculated as [Jain and Mani (2011)]

$$\mathrm{K} \times \mathrm{N}_{\mathrm{variable}} \times \mathrm{S}_{\mathrm{space}} \times \mathrm{I}_{\mathrm{iteration}} \tag{3.15}$$

where K is number of angles at which array factor is being calculated, $N_{variable}$ is the number of variables involved in optimization, S_{space} is population size, $I_{iteration}$ is number of iterations required till convergence. In proposed method, as per the novel chromosome arrangement described earlier in section A1.3.2 (Appendix-A) out of 25 elements in one quadrant for 10×10-elements array, only 16 peripheral elements are required to be involved in optimization. Consequently, as per the foregoing expression for computational cost, for a given precision (number of angles for array factor calculation), the total number of computations required till the convergence in present method is 6.72×10^5, whereas it is 5×10^5 in BDE [Zhang *et al.* (2010)], 7.36×10^5 in PSO

[Deb *et al.* (2012)] and 10×10^5 in TLBO [Nihad (2014)]. It shows that computational load is almost comparable to the techniques reported in [Zhang *et al.* (2010)], [Deb *et al.* (2012)] and [Nihad (2014)]. Thus, the foregoing results and theoretical facts evidenced that IBc-GA is an efficacious synthesis tool which has provided more degrees of freedom and affordable computational complexity in attaining the maximum possible reduction in PSLL.

Furthermore, most of the array thinning methods including those reported in [Zhang *et al.* (2010)], [Deb *et al.* (2012)], and [Nihad (2014)] have only considered the optimization of an array at antenna boresight. However, when these arrays are steered to some angle off the boresight, grating lobes would commence to emerge. The maximum scan angle that an antenna array can be steered away from the boresight is given by Eq. (3.16)

$$\theta = \sin^{-1}(\frac{\lambda}{d}-1) \tag{3.16}$$

where θ is the maximum scan angle off boresight, d is the inter-element spacing and λ is the wavelength of operating signal. It is observable from Eq. (3.16) that maximum scan angle is $\pm$ 90^0 when the inter-element spacing is $\lambda/2$, and scan volume decreases as the inter-element spacing increases.

In this study, a method for thinning of planar antenna arrays to attain reduced side lobe level over wide steering angle using IBc-GA was investigated. The radiation characteristics of the 10×10-element UE-TPA array obtained through the proposed method when array is steered to 20^0 in both azimuth and elevation planes are shown in Figs. 3-15 – 3-18 and when array is steered to 40^0 in both planes, these are depicted in Figs. 3-19 - 3-22. The radiation parameters extracted from Figs. 3-15 - 3-18 and Figs. 3-19- 3-22 are listed in Table 3-3. It may be noticed from Figs. 3-15 - 3-18 and Figs. 3-19-3-22 and Table 3-3 that best PSLLs obtained through the proposed technique are -25.86 dB and -24.96 dB respectively when array is steered to 20^0 and 40^0 away from the

boresight. This shows that there is no significant degradation in PSLL and appearance of grating lobes when the array is steered at specified angles away from boresight. Thus, the proposed method serves the purpose of synthesizing thinned arrays which are capable of beam steering over the pre-specified scan volume.

The utilization of multi-segment chromosome approach in IBc-GA results into reduced number of variables for computation and hence, it is expected to be more suitable for solving the problem of thinned planar arrays dealing with large number of antenna elements of the order of thousands or multiple of thousands.

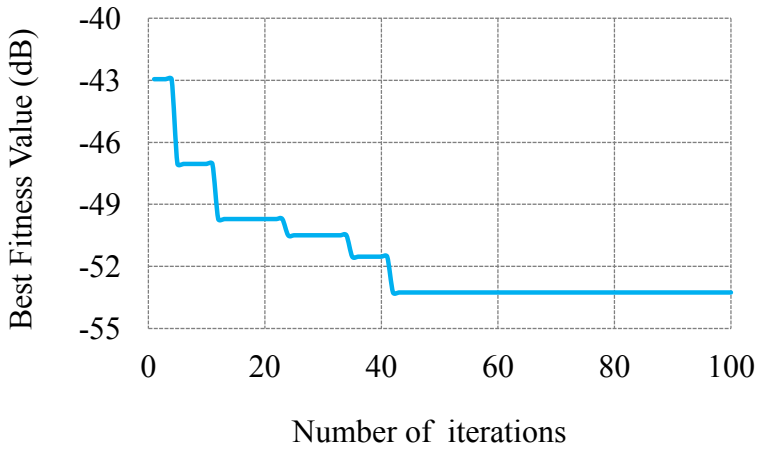

Fig. 3-9: Variation of mean fitness value with number of iterations in the optimization of proposed 10×10-element UE-TPA array.

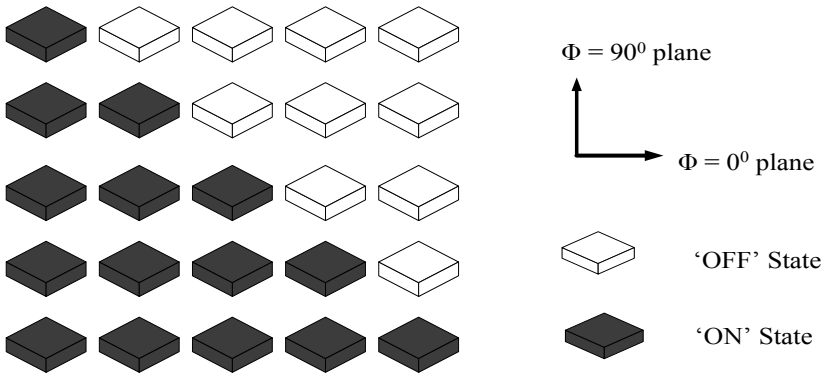

Fig. 3-10: Optimal combination of 'ON' and 'OFF' elements of one quadrant (X-positive and Y-positive plane) of the proposed 10×10-element UE-TPA array. The dark gray blocks represent the 'ON' state of antenna element while the white ones represents 'OFF' state.

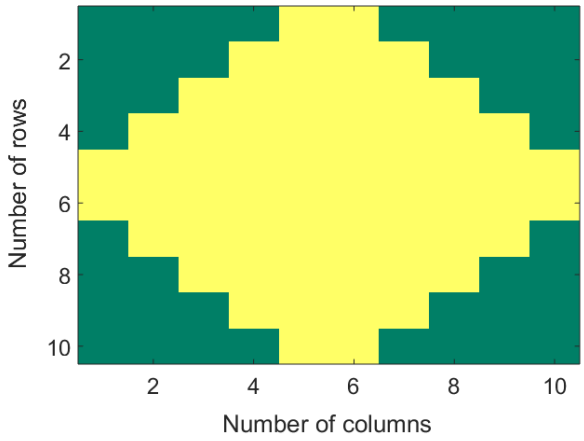

Fig. 3-11: Optimal arrangement of 'ON' (yellow) and 'OFF' (green) antenna elements on the aperture of the proposed 10×10-element UE-TPA array.

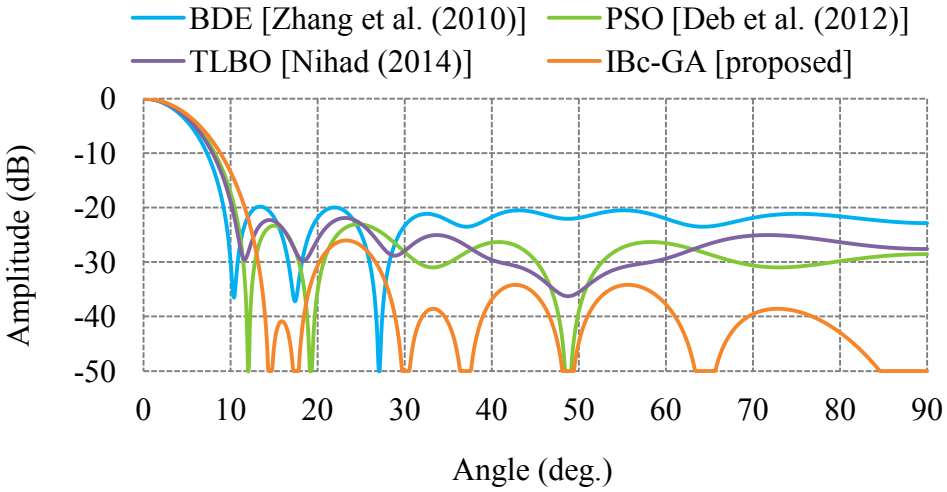

Fig. 3-12: Comparison of radiation pattern of the proposed 10×10-element UE-TPA array with those of arrays reported in [Zhang *et al.* (2010)], [Deb *et al.* (2012)], and [Nihad (2014)].

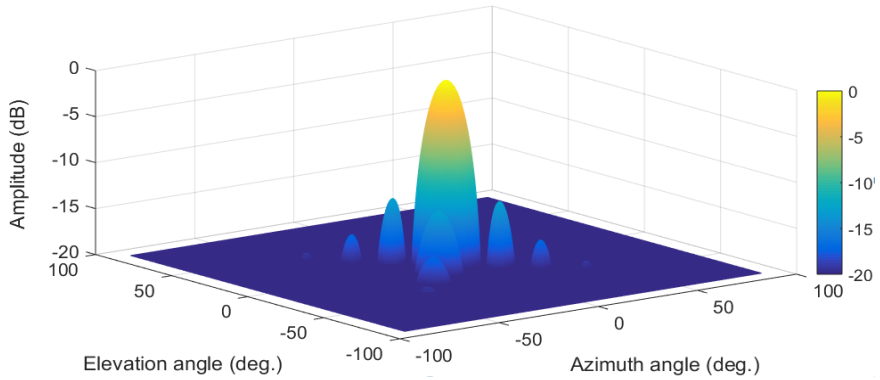

Fig. 3-13: 3D radiation pattern of the proposed 10×10-element UE-TPA array at antenna boresight.

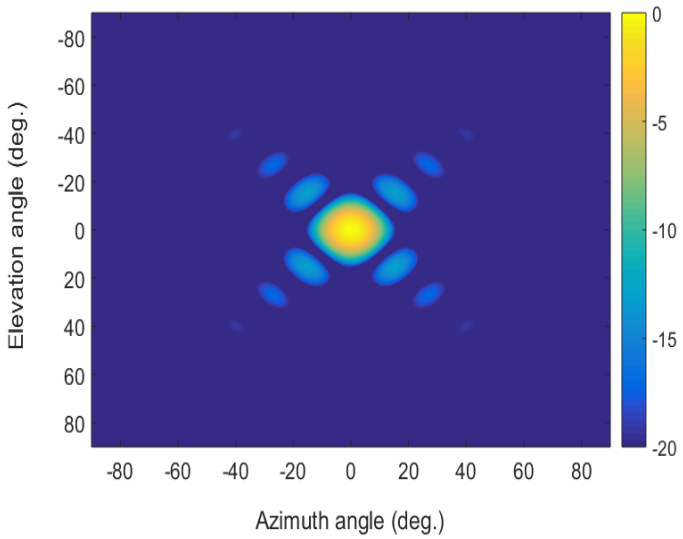

Fig. 3-14: Intensity plot of the proposed 10×10-element UE-TPA array at antenna boresight.

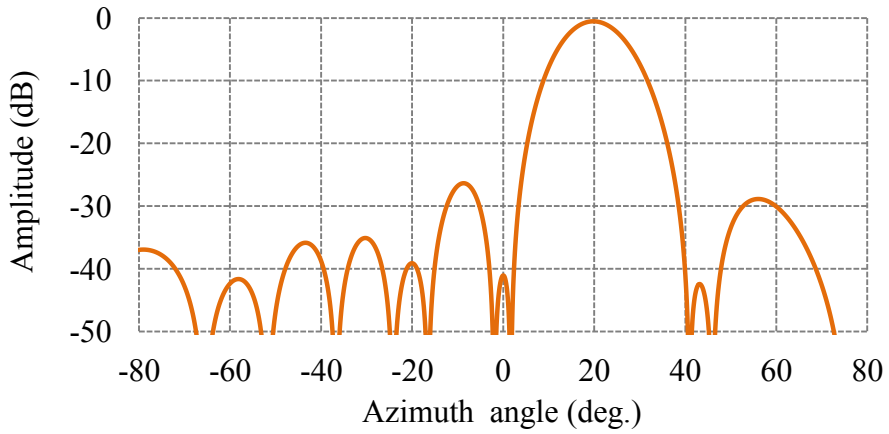

Fig. 3-15: Radiation pattern of the proposed 10×10-element UE-TPA array scanned at an angle $\theta = 20^0$ with respect to antenna array boresight in azimuth ($\Phi = 0^0$) plane.

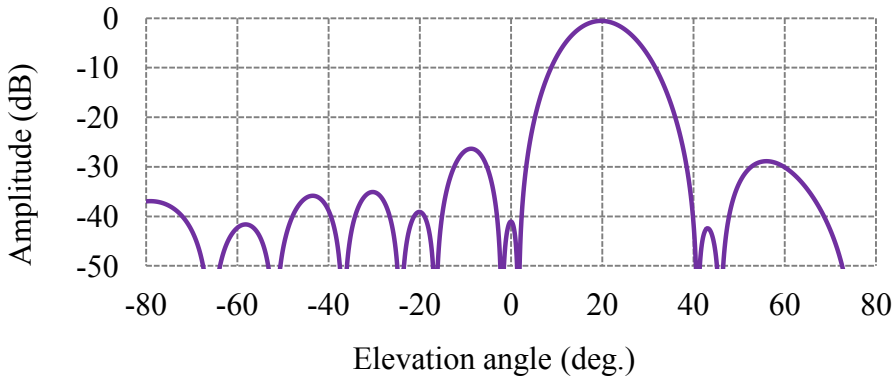

Fig. 3-16: Radiation pattern of the proposed 10×10-element UE-TPA array scanned at an angle $\theta = 20^0$ with respect to antenna array boresight in elevation ($\Phi = 90^0$) plane.

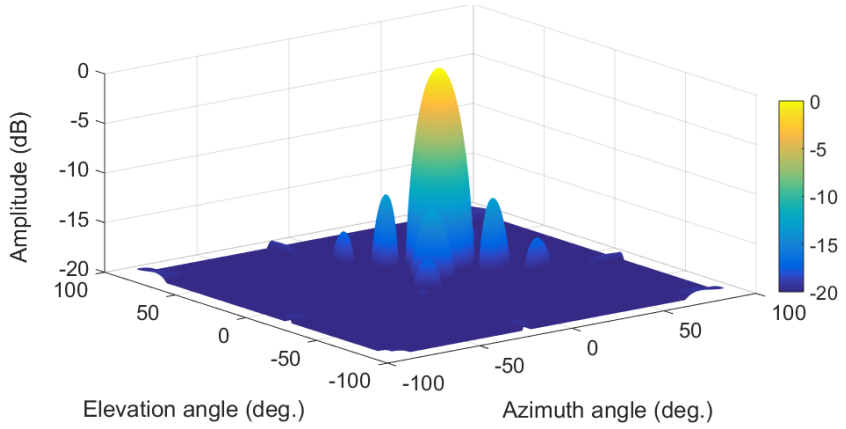

Fig. 3-17: 3D radiation pattern of the proposed 10×10-element UE-TPA array scanned at an angle θ = 20^0 with respect to antenna array boresight in both azimuth ($\Phi = 0^0$) and elevation ($\Phi = 90^0$) planes.

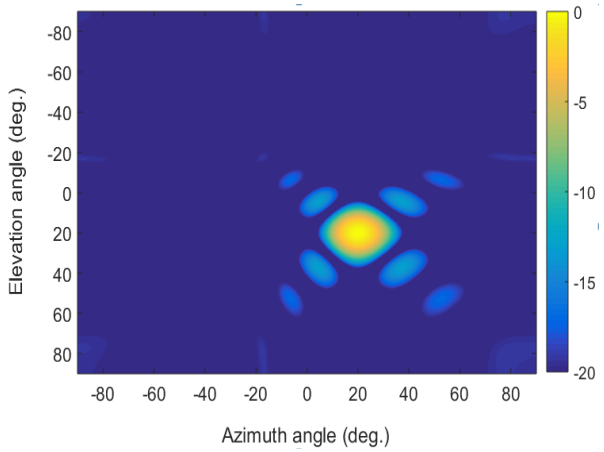

Fig. 3-18: Intensity plot of the proposed 10×10-element UE-TPA array scanned at an angle θ = 20^0 with respect to antenna array boresight in both both azimuth ($\Phi = 0^0$) and elevation ($\Phi = 90^0$) planes.

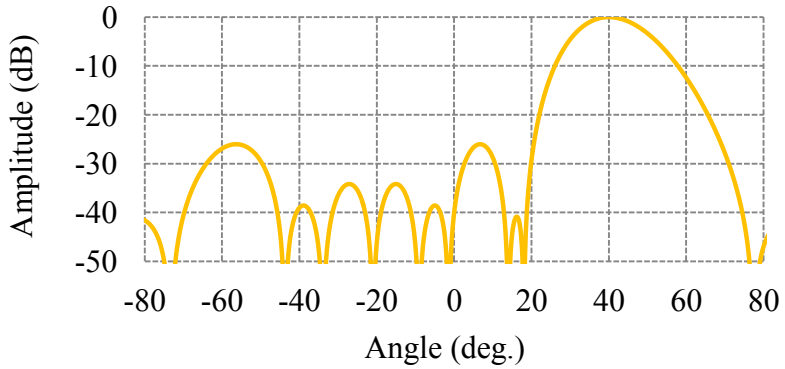

Fig. 3-19: Radiation pattern of the proposed 10×10-element UE-TPA array scanned at an angle θ = 40^0 with respect to antenna array boresight in azimuth ($\Phi = 0^0$) plane.

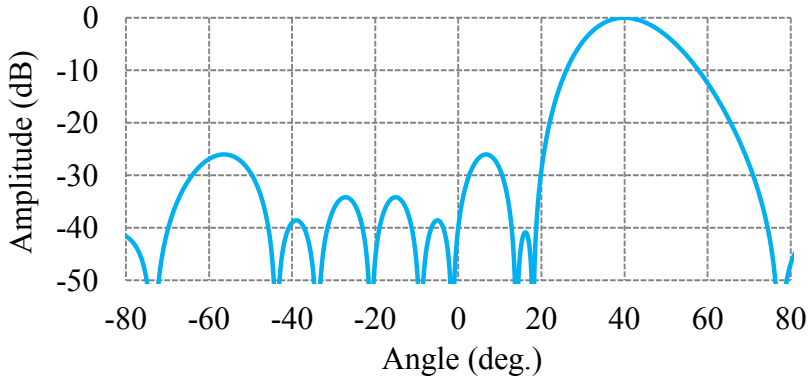

Fig. 3-20: Radiation pattern of the proposed 10×10-element UE-TPA array scanned at an angle $\theta = 40^0$ with respect to antenna array boresight in elevation ($\Phi = 90^0$) plane.

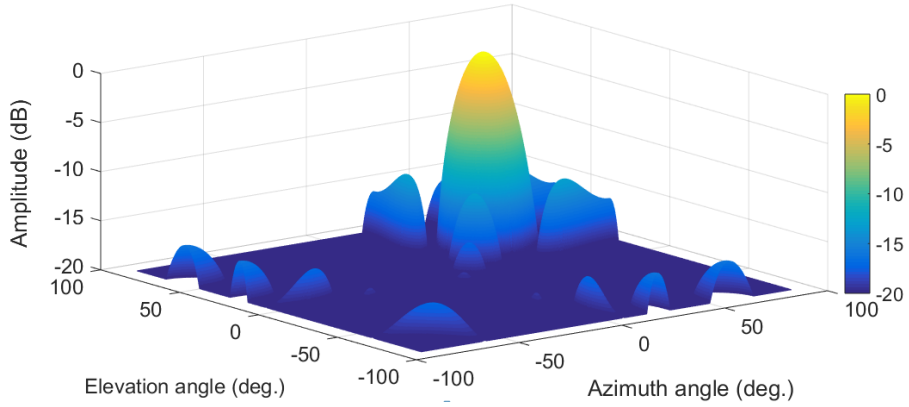

Fig. 3-21: 3D radiation pattern of the proposed 10×10-element UE-TPA array scanned at an angle $\theta = 40^0$ with respect to antenna array boresight in both azimuth ($\Phi = 0^0$) and elevation ($\Phi = 90^0$) planes.

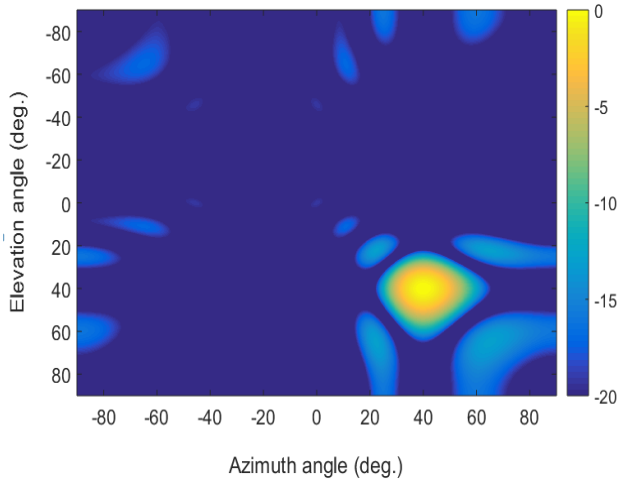

Fig. 3-22: Intensity plot of the proposed 10×10-element UE-TPA array scanned at an angle $\theta = 40^0$ with respect to antenna array boresight in both both azimuth ($\Phi = 0^0$) and elevation ($\Phi = 90^0$) planes.

Table 3-3: Comparison of numerically evaluated results of the proposed 10×10-element UE-TPA array at boresight with those of the proposed array at (20^0, 20^0) and (40^0, 40^0) and with those of the arrays reported in [Zhang *et al.* (2010)], [Deb *et al.* (2012)], and [Nihad (2014)].

Radiation Parameters	**BDEA [Zhang *et al.* (2010)]**	**PSO [Deb *et al.* (2012)]**	**TLBO [Nihad (2014)]**	**IBc-GA [Proposed] (boresight)**	**IBc-GA [Proposed] (20^0, 20^0) scan angle**	**IBc-GA [Proposed] (40^0, 40^0) scan angle**
PSLL (dB) in $\Phi = 0^0$ plane	-19.56	-23.04	-19.64	-26.73	-25.86	-24.96
PSLL (dB) in $\Phi = 90^0$ plane	-19.56	-23.04	-19.64	-26.73	-25.86	-24.96
HPBW (deg.) in $\Phi = 0^0$ plane	-	-	-	13.18	14.08	17.34
HPBW (deg.) in $\Phi = 90^0$ plane	-	-	-	13.18	14.08	17.34
Directivity (dB)	-	-	-	23.74	23.15	21.44
Thinning percentage	24	48	35	40	40	40

3.2.4.2.2 14×14-element UE-TPA Array

In this case, a 14×14-element UE-TPA array with inter-element spacing of 0.5λ is assumed for optimizing positions of 'ON' and 'OFF' elements related to lowest achievable PSLL over the pre-specified scan angles. In addition, number of 'OFF' elements is maximized to further reduce weight, volume and cost of the antenna system.

The initial parameters of IBc-GA are assumed to be same as in previous case and algorithm iterated 100 times to achieve the best desired value of fitness function expressed in Eq. (3.8). The amplest PSLL out of 50 trials evolved during number of generations is depicted in Fig. 3-23, where the best value of PSLL equal to -57.46 dB is

reached within 50 iterations. The most desirable arrangement of 'ON' and 'OFF' array elements achieved through the said IBc-GA settings is pictured in Fig. 3-24 and the element distribution on array aperture is depicted in Fig. 3-25. The radiation patterns of the proposed 14×14-element UE-TPA array obtained through IBc-GA at antenna boresight are shown in Figs. 3-26 – 3-29, where 2D patterns in $\Phi = 0^0$ and $\Phi = 90^0$ planes are depicted in Figs. 3-26 and 3-27 respectively, 3D radiation pattern in Fig. 3-28 and intensity plot in Fig. 3-29. Radiation patterns at 20^0 and 40^0 scan angles are depicted in Figs. 3-30 – 3-33 and Figs. 3-34-3-37 respectively. The radiation parameters interpreted from Figs. 3-30-3.37 are shown in Table 3-4. It can be noticed from Figs. Figs 3-30-3.37 and Table 3-4 that the PSLL averaged over 50 trials is -28.65 dB at boresight, -26.91 dB at 20^0 scan angle, and -25.54 dB at 40^0 scan angle in both azimuth and elevation planes. This signifies that bare amount of degradation occurs when antenna array is steered over desired scan volume. It can also be observed that there is no grating lobe formation in entire antenna visible region and ~ 57% of thinning

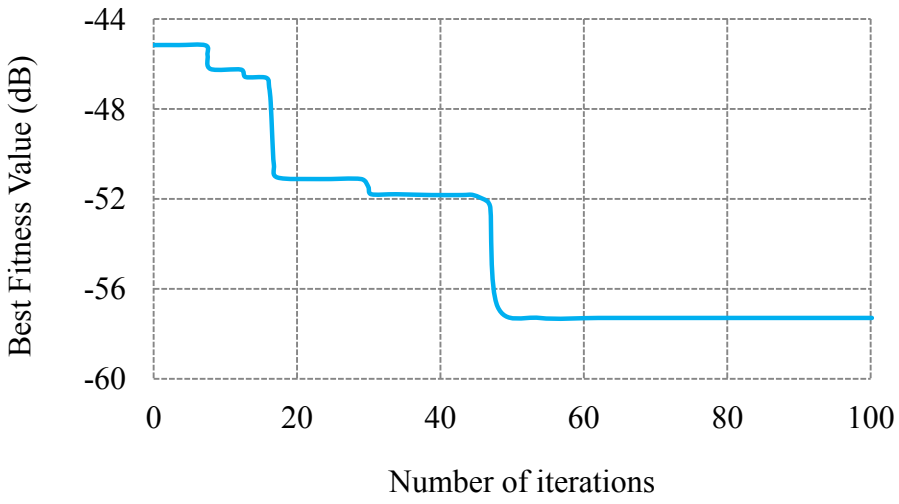

Fig. 3-23: Variation of best fitness value with number of iterations in the optimization of proposed 14×14-element UE-TPA array.

is accomplished through the suggested modification in binary coded GA which is much greater than 40 % obtained in the previous example of 10×10-element UE-TPA array.

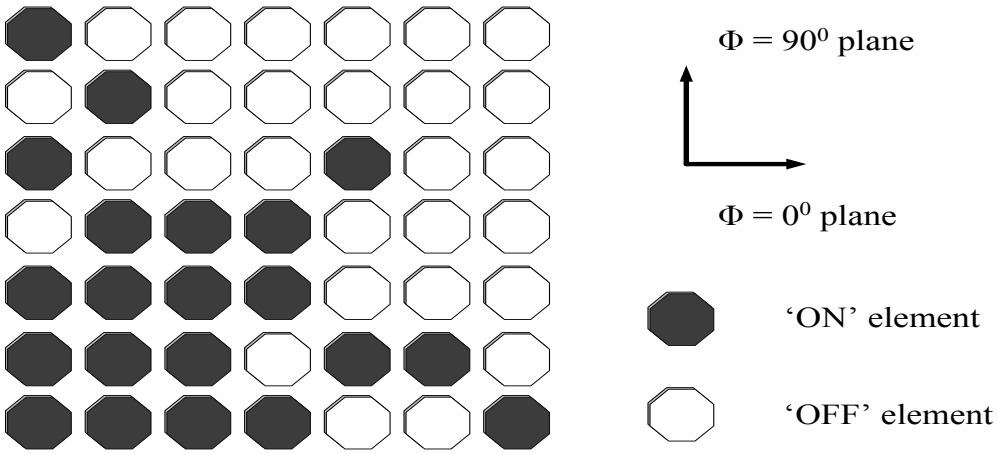

Fig. 3-24: Optimal positions of 'ON' and 'OFF' elements of one quadrant (X-positive and Y-positive plane) of the proposed 14×14-element UE-TPA array. The black blocks represent positions of 'ON' elements, while the white ones of 'OFF' elements.

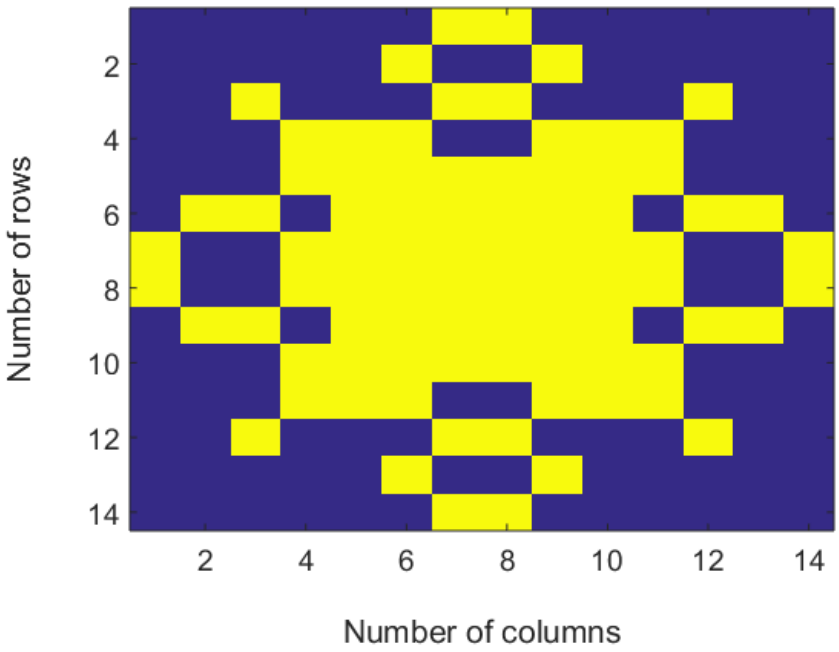

Fig. 3-25: Optimal arrangement of 'ON' (yellow) and 'OFF' (blue) elements on the aperture of the proposed 14×14-element UE-TPA array.

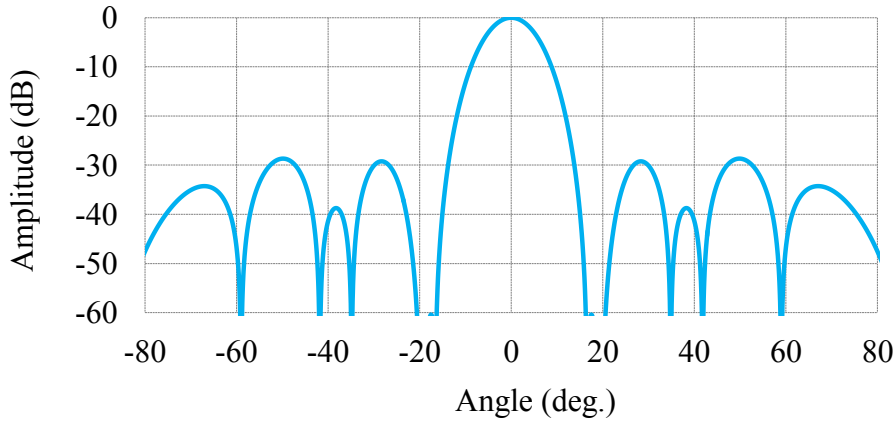

Fig. 3-26: Radiation pattern of the proposed 14×14-element UE-TPA array at antenna array boresight in azimuth ($\Phi = 0^0$) plane.

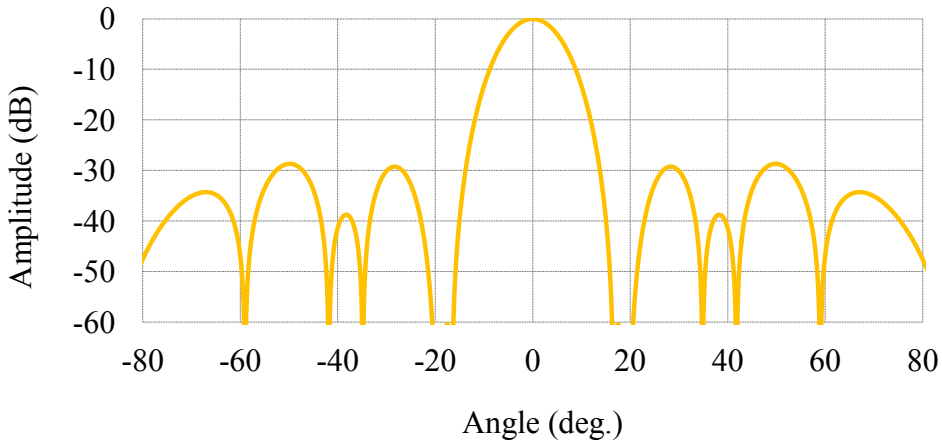

Fig. 3-27: Radiation pattern of the proposed 14×14-element UE-TPA array at antenna array boresight in elevation ($\Phi = 90^0$) plane.

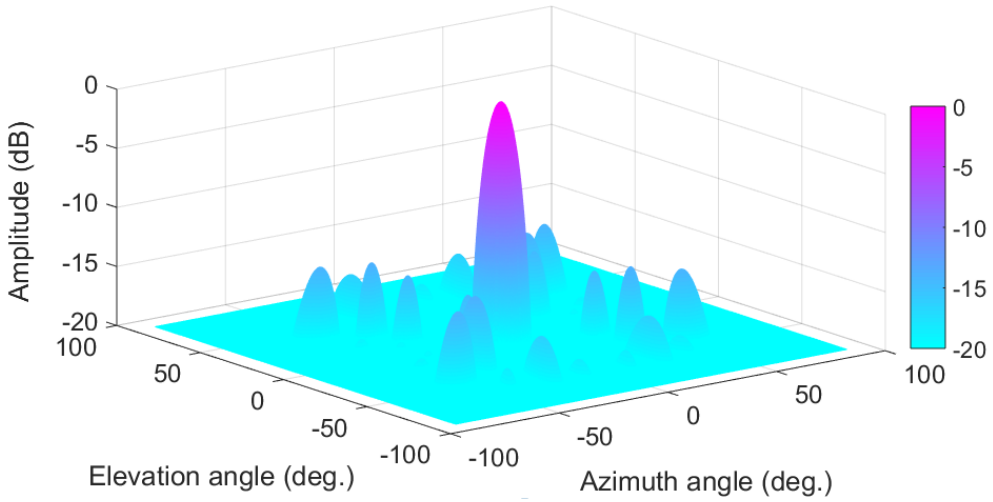

Fig. 3-28: 3D radiation pattern of the proposed 14×14-element UE-TPA array at antenna boresight.

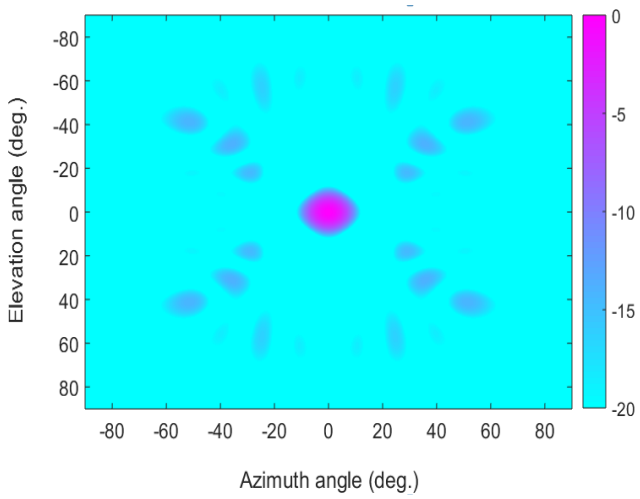

Fig. 3-29: Intensity plot of the proposed 14×14-element UE-TPA array at antenna boresight.

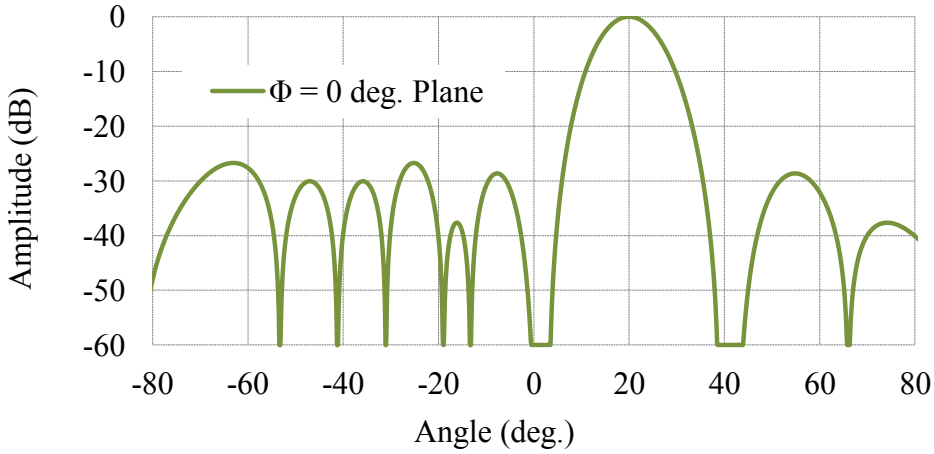

Fig. 3-30: Radiation pattern of the proposed 14×14-element UE-TPA array scanned at an angle $\theta = 20^0$ with respect to antenna array boresight in azimuth ($\Phi = 0^0$) plane.

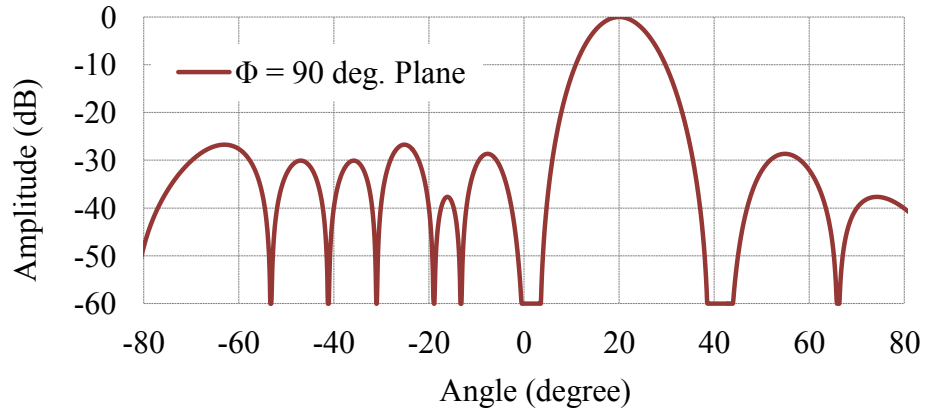

Fig. 3-31: Radiation pattern of the proposed 14×14-element UE-TPA array scanned at an angle $\theta = 20^0$ with respect to antenna array boresight in elevation ($\Phi = 90^0$) plane.

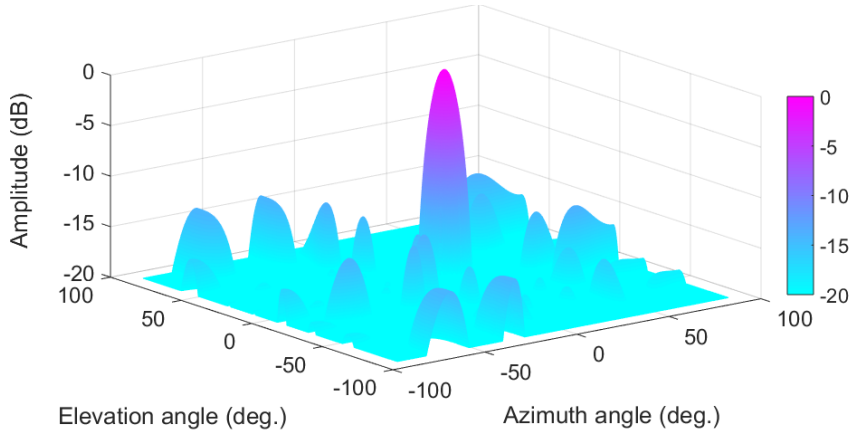

Fig. 3-32: 3D radiation pattern of the proposed 14×14-element UE-TPA array scanned at an angle $\theta = 20^0$ with respect to antenna array boresight in both azimuth ($\Phi = 0^0$) and elevation ($\Phi = 90^0$) planes.

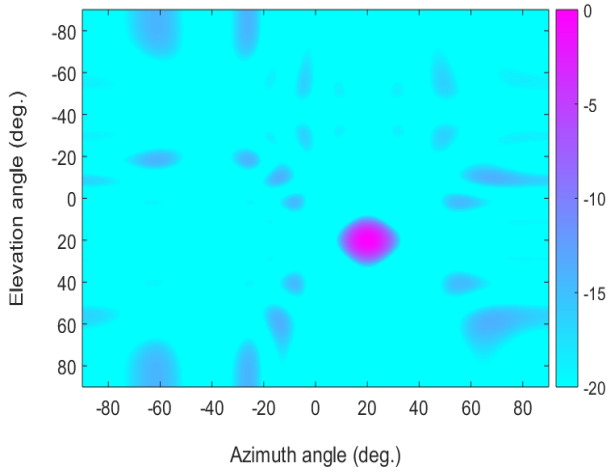

Fig. 3-33: Intensity plot of the proposed 14×14-element UE-TPA array scanned at an angle $\theta = 20^0$ with respect to antenna array boresight in both both azimuth ($\Phi = 0^0$) and elevation ($\Phi = 90^0$) planes.

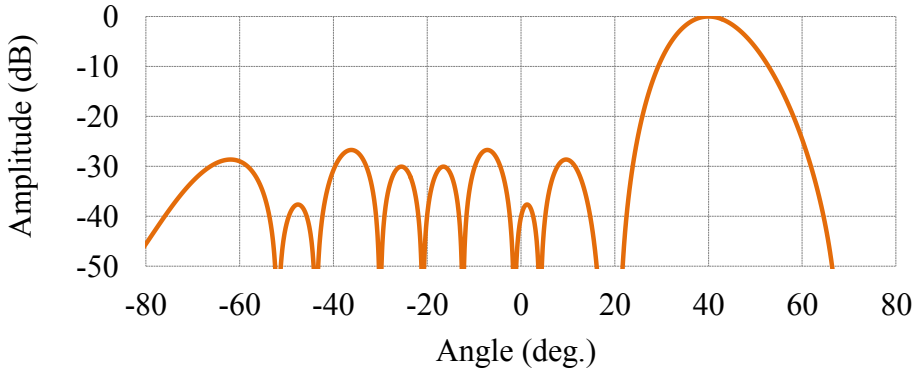

Fig. 3-34: Radiation pattern of the proposed 14×14-element UE-TPA array scanned at an angle $\theta = 40^0$ with respect to antenna array boresight in azimuth ($\Phi = 0^0$) plane.

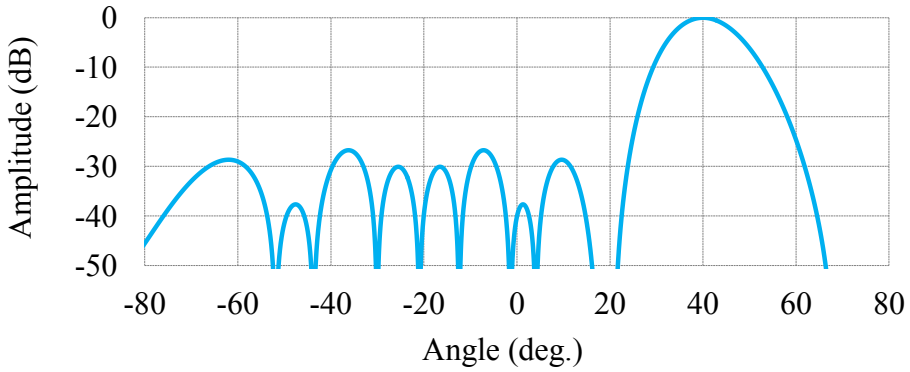

Fig. 3-35: Radiation pattern of the proposed 14×14-element UE-TPA array scanned at an angle $\theta = 40^0$ with respect to antenna array boresight in elevation ($\Phi = 90^0$) plane.

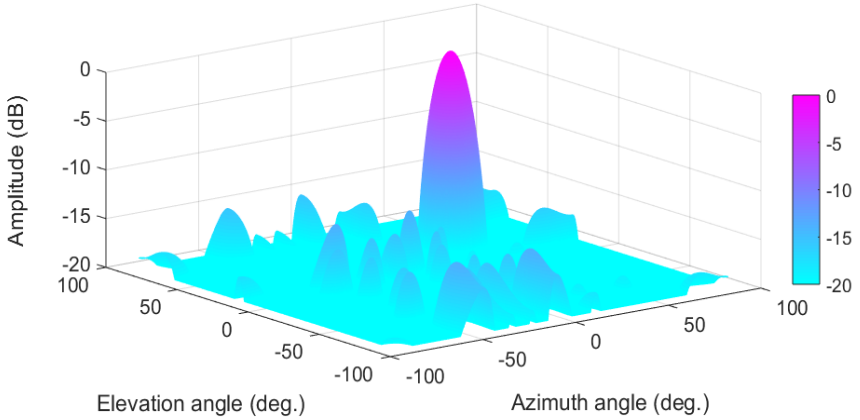

Fig. 3-36: 3D radiation pattern of the proposed 14×14-element UE-TPA array scanned at an angle $\theta = 40^0$ with respect to antenna array boresight in both azimuth ($\Phi = 0^0$) and elevation ($\Phi = 90^0$) planes.

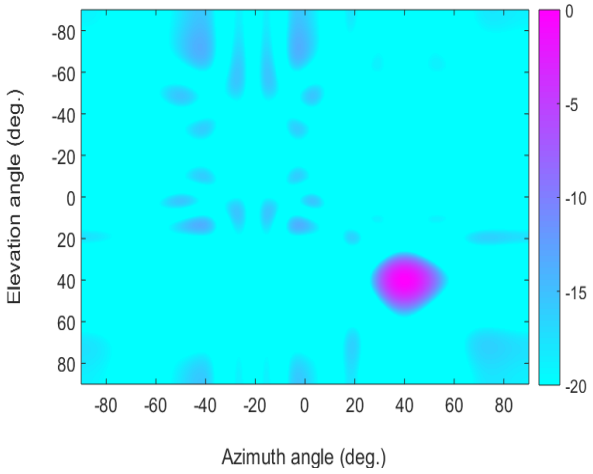

Fig. 3-37: Intensity plot of the proposed 14×14-element UE-TPA array scanned at an angle $\theta = 40^0$ with respect to antenna array boresight in both both azimuth ($\Phi = 0^0$) and elevation ($\Phi = 90^0$) planes.

Table 3-4: Comparison of numerically evaluated results for the proposed 14×14-element UE-TPA array at boresight with respect to (20^0, 20^0) and (40^0, 40^0) scan angles.

Parameters	**14×14-element (Boresight)**	**14×14-element [(20^0, 20^0) scan angle]**	**14×14-element [(40^0, 40^0) scan angle]**
Thinning percentage	~ 57	~ 57	~ 57
PSLL (dB) in $\Phi = 0^0$ plane	-28.65	-26.91	-25.54
PSLL (dB) in $\Phi = 90^0$ plane	-28.65	-26.91	-25.54
HPBW (deg.) in $\Phi = 0^0$ plane	9.83	10.42	12.78
HPBW (deg.) in $\Phi = 90^0$ plane	9.83	10.42	12.78
Directivity (dB)	26.33	25.75	24.12

3.2.4.3. Optimization of Peak, Average and RMS SLL in 10×20-element TPA Array Using PSO

In present study, thinning of 10×20-element planar rectangular array has been considered. In optimization of assumed case, PSO algorithm was commenced with a swarm of 1000 particles and iterated over 500 times in order to minimize fitness function mentioned in Eq. (3.9). The comparison of design parameters of the proposed TPA array with those of fully dense array and arrays reported in [Haupt (1994)], [Teruel and Iglesias (2006)], and [Zhang *et al.* (2010)] is given in Table 3-5. The values of fitness function i.e. peak side lobe levels in $\phi = 0^0$ and $\phi = 90^0$ planes as functions of number of iterations are demonstrated in Fig. 3-38. It can be observed from Fig. 3-38 that fitness function values attain their most estimable values (minimum possible peak SLLs of -26.58 dB and -28.32 dB in $\phi = 0^0$ and $\phi = 90^0$ planes respectively) within less

than 120 iterations. The optimum combinations of active ('1') and inactive ('0') elements achieved using aforementioned algorithm settings is described in Fig 3-47 and associated elements distribution on array aperture of the proposed TPA array is shown in Fig. 3-40. The yellow denotes that the element is 'active' while the green one represents that the element is 'inactive'. As mentioned in Table 3-5, results for the array having inter-element spacings equal to 0.5λ (15.7895 mm) in both $\phi = 0^0$ and $\phi = 90^0$ planes are obtained at 9.5 GHz in X-band. The computation of array radiation pattern was carried out using element-by-element superposition principle [Zhang *et al.* (2010)]. During optimization process, calculation was done at 1801 points in the angular range of -90 deg. to +90 deg. (at a step of 0.1 deg.) in both $\phi = 0^0$ and $\phi = 90^0$ planes.

Table 3-5: Comparison of design parameters of the proposed TPA array with those of fully dense array and arrays reported in [Haupt (1994)], [Teruel and Iglesias (2006)], and [Zhang *et al.* (2010)].

Design parameters	**Fully dense array**	**GA [Haupt (1994)]**	**ACO [Teruel and Iglesias (2006)]**	**BDE [Zhang *et al.* (2010)]**	**PSO [Proposed]**
Frequency of analysis	X-band (9.5GHz)	X-band (9.5GHz)	X-band (9.5GHz)	X-band (9.5GHz)	X-band (9.5GHz)
Inter-element spacings ($d_x = d_y$)	0.5λ	0.5λ	0.5λ	0.5λ	0.5λ
Rows × columns	10×20	10×20	10×20	10×20	10×20
Size (X-axis×Y-axis)	10λ×5λ	10λ×5λ	10λ×5λ	10λ×5λ	10λ×5λ
Thinning percentage	-	46	32	46	42

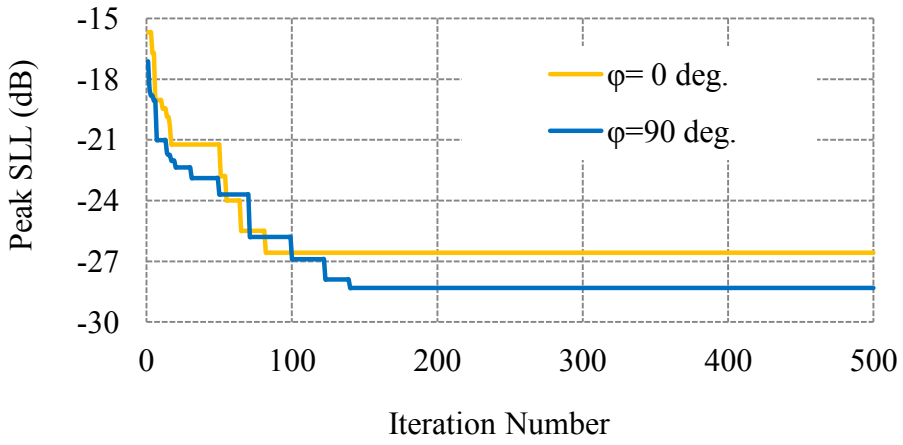

Fig. 3-38: Variations of PSLL values as functions of number of iterations in the optimization of proposed TPA array.

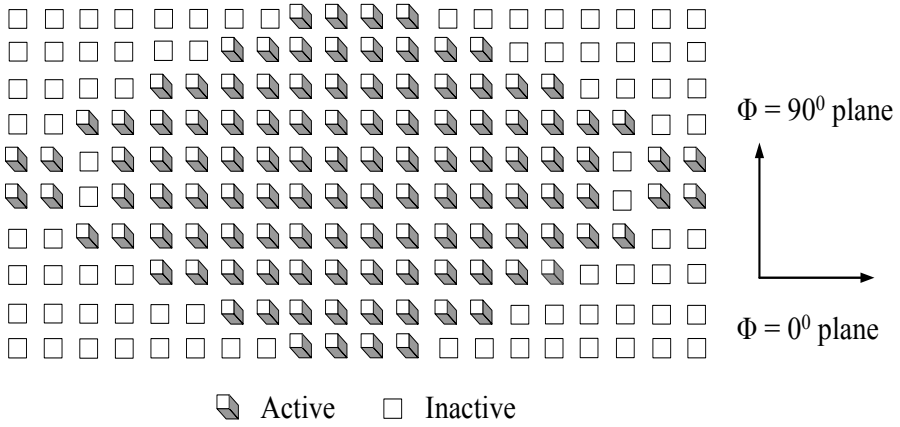

Fig. 3-39: Optimum geometrical congfiguration of the 10×20-elements TPA array obtained by proposed technique.

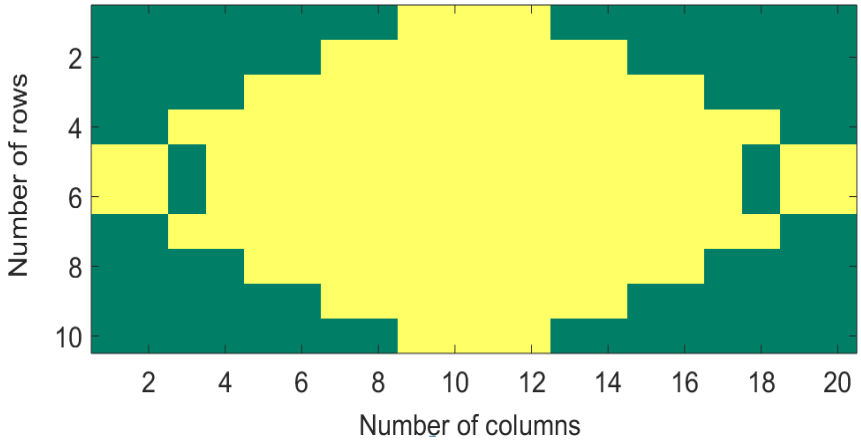

Fig. 3-40: Optimal arrangement of 'ON' (yellow) and 'OFF' (green) elements on the aperture of the proposed 10×20-element TPA array.

However, the results were obtained at 18001 points (at a step of 0.01 deg.) in order to estimate array parameters more precisely. The radiation patterns of the proposed 10×20-element TPA array along with those of the arrays reported in [Haupt (1994)], [Teruel and Iglesias (2006)], and [Zhang *et al.* (2010)] in $\phi = 0^0$ and in $\phi = 90^0$ planes are shown in Figs. 3-41, 3-42, and Figs. 3-43, 3-44 respectively. The 3D radiation pattern of the proposed array and intensity plot are shown in Figs. 3-45 and 3-46 respectively. It can be noticed from Figs. 3-45 and 3-46 that PSLL in only some of inter-cordinal planes is about -19 dB and elsewhere it is better than - 26.58 dB, which results in better average SLL. The thinning percentage of the array obtained by present technique is 42% (as showed in Table 3-5), which is more than 32% reported in [Teruel and Iglesias (2006)] and slightly less than 46% reported in [Haupt (1994)] and [Zhang *et al.* (2010)]. The radiation parameters extracted from Figs. 3-41 - 3-46 for the proposed array, therefore the arrays reported in [Haupt (1994)], [Teruel and Iglesias (2006)], and [Zhang *et al.* (2010)] and computed for fully dense array are indicated in Table 3-6. It can be seen from Figs. 3-41 - 3-46 and Table 3-6 that peak SLL in $\phi = 0^0$ plane obtained by present technique is lower (in the range 0.82 - 6.51 dB) as compared to those obtained in [Haupt (1994)], and [Teruel and Iglesias (2006)]. Further PSLL in $\phi = 90^0$ plane obtained for the proposed array is lower (in the range of 2.42 - 8.56 dB) in comparison to those obtained in [Haupt (1994)], [Teruel and Iglesias (2006)], and [Zhang *et al.* (2010)]. The RMS SLL of the proposed array is lower by 5.26 dB with that obtained in [Haupt (1994)] in $\phi = 0^0$ plane. It is lower (in the range 3.4 - 11.34 dB) as compared to those obtained in [Haupt (1994)], [Teruel and Iglesias (2006)], and [Zhang *et al.* (2010)]. Average SLL is better (in the range 0.16 - 1.86 dB) as compared with those obtained in [Haupt (1994)], [Teruel and Iglesias (2006)], and [Zhang *et al.*

(2010)]. The HPBW and directivity obtained for the proposed array are almost same as those of equivalently Taylor-tapered fully dense array of equal size.

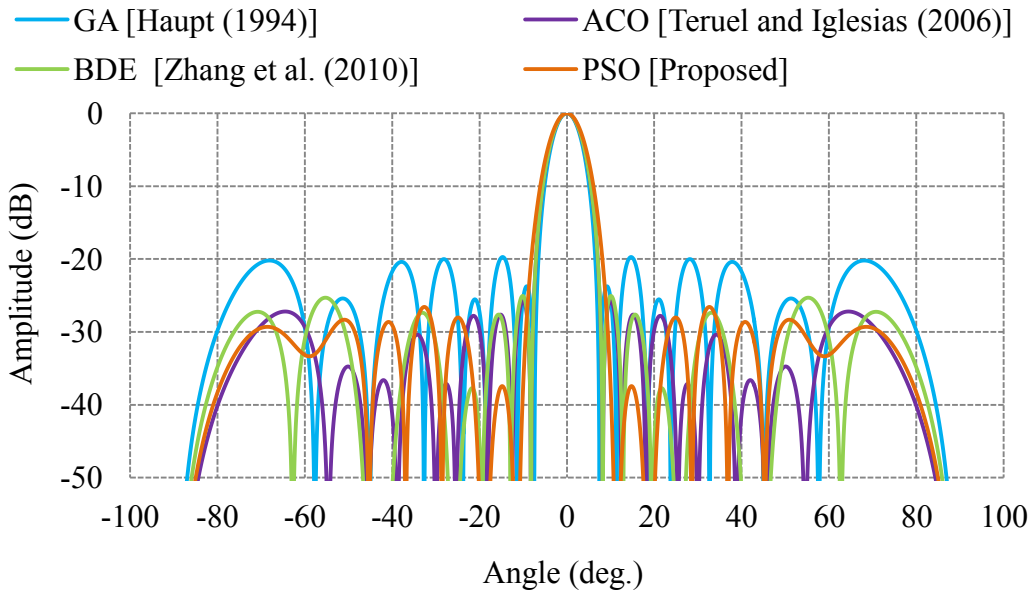

Fig. 3-41: Comparison of radiation pattern of the proposed 10×20-element TPA array in $\phi = 0^0$ plane with those of the arrays reported in [Haupt (1994)], [Teruel and Iglesias (2006)], and [Zhang *et al.* (2010)].

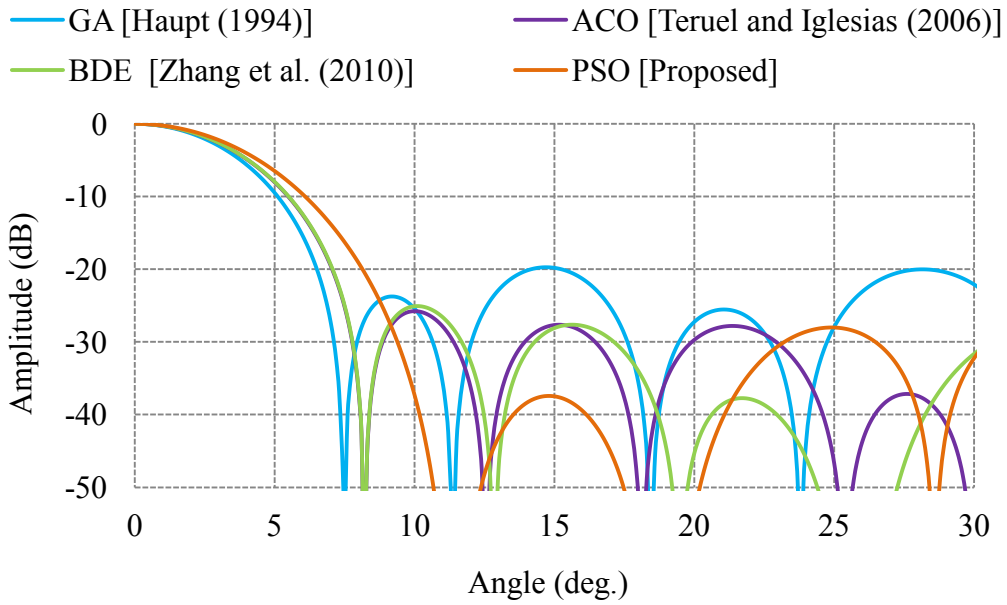

Fig. 3-42: Comparison of radiation pattern of the proposed 10×20-element TPA array in $\phi = 0^0$ plane with those of the arrays reported in [Haupt (1994)], [Teruel and Iglesias (2006)], and [Zhang *et al.* (2010)] in the angular region ($\theta = 0^0 - 30^0$).

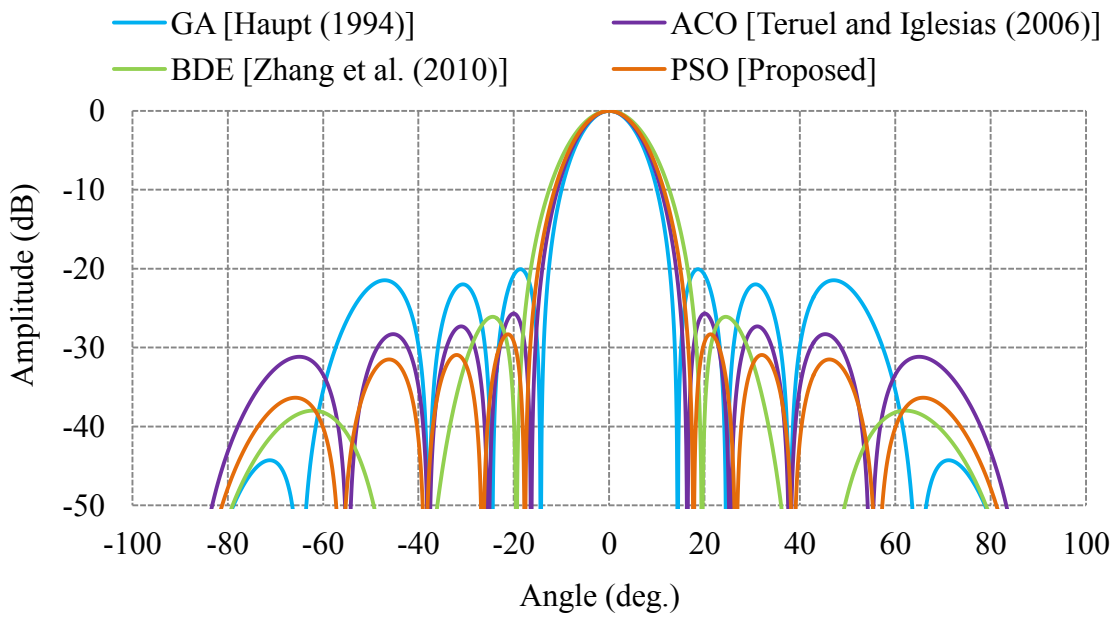

Fig. 3-43: Comparison of radiation pattern of the proposed 10×20-element TPA array in $\phi = 90^0$ plane with those of the arrays reported in [Haupt (1994)], [Teruel and Iglesias (2006)], and [Zhang *et al.* (2010)].

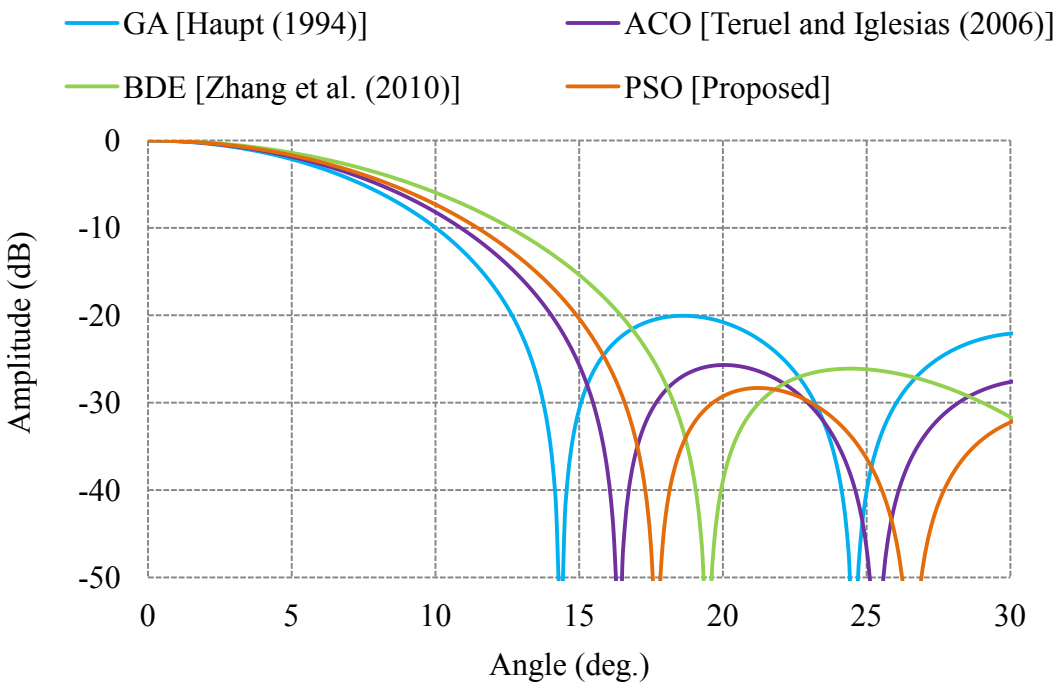

Fig. 3-44: Comparison of radiation pattern of the proposed 10×20-element TPA array in $\phi = 90^0$ plane with those of the arrays reported in [Haupt (1994)], [Teruel and Iglesias (2006)], and [Zhang *et al.* (2010)] in the angular region ($\theta = 0^0 - 30^0$).

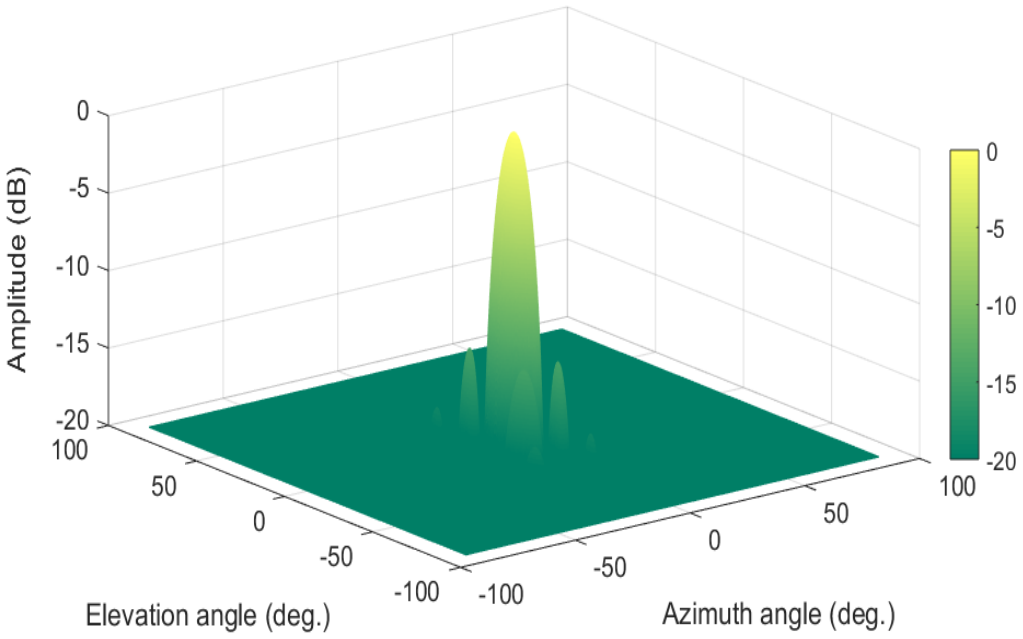

Fig. 3-45: 3D radiation pattern of the proposed 10×20-element TPA array.

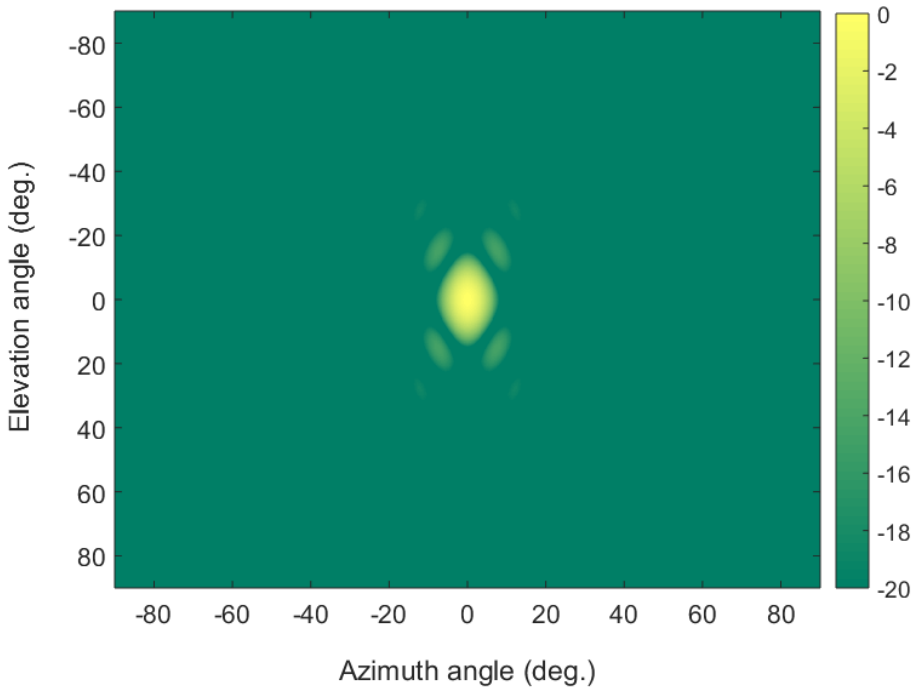

Fig. 3-46: Intensity plot of the proposed 10×20-element TPA array.

Table 3-6: Comparison of radiation pattern characteristics of the proposed TPA array with those of arrays reported in [Haupt (1994)], [Teruel and Iglesias (2006)], and [Zhang *et al.* (2010)] and Taylor-tapered fully dense array of equal size.

Design parameters	Fully dense array (10×20)	Thinned planar antenna arrays			
		GA [Haupt (1994)]	ACO [Teruel and Iglesias (2006)]	BDE [Zhang *et al.* (2010)]	PSO [Proposed]
PSLL (dB) in $\phi = 0^0$ plane	-26	-20.07	-25.76	-26.90	-26.58
PSLL (dB) in $\phi = 90^0$ plane	-28	-19.76	-25.67	-25.90	-28.32
RMS SLL (dB) in $\phi = 0^0$ plane	-32	-26.74	-32.5	-34.89	-32
RMS SLL (dB) in $\phi = 90^0$ plane	-34.9	-24.56	-32.5	-31.14	-35.9
Average SLL (dB)	-32.3	-26.37	-28.07	-27.8	-28.23
HPBW (deg.) in $\phi = 0^0$ plane	6.2	5.8	6.3	6.2	6.8
HPBW (deg.) in $\phi = 90^0$ plane	12.6	11.6	12.8	14.4	13.2
Directivity (dB)	24	22.42	23.8	23.10	23.23

3.2.4.4. Optimization of PSLL by Jointly Determining Thinned Configuration and Amplitude Weights in 10×20- and 8×8-elements TPA Array Using MBC-GA

3.2.4.4.1 10×20-element TPA Array

In this case, the effectualness of the proposed MBC-GA is manifested by considering 10×20-element TPA array synthesis as optimization design problems. Algorithm began with a population of 10000 chromosomes and iterated over 500 times to minimize fitness functions as formulated in Eqs. (3-11) and (3-13) corresponding to the synthesis

of uniformly excited thinned planar antenna (UE-TPA) and amplitude weight thinned planar antenna (AW-TPA) arrays respectively. The initial goal is to determine optimum thinned configuration corresponding to lowest possible PSLL. Furthermore, it is also aimed to optimize both discrete amplitude weight and thinned arrangements simultaneously for the synthesis of AW-TPA array in order to get further reduction in PSLL without altering HPBW.

Both UE-TPA and AW-TPA arrays are examined assuming inter-element spacing equal to 15.79 mm (0.5λ at 9.5 GHz) in both $\phi = 0^0$ and $\phi = 90^0$ planes.

It is aimed to determine optimum density of antenna elements which results in density taper similar to corresponding Taylor taper. This results in PSLL <-30 dB without degrading HPBW. The Taylor taper is calculated as [Balanis (2005)]

$$A = \frac{\cosh^{-1}(R)}{\pi} \quad , \quad \sigma = \frac{\bar{n}}{\sqrt{A^2 + \left(\bar{n} - \frac{1}{2}\right)^2}} \tag{3.17}$$

$$Z_n = \pm\sigma\sqrt{A^2 + \left(n - \frac{1}{2}\right)^2}\Bigg| \text{ for } 1 \leq \bar{n} \leq n \tag{3.18}$$

$$Z_n = Z_n = \pm n \mid \text{ for } \bar{n} > n \tag{3.19}$$

$$F(n, A, \bar{n}) = \frac{[(\bar{n}-1)!]^2}{\left((\bar{n}-1+n)!\left((\bar{n}-1+n)!\right)\right)} \prod_{m=1}^{n-1}\left[1 - \frac{n^2}{z_m^2}\right] \tag{3.20}$$

$$I(Z') = \frac{\lambda}{l}\left[1 + 2\sum_{n=1}^{n-1} F(n, A, \bar{n})\cos\left(2\pi n\frac{Z'}{l}\right)\right] \tag{3.21}$$

where A is constant related to maximum desired side lobe level R (voltage ratio), σ is the scaling factor, Z_n is the locations of nulls and $F(n, A, \bar{n})$ is the Taylor space factor. For a -30 dB side lobe, voltage ratio of maximum to side lobe level (R) is equal to 31.62.

The variations in the fitness function values as functions of number of iterations for the synthesis of UE-TPA and AW-TPA arrays are pictured in Fig. 3-47 which demonstrates that fitness values accomplish their most desirable ones (minimum possible peak SLLs) in less than 170 and 190 generations for the synthesis of UE-TPA and AW-TPA arrays respectively. The optimum sequences of 'ON' and 'OFF' elements for UE-TPA array and corresponding antenna element distribution on array aperture are shown in Figs. 3-48 and 3-49 respectively. The optimum combinations of 'ON','OFF' and 'amp weighted' elements in case of AW-TPA array attained through proposed MBC-GA and antenna element population on the array aperture are presented in Figs. 3-50 and 3-51 respectively. The comparison of synthesized normalized taper with that of standard Taylor taper are depicted in Figs. 3-52 and 3-53 in $\phi = 0^0$ and in $\phi = 90^0$ planes respectively. The radiation patterns obtained through the synthesis of both arrays in $\phi = 0^0$ and in $\phi = 90^0$ planes are shown in Figs. 3-54 – 3-59. The radiation parameters extracted from Figs. 3-54 – 3-59 for the proposed UE-TPA and AW-TPA arrays and those of arrays reported in [Teruel and Iglesias (2006), Zhang *et al.* (2010), Wang *et al.* (2012), and Liu and Wu (2014)] are indicated in Table 3-7. It can be seen from Figs. 3-54 – 3-59 and Table 3-7 that in case of UE-TPA array synthesis, PSLL in $\phi = 0^0$ plane obtained by proposed MBC-GA is -27.49 dB, which is 1.73 dB lower than that obtained using ACO [Teruel and Iglesias (2006)], 1.4 dB lower than that attained using BDE [Zhang *et al.* (2010)], 1.1 dB lower than that obtained using CBPSO [Wang *et al.* (2012)], and 0.91 dB lower than that attained using IBIWO [Liu and Wu (2014)]. PSLL in $\Phi = 90^0$ plane achieved through our technique is -27.82 is the best with respect to those reported in Teruel and Iglesias (2006), Zhang *et al.* (2010), and Wang *et al.* (2012).

Additionally, The HPBWs in both the planes obtained through UE-TPA array synthesis are better than those reported in [Teruel and Iglesias (2006), Zhang *et al.* (2010), Wang *et al.* (2012), and Liu and Wu (2014)]. However, HPBWs in both the planes obtained through AW-TPA synthesis are almost equal to those obtained through UE-TPA array synthesis while further PSLL reduction of 5.04 dB in $\phi = 0^0$ plane and 7.16 dB in $\phi = 90^0$ plane occurs when using AW-TPA synthesis.

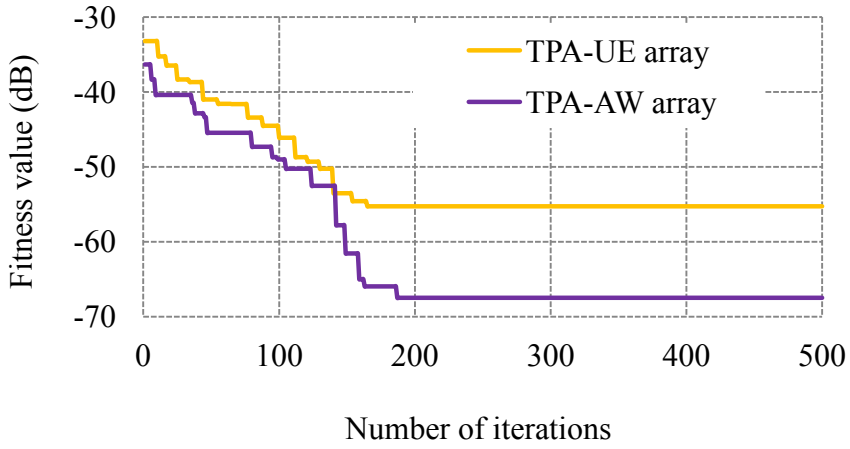

Fig. 3-47: Variations of PSLL value as a function of number of iterations during the optimization of proposed 10×20-element TPA array.

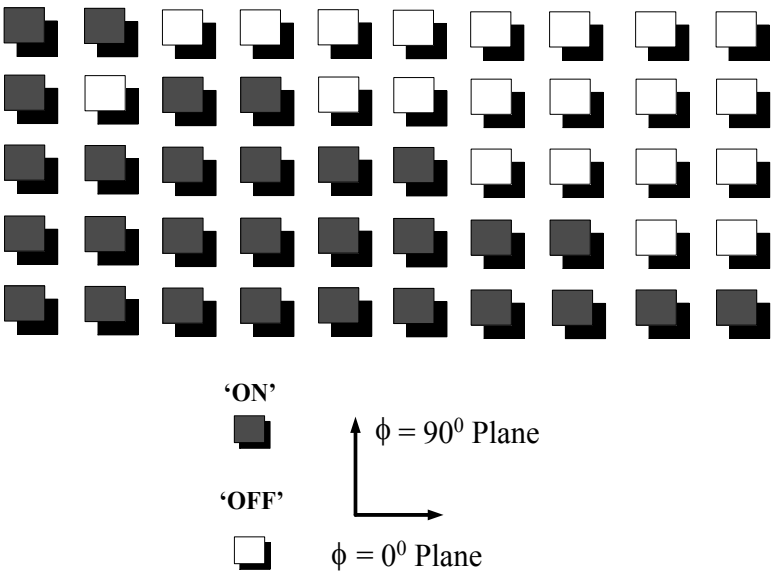

Fig. 3-48: Optimum combinations of 'ON' and 'OFF' elements for one quadrant (X-positive Y-positive plane) of the proposed 10×20-element UE-TPA array.

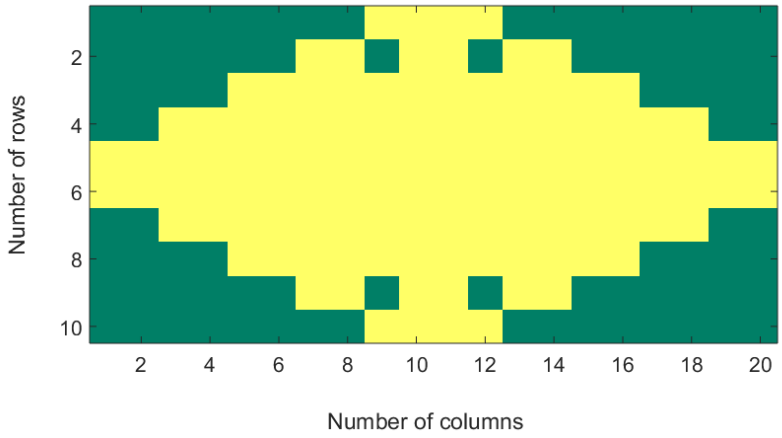

Fig. 3-49: Optimal arrangement of 'ON' (yellow) and 'OFF' (green) elements on the aperture of the proposed 10×20-element UE-TPA array.

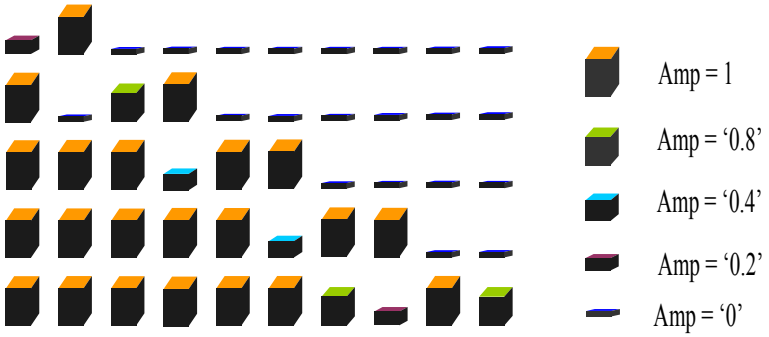

Fig. 3-50: Optimum combinations of 'ON' (Amp = '1'), OFF' (Amp = '0') and amplitude weighted elements one quadrant (X-positive Y-positive plane) of proposed 10×20-element AW-TPA Array.

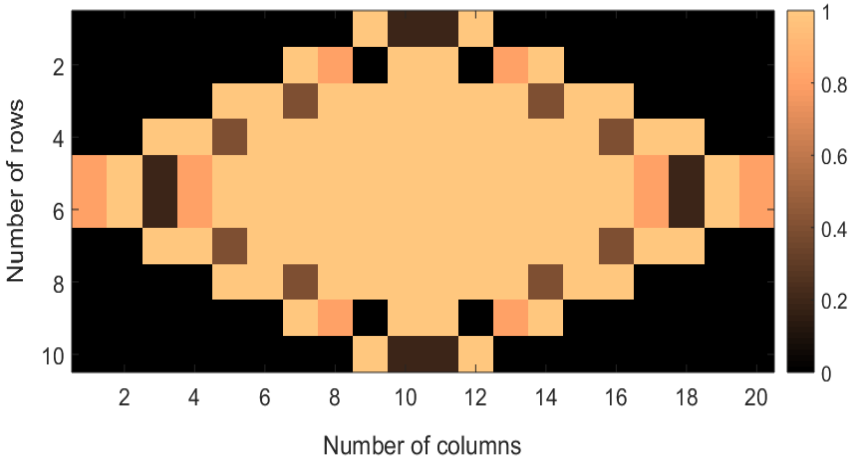

Fig. 3-51: Optimum arrangement of 'ON' (Amp = '1'), OFF' (Amp = '0') and amplitude weighted ('0' < Amp <'1') antenna elements on the aperture of the proposed 10×20-element AW-TPA Array.

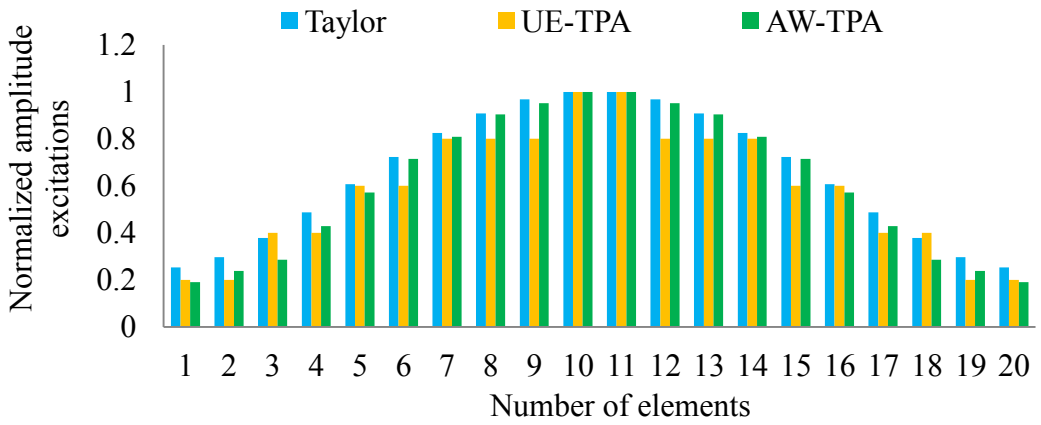

Fig. 3-52: Normalized amplitde distributions across the array elements of the fully filled 30 dB Taylor tapered and the proposed 10×20-element arrays in $\phi = 0^0$ plane.

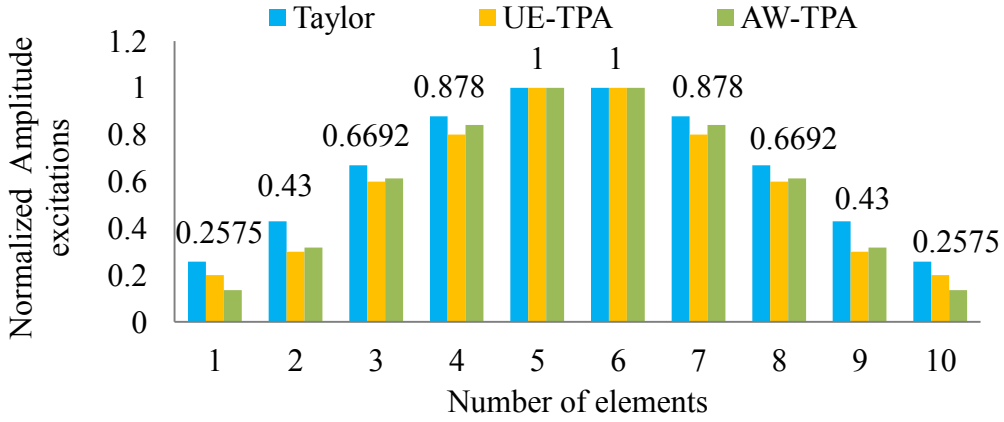

Fig. 3-53: Normalized amplitde distributions across the array elements of the fully filled 30 dB Taylor tapered and the proposed 10×20-element arrays in $\phi = 90^0$ plane.

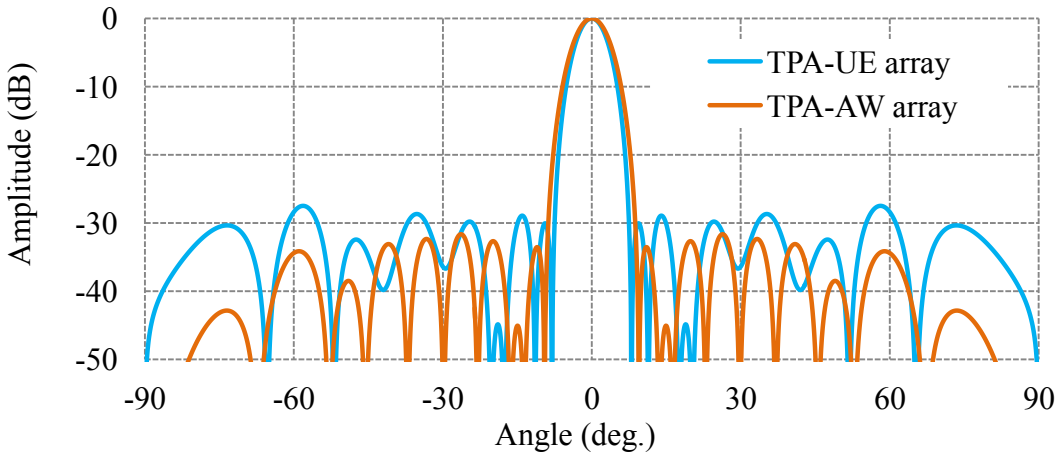

Fig. 3-54: Comparison of radiation patterns of the proposed 10×20-element UE-TPA and AW-TPA arrays in $\phi = 0^0$ plane.

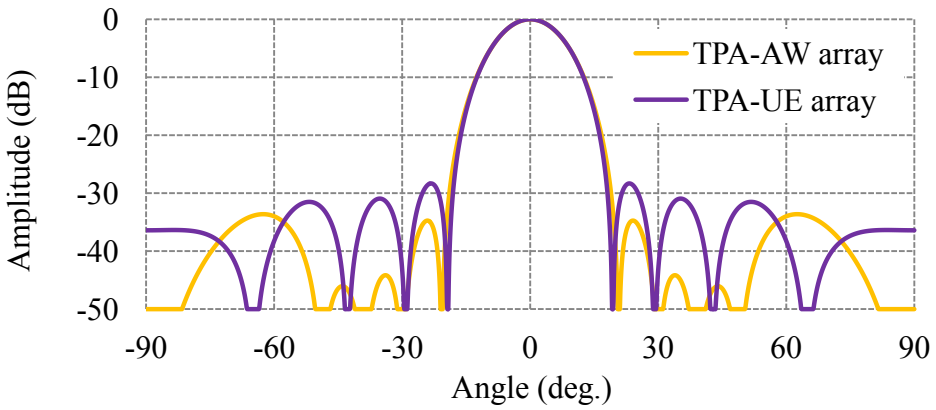

Fig. 3-55: Comparison of radiation patterns of the proposed 10×20-element UE-TPA and AW-TPA arrays in $\phi = 90^0$ plane.

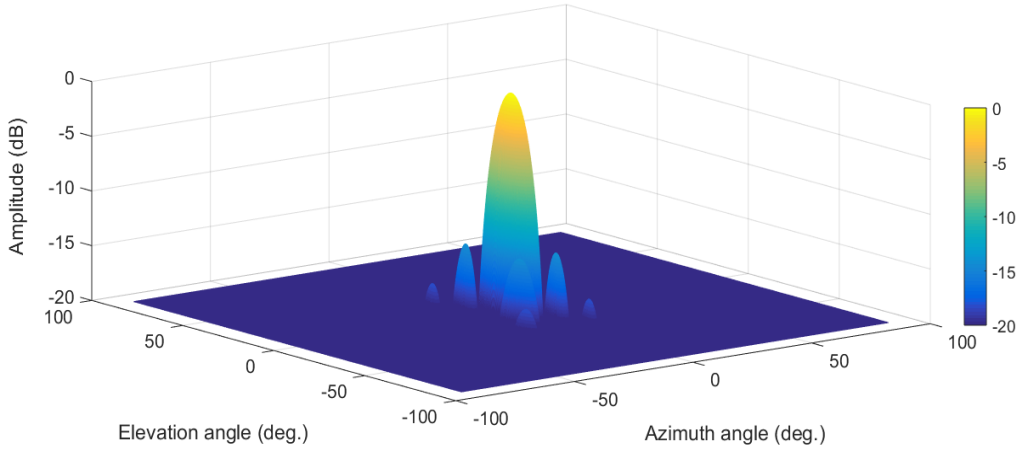

Fig. 3-56: 3D radiation pattern of the proposed 10×20-element UE-TPA array.

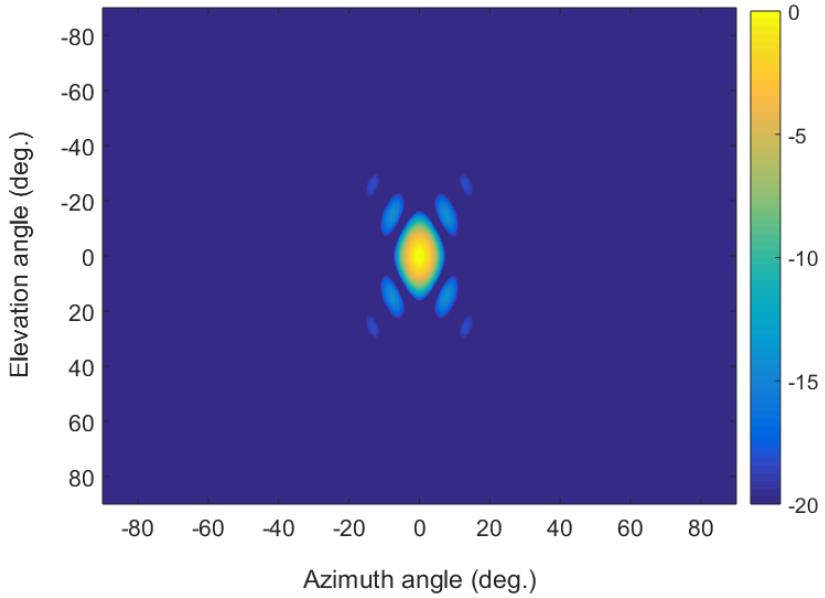

Fig. 3-57: Intensity plot of the proposed 10×20-element TPA array.

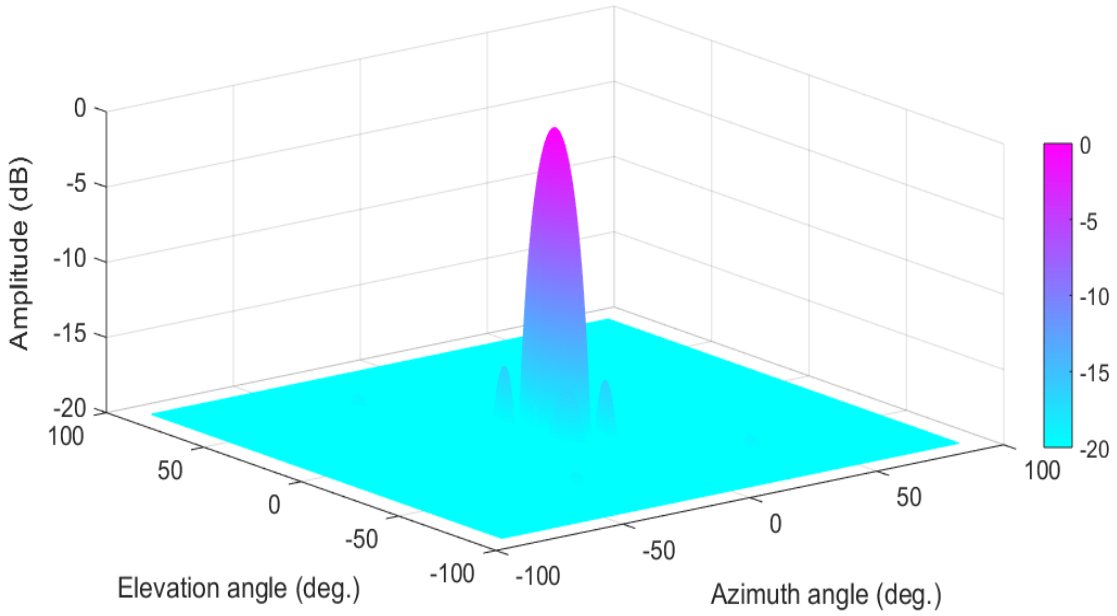

Fig. 3-58: 3D radiation pattern of the proposed 10×20-element AW-TPA array.

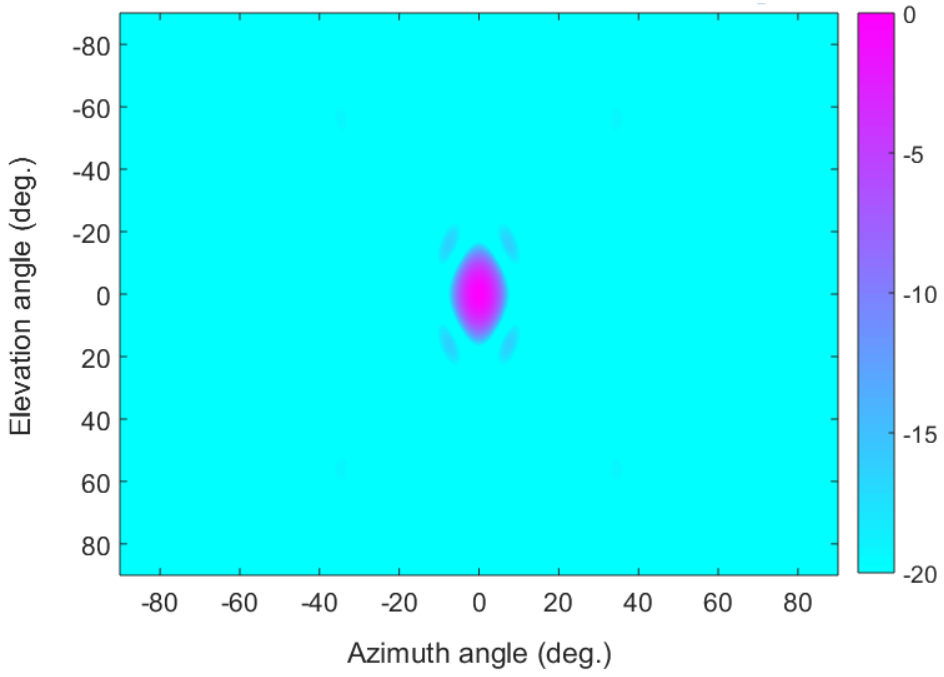

Fig. 3-59: Intensity plot of the proposed 10×20-element AW-TPA array.

Table 3-7: Comparison of radiation parameters of the proposed 10×20- elements TPA array with those of the arrays reported in [Teruel and Iglesias (2006), Zhang *et al.* (2010), Wang *et al.* (2012), and Liu and Wu (2014)].

Parameters	ACO [Teruel and Iglesias (2006)]	BDE [Zhang et al. (2010)]	CBPSO [Wang *et al.* (2012)]	IBIWO [Liu and Wu (2014)]	MBC-GA [UE-TPA]	MBC-GA [AW-TPA]
Fill factor (%)	68	54	54	52	58	58
Peak SLL (dB) in $\phi = 0^0$ plane	-25.76	-26.09	-26.39	-26.58	-27.49	-32.53
Peak SLL (dB) in $\phi = 90^0$ plane	-25.67	-25.09	-26.33	-28.32	-27.82	-34.98
Average SLL (dB)	-28.07	-27.8	-28.05	-27.3	-30.23	-34.25
HPBW (deg.) in $\phi = 0^0$ plane	6.3	6.2	6.1	6.4	5.75	5.98
HPBW (deg.) in $\phi = 90^0$ plane	12.8	14.4	13.9	13.8	12.6	12.68

3.2.4.4.2 8×8-element TPA Array

All the parameters of MBC-GA are assumed same as in the previous case. Both UE-TPA and AW-TPA arrays are examined taking inter-element spacing equal to 15.79 mm (0.5λ at 9.5 GHz) in both $\phi = 0^0$ and $\phi = 90^0$ planes

The variations of fitness values as a function of number of iterations for the synthesis of both the UE-TPA and AW-TPA arrays are shown in Fig. 3-60. It can be noticed from Fig. 3-60 that the best fitness values of -51.54 dB for the synthesis of UE-TPA array and -59 dB for the synthesis of AW-TPA array are accomplished within 150 and 180 generations respectively. The optimum sequences of 'ON', and 'OFF' elements and their distribution on the aperture of UE-TPA array are demonstrated in Figs. 3-61

and 3-62 respectively. The optimum sequences of 'ON', 'OFF' as well as 'amp weighted' elements and corresponding antenna element distribution on the aperture of AW-TPA array achieved using aforesaid settings are reported in Figs. 3-63 and 3-64 respectively. The comparison of synthesized taper with conventional Taylor taper is demonstrated in Fig. 3-65. Analysis is performed by assuming inter-element spacing of 25 mm (0.79λ at 9.5 GHz) in both $\phi = 0^0$ and $\phi = 90^0$ planes. Since the resulting radiation patterns are symmetric in both $\phi = 0^0$ and $\phi = 90^0$ planes, only one plane ($\phi = 0^0$ plane) patterns of the proposed UE-TPA and AW-TPA arrays are shown in Fig. 3-66. The 3D radiation patterns and intensity plots of the proposed UE-TPA array are depicted in Figs. 3-67 and 3-68 respectively whereas those of the proposed AW-TPA array are shown in Figs 3-69 and 3-70 respectively. The radiation parameters extracted from Figs. 3-66 - 3-70 are given in Table 3-8. It can be pointed out from Figs. 3-66 - 3-70 and Table 3-8 that PSLLs in $\phi = 0^0$ plane obtained through the present technique are -25.76 dB and -29.5 dB for the synthesis of UE-TPA and AW-TPA arrays respectively. In addition, HPBW obtained through the synthesis of AW-TPA array is almost equal to that obtained using UE-TPA synthesis while further reduction of -3.74 dB in PSLL occurs through AW-TPA array synthesis.

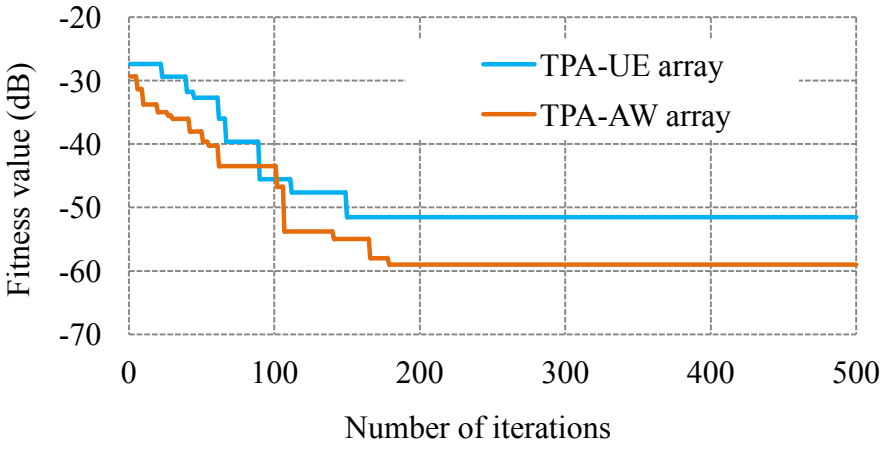

Fig. 3-60: Variations of best fitness i.e. PSLL value as a function of number of iterations in the optimization of the proposed 8x8-element TPA arrays.

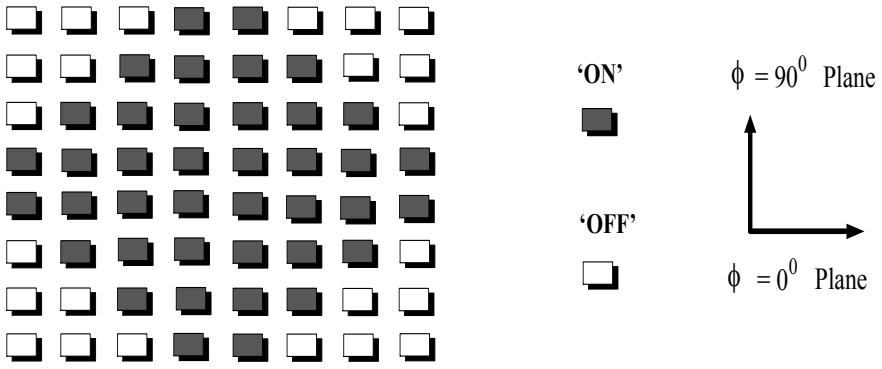

Fig. 3-61: Optimum combinations of 'ON' and 'OFF' elements for the proposed 8×8-element UE-TPA Array.

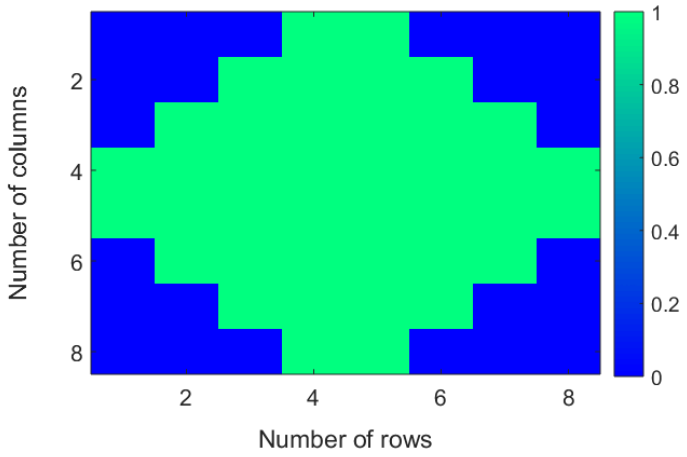

Fig. 3-62: Optimal arrangement of 'ON' (green) and 'OFF' (blue) elements on the aperture of the proposed 8×8-element UE-TPA array.

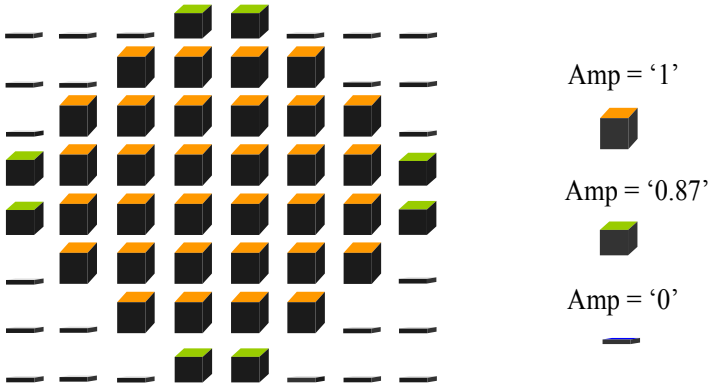

Fig. 3-63: Optimum combinations of 'ON' and 'OFF' elements for the proposed 8×8-element AW-TPA array.

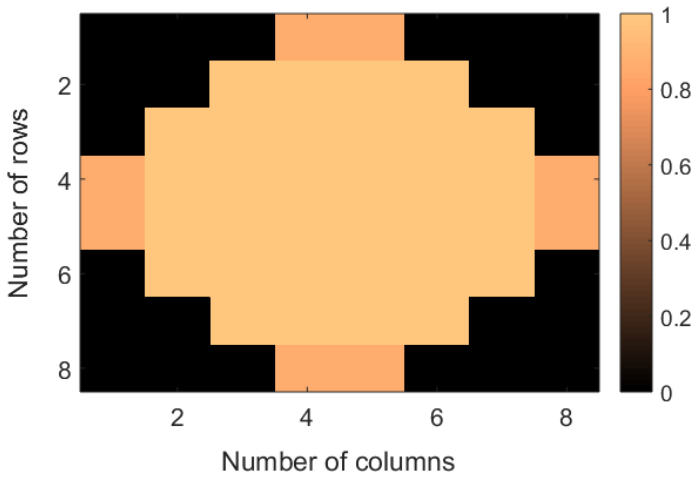

Fig. 3-64: Optimum arrangement of 'ON' (Amp = '1'), OFF' (Amp = '0') and amplitude weighted ('0' < Amp <'1') elements on the aperture of the proposed 8×8-element AW-TPA array.

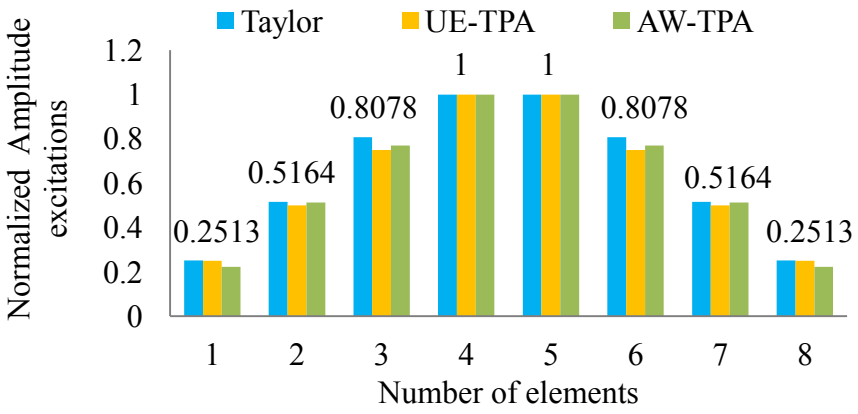

Fig. 3-65: Normalized amplitde distributions across the array elements of the fully filled 30 dB Taylor tapered and the proposed 8×8-element UE-TPA and AW-TPA arrays.

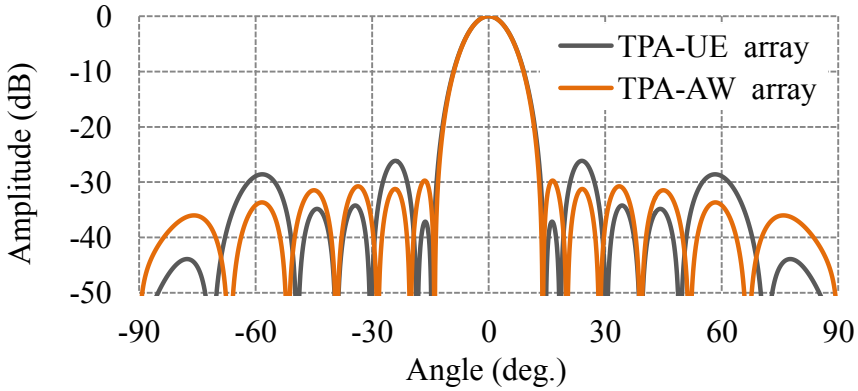

Fig. 3-66: Comparison of radiation patterns of the proposed 8x8-element UE-TPA and AW-TPA arrays.

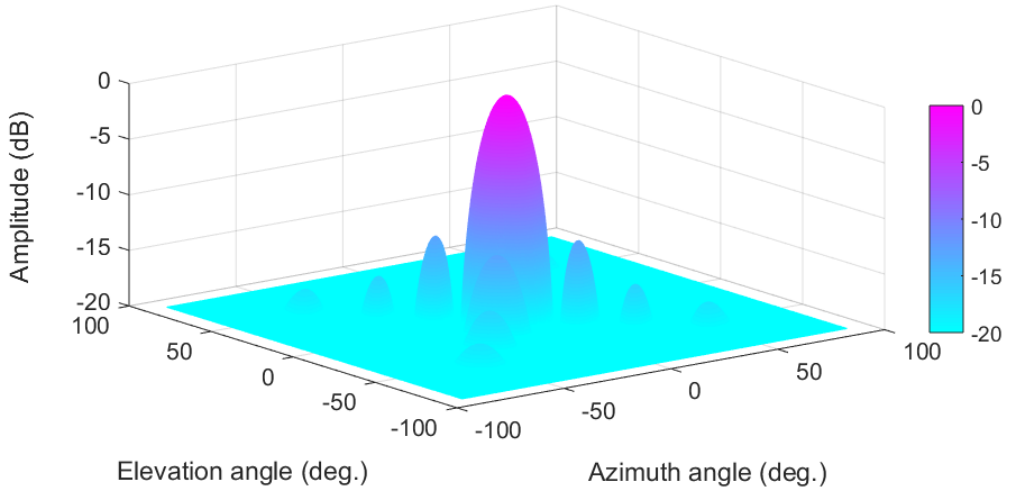

Fig. 3-67: 3D radiation pattern of the proposed 8×8-element UE-TPA array.

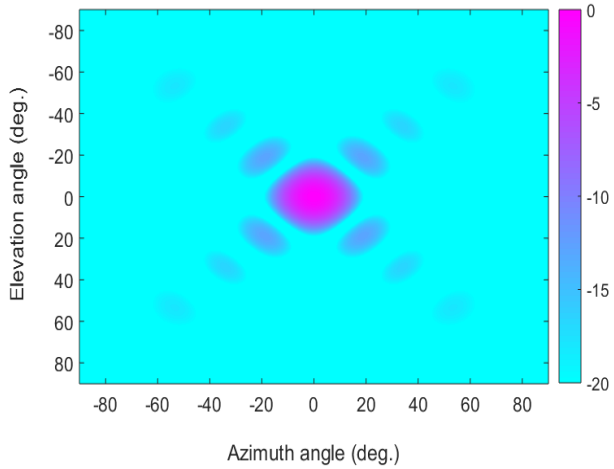

Fig. 3-68: Intensity plot of the proposed 8×8-element UE-TPA array.

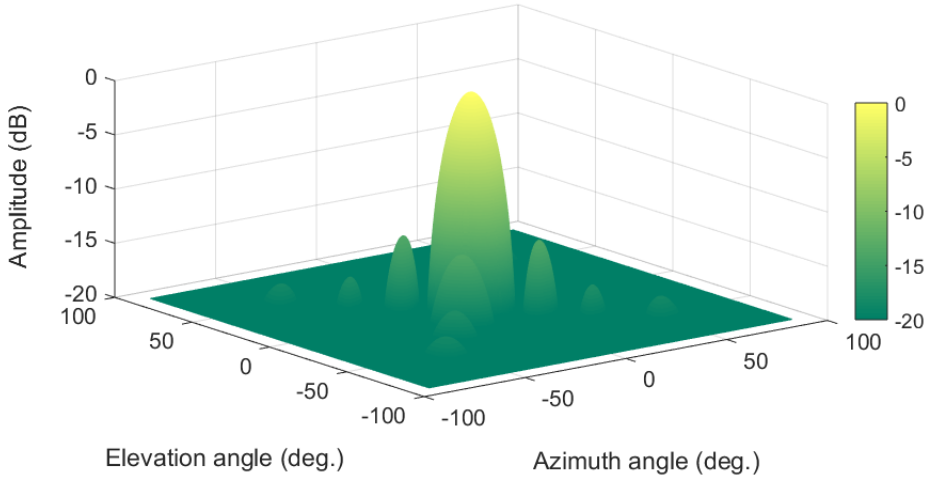

Fig. 3-69: 3D radiation pattern of the proposed 8×8-element AW-TPA array.

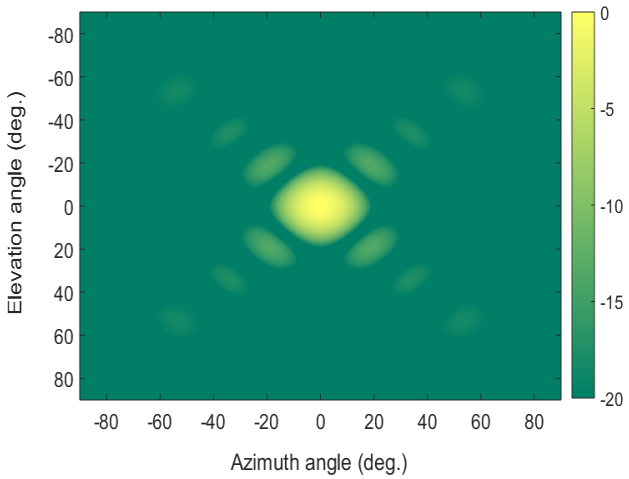

Fig. 3-70: Intensity plot of the proposed 8×8-element AW-TPA array.

Table 3-8: Summary of the Computed Radiation Pattern Parameters of the Proposed 8x8 TPA-UA and AW-TPA Arrays.

Parameters	**UE-TPA array**	**AW-TPA array**
Peak SLL (dB) in $\phi = 0^0$ plane	-25.77	-29.50
Peak SLL (dB) in $\phi = 90^0$ plane	-25.77	-29.50
HPBW (deg.) in $\phi = 0^0$ plane	12.30	12.40
HPBW (deg.) in $\phi = 90^0$ plane	12.30	12.40
Average SLL (dB)	-25.78	-27.17

3.2.5 EM Simulation and Experimental Validation of 8×8-element AW-TPA Array

This section describes the architecture and the EM simulation of the proposed 8×8-element AW-TPA array as synthesized in previous section. M-shaped patch element [Aggarwal and Gangwar (2014)] is assumed to realize the antenna array. The architecture of complete array assembly with its geometrical parameters (in mm at 9.5 GHz) is depicted in Fig. 3-71 which consists of 40 M-shaped patch antenna elements and a 1:40 ways microstrip line feed network to excite each one of them with required amplitude and equal phase.

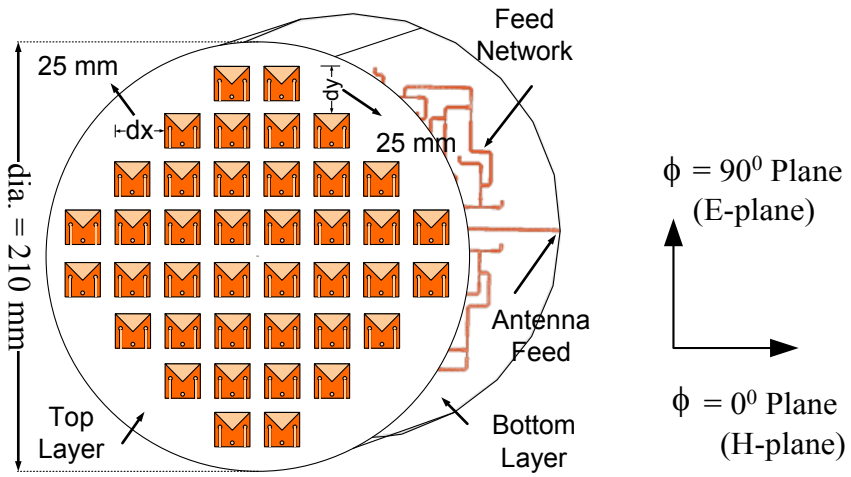

Fig. 3-71: Architecture of the proposed 8×8-element AW-TPA array assembly with its geometrical parameters.

3.2.5.1 Simulation and Design of Radiating Layer of the Array

The radiating layer of the antenna array is designed and optimized using HFSS/CST 3D EM simulator software and built on a RT Duroid 5880 substrate with dielectric constant (ε_r) equal to 2.2 and thickness equal to 3.16 mm. Inter-element spacings in both E- and H- planes are kept same equal to 25 mm (0.79λ at 9.5 GHz). Fig. 3-72 shows the 3D model of the radiating layer in which 40 M-shaped patch radiating elements are distributed over the circular aperture of 210 mm diameter. The variations of return loss of different ports (port designation is shown in Fig. 3-76) with frequency for one quadrant (X-negative Y-positive plane) of the radiating elements' layer are shown in Fig. 3-73. It can be seen from Fig. 3-73 that return loss better than -15 dB has been obtained through simulation over the entire frequency band of 800 MHz. Figure 3-74 shows the variations of simulated mutual coupling with frequency between different elements (port designation is shown in Fig. 3-76) in both E- and H-planes. It can be observed that the worse mutual coupling < - 20 dB is obtained in both E- and H-planes.

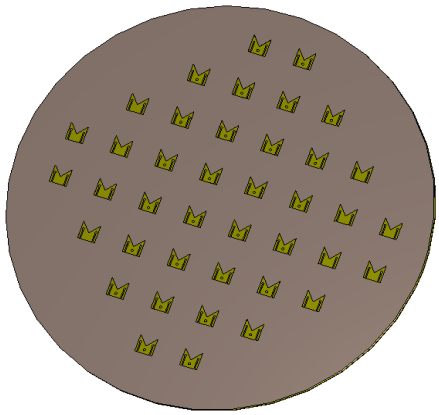

Fig. 3-72: 3D Model of radiating layer of the proposed 8×8-element AW-TPA antenna array.

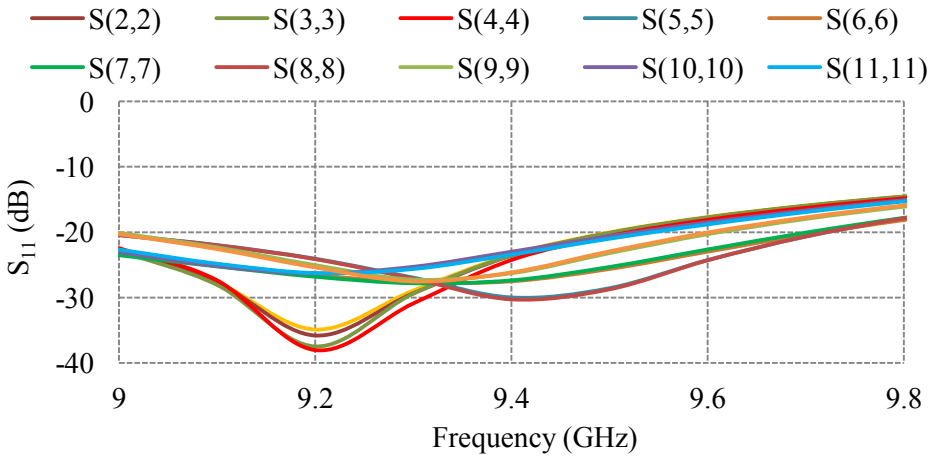

Fig. 3-73: Variations of return loss with frequency for one quadrant (X-negative Y-positive plane) elements of the proposed 8×8-element AW-TPA array.

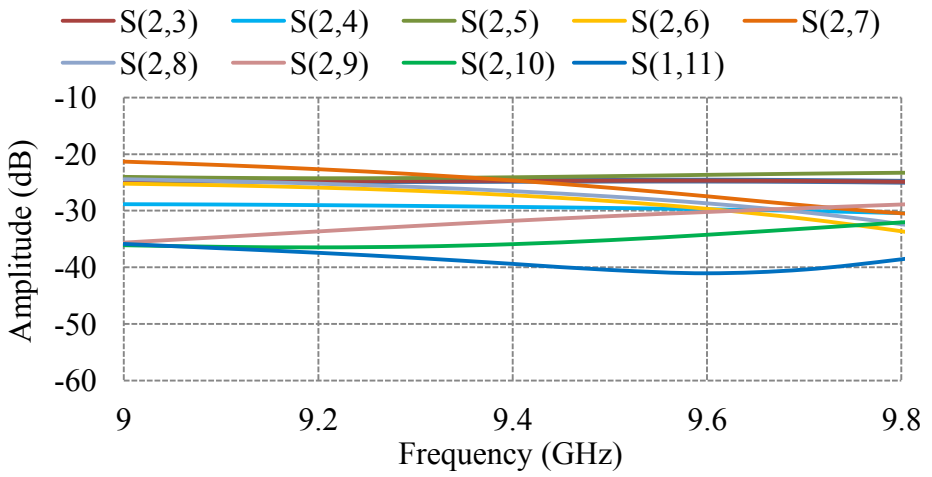

Fig. 3-74: Variations of mutual couplings with frequency for one quadrant (X-negative Y-positive plane) elements of the proposed 8×8-element AW-TPA array.

3.2.5.2 Simulation and Design of Feed Network Layer of the Array

The feed network configuration proposed for this design is shown in Fig. 3-75. It consists of 1:40 way microstrip line corporate power dividers/combiners to excite every element of array with equal phase and required amplitude signal. It is designed and optimized using ADS EM simulator ver. 9 software and built on a RT Duroid 5880 substrate with ε_r equal to 2.2 and thickness equal to 0.508 mm. In designing, sub-network concept has been resorted to optimize the amplitude and phase of each quadrant (1:10 ways) at individual level to achieve high degree of amplitude and phase accuracy. Figure 3-76 shows the port designation and Figs. 3-77 and 3-78 show the simulated magnitude and phase response of 1: 10 ways feed network. It can be observed that $|S_{11}| \leq -22$ dB, maximum amplitude imbalance ± 0.5 dB and maximum phase imbalance among the ports ± 5 deg have been obtained through simulation over entire frequency band of operation.

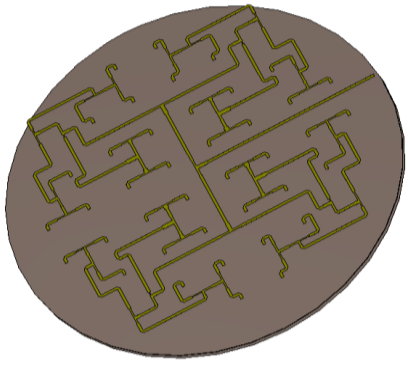

Fig. 3-75: 3D Model of feed network layer of the proposed 8×8-element AW-TPA antenna array.

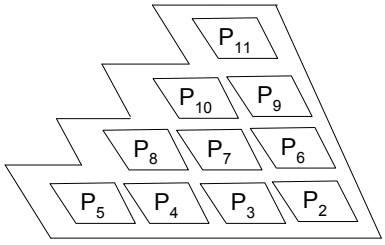

Fig. 3-76: Port designation for one quadrant (X-negative Y-positive plane) of the proposed 8×8-element AW-TPA array .

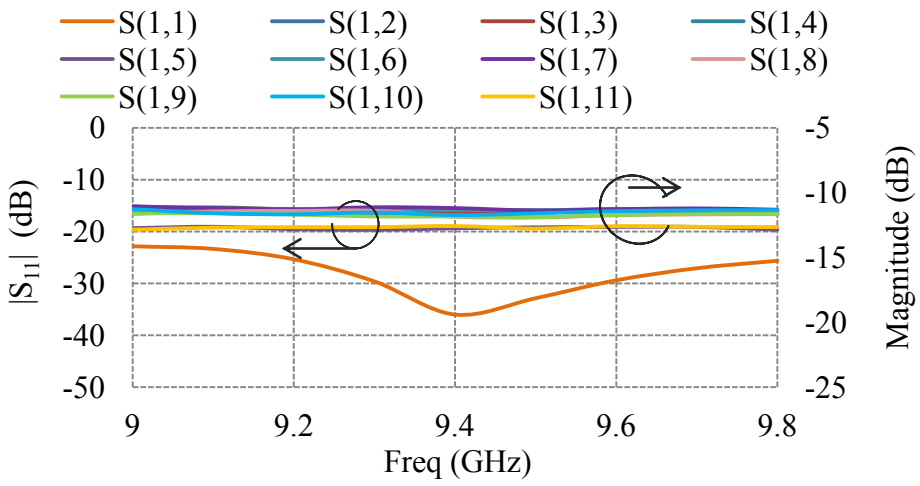

Fig. 3-77: Variations of return loss and amplitude distributions with frequency for one quadrant (X-negative Y-positive plane) for the feed network of the proposed 8×8-element AW-TPA array.

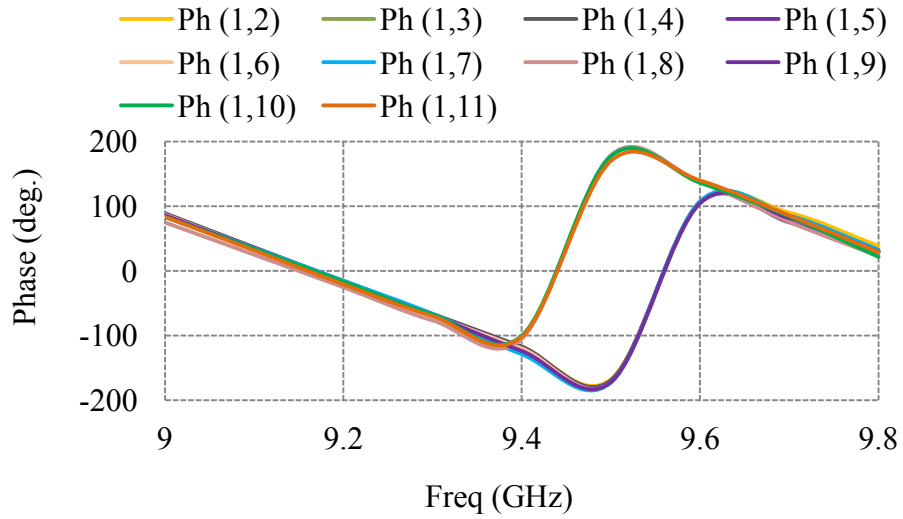

Fig. 3-78: Variations of phase with frequency for one quadrant (X-negative Y-positive plane) for the feed network of the proposed 8×8-element AW-TPA array.

3.2.5.3 Design and Simulation of Complete Array Assembly

The configuration of complete array assembly is shown in Fig. 3-79. The radiating elements and feed network layers as designed in previous sub-sections are arranged in a stacked configuration and individual antenna element is fed through a coaxial conductor

where one end of the conductor is connected to the antenna element and other end to the respective port of feed network. The radiating element layer integrated with feed network is assembled with metal plate at the back in order to provide mechanical support to antenna system as well as to interface with other sub-systems for characterization/operation. The gap between antenna array PCB and metal plate has been optimized in order to nullify the effect of metal on the microstrip lines as well as to maintain the total antenna thickness as less as possible. It was found that at the gap of 10 mm or beyond, there is negligible effect of metal on feed network microstrip lines and performance was optimum. This spacing between antenna array PCB and metal plate is filled with a rigid foam material rohacell 51 HF (ε_r =1.06, thickness = 10 mm) in order to provide mechanical support to the antenna array PCB. The simulated return loss of the complete array assembly is shown in Fig. 3-80. It can be noticed from Fig. 3-80 that return loss <-15 is obtained over the frequency band 9.0-9.8 GHz. Figs. 3-81 and 3-82 show the simulated radiation patterns of the array in H-and E-planes respectively. It can be seen that PSLL better than -29 dB is obtained in both the planes in spite of presence of strong mutual coupling.

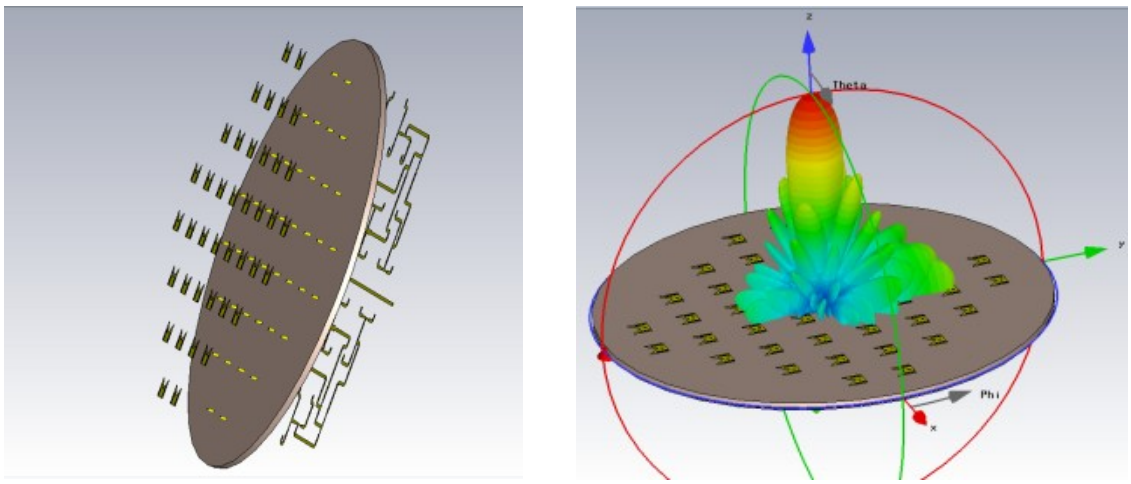

Fig. 3-79: Assembly of the proposed 8×8-element AW-TPA array.

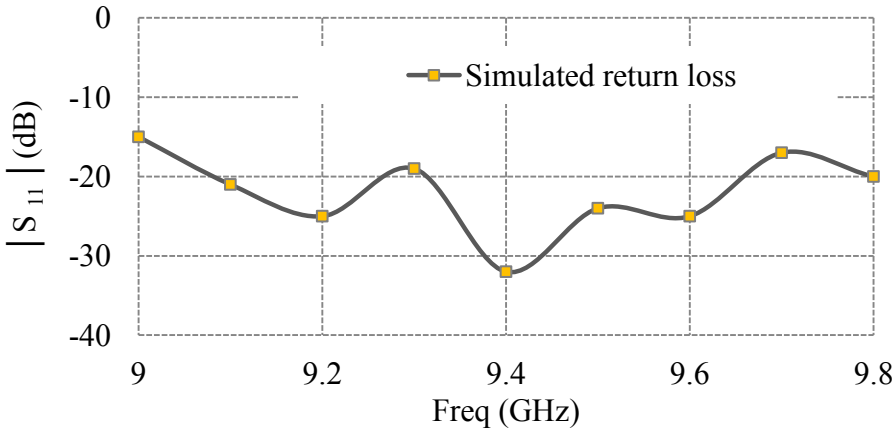

Fig. 3-80: Variation of simulated return loss with frequency for the sum port of the proposed 8×8-element AW-TPA array.

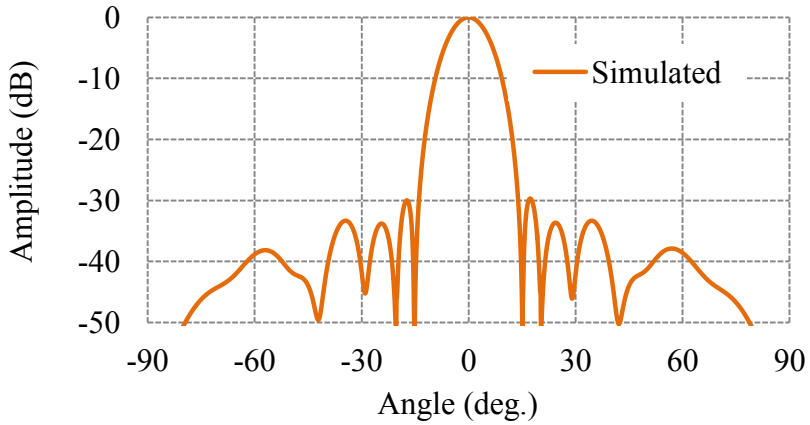

Fig. 3-81: Simulated radiation pattern of the proposed 8×8-element AW-TPA array in $\phi = 0^0$ plane (H-plane) .

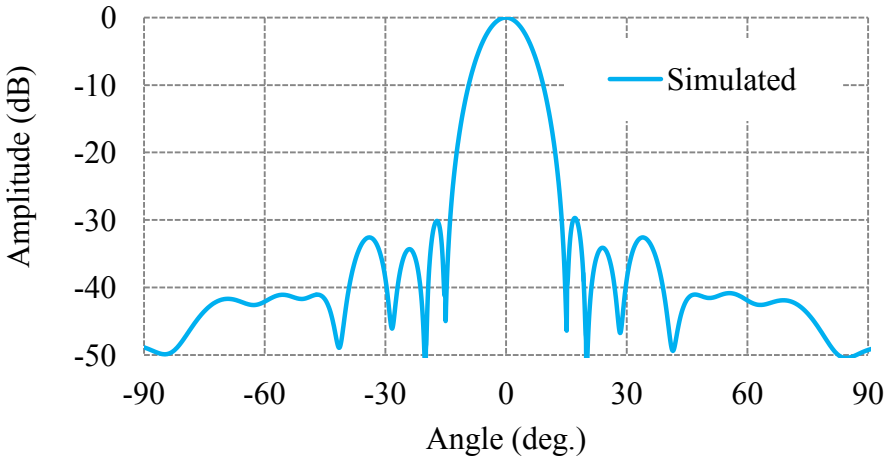

Fig. 3-82: Simulated radiation pattern for the proposed 8×8-element AW-TPA array in $\phi = 90^0$ plane (E-plane).

3.2.5.4 Experimental Evaluation and Results

In this section, experimental assessment of the 8×8-element AW-TPA array is reported. The complete array antenna with optimal geometrical parameters is fabricated, integrated and tested. The realized antenna array is shown in Fig. 3-83. The S-parameters of the array were measured using an Agilent E5071C Network Analyser as per the setup shown in Fig. 3-84. Figure 3-85 depicts the radiation pattern characteristics measurement in spherical Near/Far Field Test Range (SN/SF TR). This antenna array was characterized in far-field mode of test range (SFTR). Herein, the antenna array under test was kept in receive mode of operation and separation between antenna array under test and source antenna was about 10 meter to ensure the far-field criterion. Source antenna position was kept fixed and antenna array under test was rotated form -90^0 to $+90^0$ in horizontal plane and the far -field data corresponding to each angle (step 0.1 deg.) was recorded by data acquisition software.

The comparison of simulated and measured return loss of the fabricated antenna array is shown in Fig. 3-86. It can be seen from Fig. 3-86 that the measured $|s_{11}|$ of antenna array is < -12 dB over the band (8.5% impedance bandwidth) and is in close agreement with the simulated one. Figures 3-87 and 3-88 demonstrate simulated and measured co-pol and measured cross-pol in H-plane ($\phi = 0^0$, $-90^0 \leq \theta \leq 90^0$) and in E-plane ($\phi = 90^0$, $-90^0 \leq \theta \leq 90^0$) of the antenna array at a freq. of 9.5 GHz respectively. Radiation parameter extracted from Figs. 3-87 and 3-88 are tabulated in Table 3-9. It can be seen from Figs. 3-87 and 3-88 and Table 3-9 that peak SLL <- 28 dB, and cross-pole < -25 dB have been obtained through measurements. The measured 3 dB beam widths are around 12.4 deg. in both E- and H- planes. It can be observed that there is acceptable change in the measured performance and all the results are in good agreement with the simulated ones which validate the proposed array design.

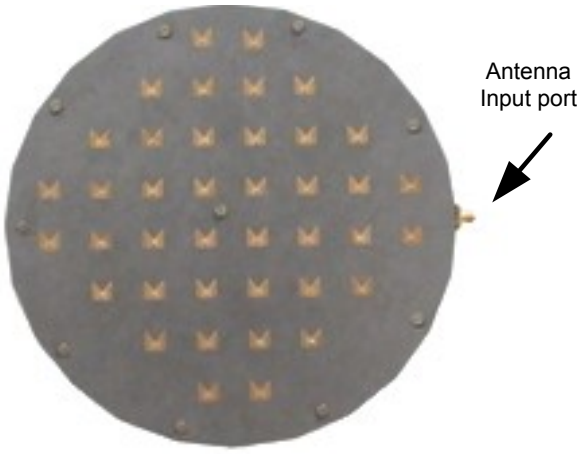

Fig. 3-83: Realized 8×8-element AW-TPA array.

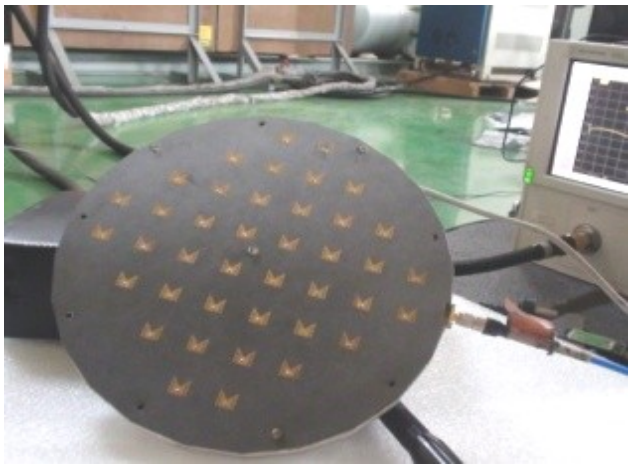

Fig. 3-84: VSWR measurement setup of the realized 8×8-element AW-TPA array.

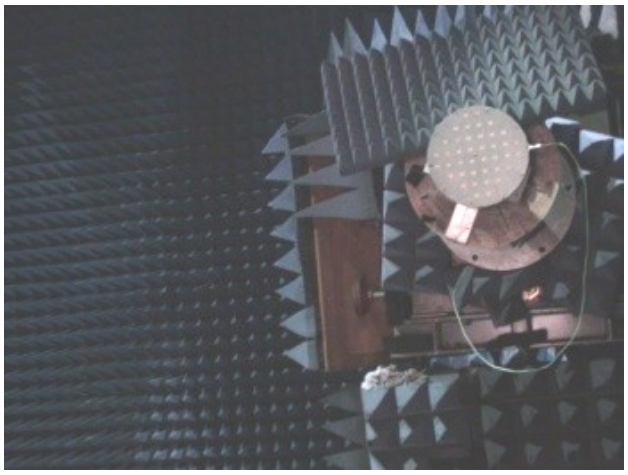

Fig. 3-85: Pattern measurement setup in test chamber of the realized 8×8-element AW-TPA array.

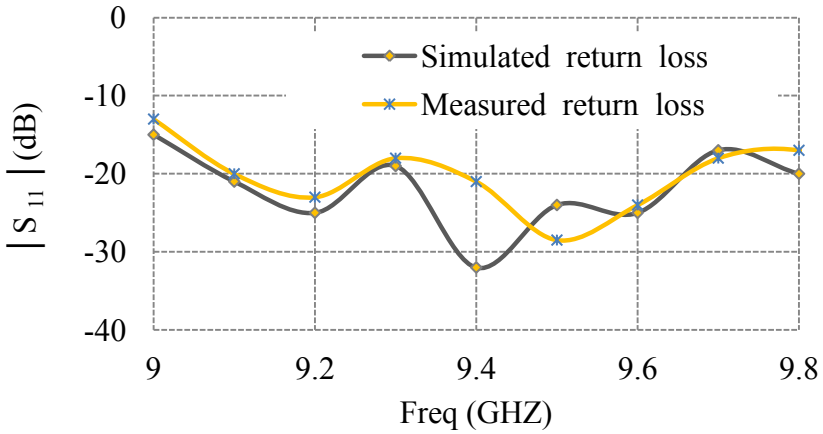

Fig. 3-86: Comparison of simulated and measured return loss of the proposed 8×8-element AW-TPA array.

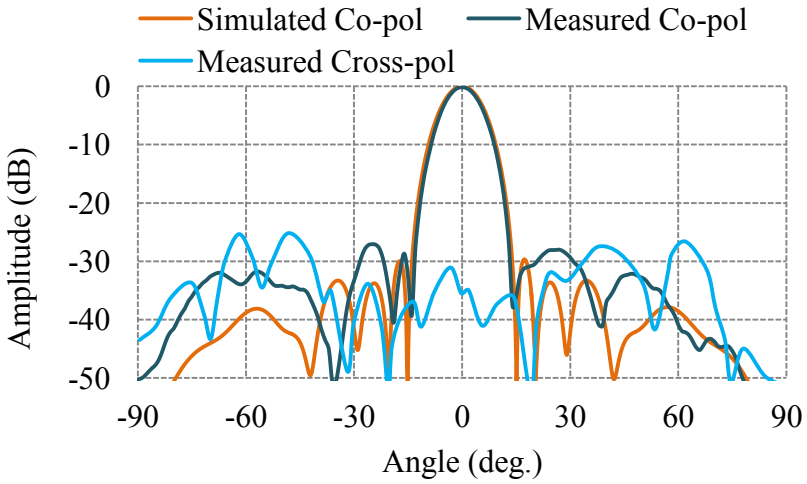

Fig. 3-87: Comparison of simulated and measured radiation patterns of the proposed 8×8-element AW-TPA array in $\phi = 0^0$ plane.

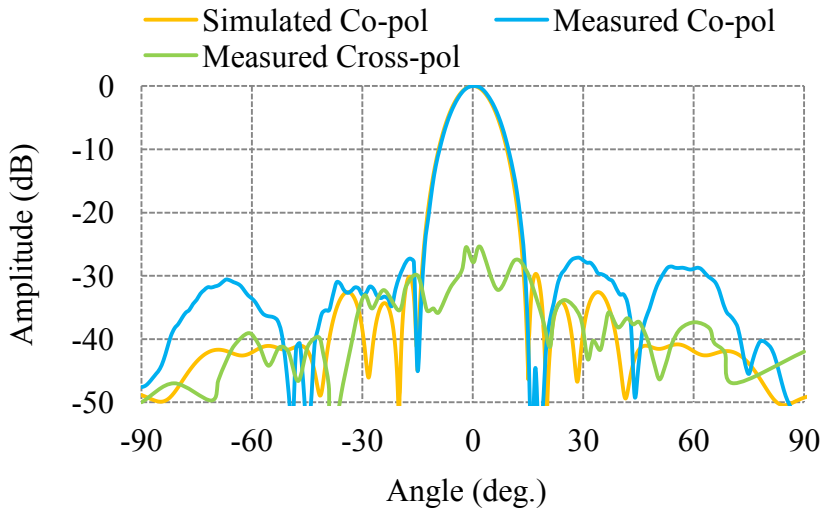

Fig. 3-88: Comparison of simulated and measured radiation patterns for the proposed 8×8-element AW-TPA array in $\phi = 90^0$ plane.

Table 3-9: Summary of the results obtained through simulation and experiment for the proposed 8×8-element AW-TPA array.

Parameters	**Computed**	**Simulated**	**Experimental**
Peak SLL (dB) in $\phi = 0^0$ plane	-29.50	-29.80	-27.50
Peak SLL (dB) in $\phi = 90^0$ plane	-29.50	-29.90	-28.40
Cross-pol (dB) in $\phi = 0^0$ plane	-	-	-25.10
Cross-pol (dB) in $\phi = 90^0$ plane	-	-	-25.46
HPBW (deg.) in $\phi = 0^0$ plane	12.40	12.23	12.25
HPBW (deg.) in $\phi = 90^0$ plane	12.40	12.27	12.30
Directivity (dB)	24.40	24.50	24.46

3.3. Non-uniformly Spaced Planar Antenna (NUSPA) Arrays

3.3.1 Introduction

The research work on NUSPA arrays is broadly divided into the following two categories.

- Peak SLL Optimization in 8×16-element UE-NUSPA Array Using PSO
- Peak SLL Optimization in 8×16-element AW-NUSPA Array Using PSO

Details of each category are described subsequently in different sub-sections.

3.3.1.1 Peak SLL Optimization in 8×16-element UE-NUSPA Array Using PSO

In practical applications, unequally spaced antenna arrays exhibit distinguishable advantages compared with conventional uniformly spaced arrays, as they reduce the number of elements, suppress the side lobe level (SLL), and simplify the design of feed network. However, due to the nonlinear dependence of phase on position, it is difficult to design and analyse unequally spaced arrays to yield the desired radiation pattern.

The aperiodic placement of uniformly excited antenna elements in sparse arrays enables one to obtain lower SLL, narrow half power beam width (HPBW), higher gain or directivity and reduces the number of elements for a specified aperture size [Haupt (2010)]. A lot of research effort has been made to suppress peak SLL (PSLL) by optimizing inter-element spacings alone (SO) while providing uniform excitation across all the elements [[Chen *et al.* (2006)], Goudos *et al.* (2010)], [Zhang *et al.* (2011)], and [Gangwar *et al.* (2017)]. The maximum reduction of SLL achieved by these techniques is of the order of -20 to -22 dB.

In general, to simulate variable elements' density over the aperture corresponding to lowest possible PSLL and higher aperture efficiency, the inner elements should have equal spacings/excitations and the edge elements should have unequal spacings/excitations. This means that if the number of edge elements is properly selected, it would result in maximum reduction of PSLL while maintaining narrow and highly directive main beam especially when array size is very large. Additionally, it also reduces the number of variables for computation.

In the present research work, an attempt is made to simulate the required current distribution on antenna aperture corresponding to lowest possible PSLL by employing PSO algorithm to find the optimum inter-element spacings. The 8×16-elements uniformly excited non-uniformly spaced planar antenna (UE-NUSPA) array is analysed and its parameters determined and compared with those of Taylor-tapered uniformly spaced array of similar size. The results show that present strategy (adjusting spacings of only optimum number of edge elements) is very effective in minimizing SLL in UE-NUSPA Arrays.

3.3.1.2 Peak SLL Optimization in 8×16-element UE-NUSPA Array Using PSO

In the present strategy, particle swarm optimization (PSO) is applied to jointly optimize the spacings and amplitude excitations of small number of elements near the edges rather than total number of elements in the array in a combined manner to simulate required current distribution on the aperture corresponding to lowest possible PSLL. A NUSLA array consisting of 8×16-element is theoretically modelled and examined.

A lot of research effort has been made to suppress peak SLL (PSLL) by optimizing inter-element spacings alone while providing uniform excitation across the

elements [Chen *et al.* (2006)], [Goudos *et al.* (2010)], [Zhang *et al.* (2011)], and [Gangwar *et al.* (2017)]. The maximum reduction of SLL achieved by these techniques is of the order of -20 to -22 dB. However, it is preferable for radar application to design an antenna array with very low SLL (< -30 dB) to minimize interference from other objects. This amount of reduction in PSLL is difficult to achieve by the aforementioned techniques. This may be due to the fact that the radiated far field does not linearly depend on the inter-element spacings.

Several solutions including those reported in [Kurup *et al.* (2003)], [Lin *et al.* (2010)], and [Cen *et al.* (2012)] have been proposed to reduce SLL by considering both the spacing-phase (SP) synthesis [Kurup *et al.* (2003)], [Lin *et al.* (2010)], and spacing-amplitude synthesis [Cen *et al.* (2012)]. In these methods, researchers jointly adjusted the positions and amplitude/phase excitations of the all the elements in the array and achieved pretty good reduction in PSLL. However, to simulate variable elements' density over the aperture corresponding to lowest possible PSLL and higher aperture efficiency, the inner elements should have equal spacings/excitations and the edge elements should have unequal spacings/excitations. This means that if the number of edge elements is properly selected, it would result in maximum reduction of PSLL while maintaining narrow and highly directive main beam especially when array size is very large. Additionally, it also reduces the number of variables for computation.

In the present research work, an attempt is made to simulate the required current distribution on antenna aperture corresponding to lowest possible PSLL by applying PSO algorithm to find optimum inter-element spacings and amplitude excitations in a combined manner. The results obtained for 8×16-element AW-NUSPA array using the proposed strategy (adjusting spacings/excitations of only optimum number of edge elements) is expected to be very effective in minimizing PSLL.

3.3.2 Geometrical Configuration and Problem Formulation for NUSPA Arrays

3.3.2.1 Peak SLL Optimization in 8×16-element UE-NUSPA Array Using PSO

The general structure of symmetrical planar array consisting of $2N_p \times 2M_p$ elements as shown in Fig. 3-89 is considered in this study. The total far-field radiated from this array can be expressed as [Haupt (2010)]

$$E(\theta,\phi) = E_{ele}(\theta,\phi) \times AF_P(\theta,\phi) \tag{3.22}$$

where $E_{ele}(\theta,\phi)$ is radiation pattern of single element (considered as cos θ pattern) and $AF_P(\theta,\phi)$ is array factor for planar array, which can be formulated as [Haupt (2010)]

$$AF_P(\theta,\phi) = \sum_{n=1}^{N_P}\sum_{m=1}^{M_P} a_{nm}\, exp[\, jkx_n\, sin\theta\, cos\phi\,] \times \exp[jky_m\, sin\theta\, sin\phi] \tag{3.23}$$

a_{nm} is the excitation amplitude of antenna element at position (n,m)th, and $k = 2\pi/\lambda$ is the wave number.

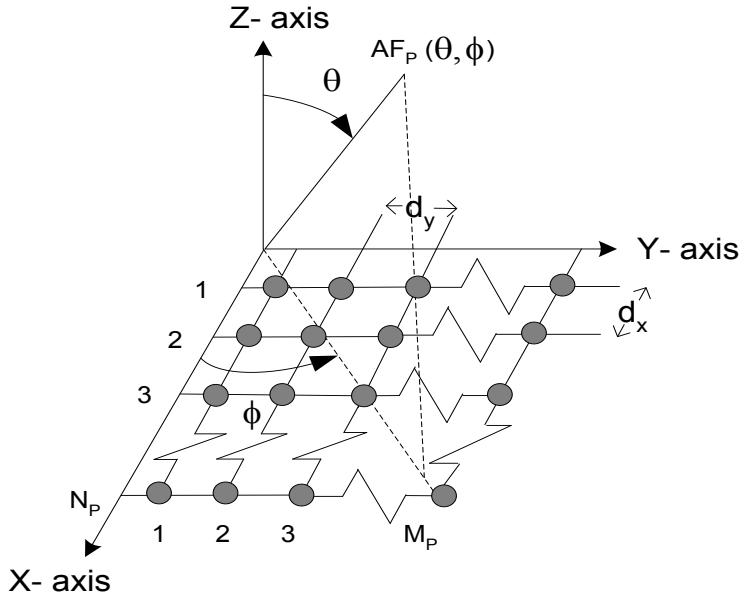

Fig. 3-89: General structure of one quadrant of the NUSPA array with $N_p \times M_p$ elements.

The aim of the present synthesis is to minimize PSLL by computing the optimum inter-element spacings with the constrants $0.5\lambda \leq d_i \leq 1.5\,\lambda$, and uniform amplitude excitations. The fitness function for evaluating peak SLL can be defined as

$$F_{SLL}(D) = \max_{\forall\theta\in AR}\left[20\log\left|\frac{AF(D,A,\theta,\phi)}{AF_{max}}\right|\right] \tag{3.24}$$

where AR denotes the angular region excluding the main beam, and AF_{max} is the maximum value of array factor. Function given in Eq. (3.25) reduces during optimization.

$$f_p(D) = F_{PSLL}(D,\theta)|_{\phi=0^o} + F_{PSLL}(D,\theta)|_{\phi=90^o} \tag{3.25}$$

3.3.2.2 Peak SLL Optimization in 8×16-element AW-NUSPA Array Using PSO

The general structure of symmetrical planar array consisting of $2N_p \times 2M_p$ elements as shown in Fig. 3-89 is considered in this study. The total far-field radiated from this array can be given by Eq. (3.22).

The aim of the present synthesis is to minimize PSLL by computing jointly the optimum inter-element spacings with the constraints $0.5\lambda \leq d_i \leq 1.5\,\lambda$, and amplitude excitations. The fitness function for evaluating peak SLL can be defined as

$$F_{SLL}(D,A) = \max_{\forall\theta\in AR}\left[20\log\left|\frac{AF(D,A,\theta,\phi)}{AF_{max}}\right|\right] \tag{3.26}$$

where AR denotes the angular region excluding the main beam, and AF_{max} is the maximum value of array factor. Function given in Eq. (3.27) reduces during optimization.

$$f_p(D,A) = F_{PSLL}(D,A,\theta)|_{\phi=0^o} + F_{PSLL}(D,A,\theta)|_{\phi=90^o} \tag{3.27}$$

3.3.3 Optimization Technique for the Synthesis of NUSPA Array

3.3.3.1 Peak SLL Optimization in 8×16-element UE-NUSPA Array Using PSO

In this study, PSO as explained in section A2.1 (Appendix -A) is used to determine the best configuration of UE-NUSPA array corresponding to optimal values of PSLL. The fitness function given in Eq. (3.25) is minimized using the PSO algorithm in order to obtain best fitness value.

3.3.3.2 Peak SLL Optimization in 8×16-element AW-NUSPA Array Using PSO

PSO as detailed in section A2.1 (Appendix-A) is used to determine the best configuration of AW-NUSPA array corresponding to optimal values of PSLL. The fitness function given in Eq. (3.27) is reduced using the PSO algorithm during search of an optimum solution.

3.3.4 Numerical Analysis, Results and Discussion

The effectiveness of the proposed technique is demonstrated by considering 8×16-element NUSPA array as optimization design problem.

3.3.4.1 Peak SLL Optimization in 8×16-element UE-NUSPA Array Using PSO

The best inter-element spacings obtained for the uniformly excited NUSPA array along $\Phi = 0^0$ and $\Phi = 90^0$ planes are listed in Table 3-10 and related array architecture is designated in Fig. 3-90. The variation of best fitness value is shown in Fig. 3-91. The achieved radiation patterns at 9.5 GHz frequency of the array in $\Phi = 0^0$ and $\Phi = 90^0$ planes are demonstrated in Figs. 3-92 and 3-93 respectively. The 3D radiation pattern

and intensity plot are shown in Figs. 3-94 and 3-95 respectively. The parameters derived from Figs. 3-92 - 3-95 are tabulated in Table 3-11 and compared with those corresponding to equally excited uniformly spaced array of similar size. It can be observed from Figs. 3-92 - 3-95 and Table 3-11 that there is slight improvement in HPBW and directivity of the proposed NUSPA array as compared with equally excited uniformly spaced array of similar size. Additionally, the side lobe levels in all the planes (inter-coodinal and principal) are better than ≤-19 dB. The number of parameters to be optimized are 45% less than those reported in [Chen *et al.* (2006)], [Lin *et al.* (2010)], [Zhang *et al.* (2011)], and [Cen *et al.* (2012)] and hence relatively less computational cost is involved in the present study.

Table 3-10: Best inter-element spacings normalized to free space wavelength for one quadrant of the proposed NUSPA array.

Inter-element spacings across $\phi = 0^0$ plane	0.25 0.51 0.60 0.77
Inter-element spacings across $\phi = 90^0$ plane	0.25 0.50 0.50 0.56 0.61 0.69 0.81 0.97

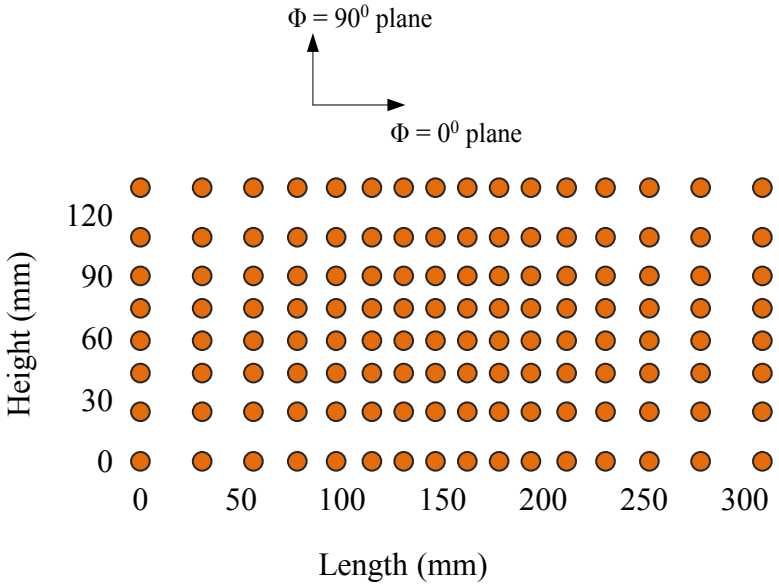

Fig. 3-90: Proposed geometry of 8×16-element NUSPA array with dimensions corresponding to a frequency of 9.5 GHz.

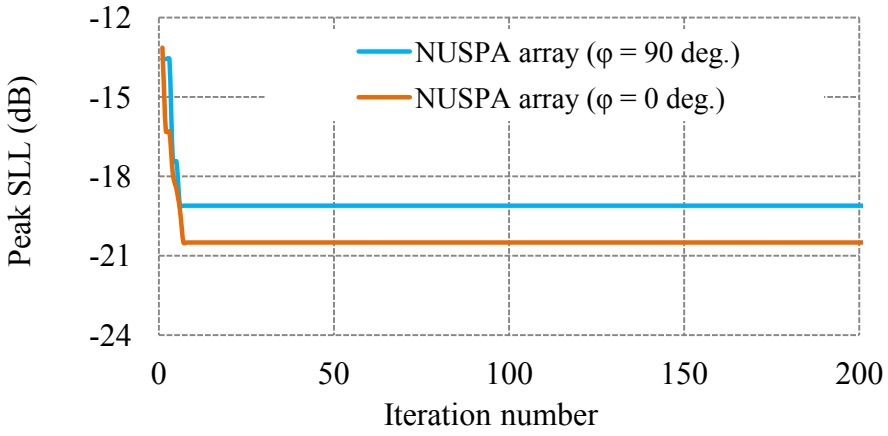

Fig. 3-91: Peak SLL vs. number of iterations for equally excited NUSPA array.

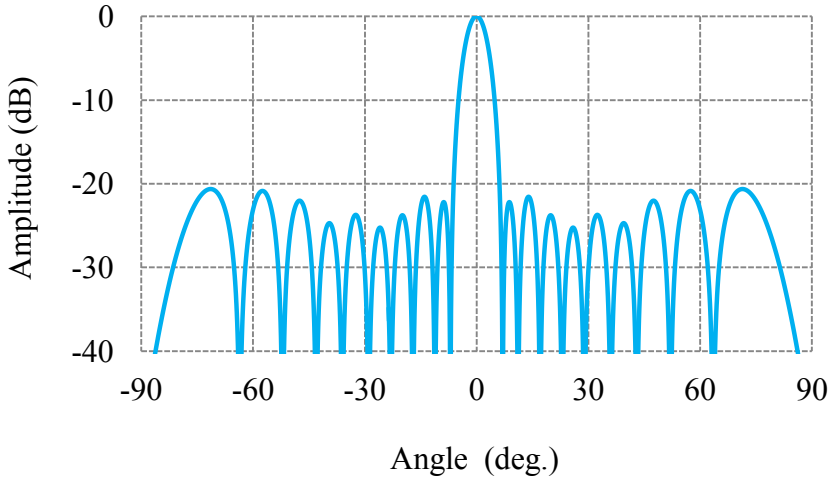

Fig. 3-92: Numerically evaluated radiation pattern of the proposed 8×16-element NUSPA array in $\phi = 0^0$ plane.

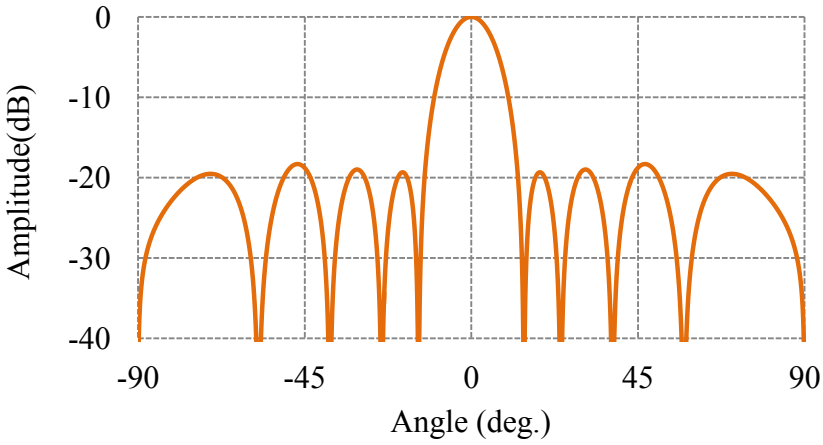

Fig. 3-93: Numerically evaluated radiation pattern of the proposed 8×16-element NUSPA array in $\phi = 90^0$ plane.

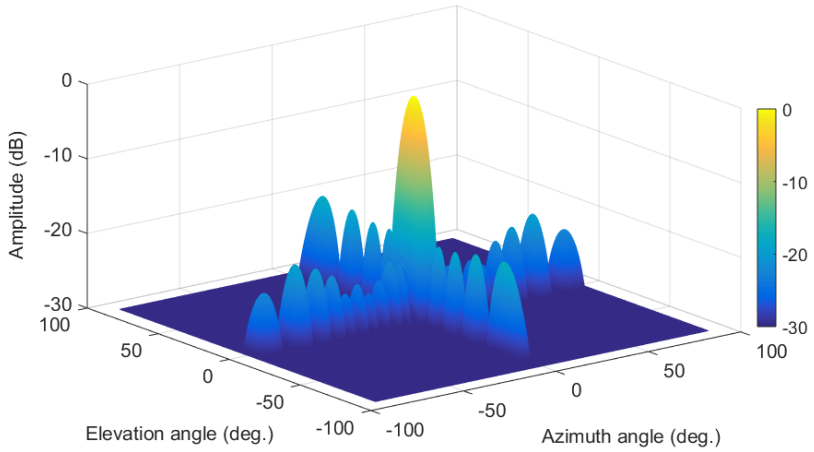

Fig. 3-94: 3D radiation pattern of the proposed 8×16-element NUSPA array.

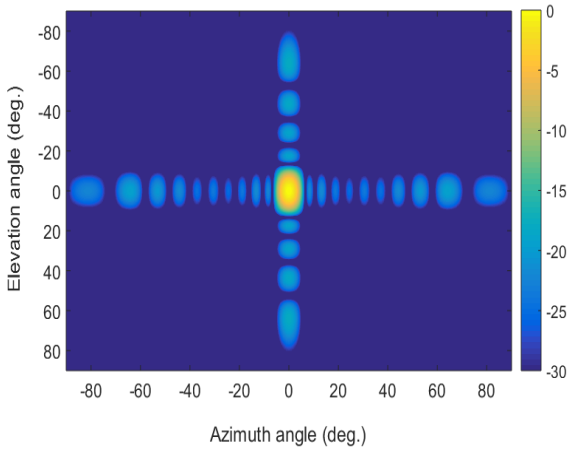

Fig. 3-95: Intensity plot of the proposed 8×16-element NUSPA array.

Table 3-11: Comparison of numerical results of the proposed NUSPA array with those of uniformly spaced Taylor tapered array of equal size.

Design parameters	**Uniformly spaced array**		**NUSPA array**	
	$\Phi = 0^0$ plane	$\Phi = 90^0$ plane	$\Phi = 0^0$ plane	$\Phi = 90^0$ plane
Size of array (λ)	9.776 λ	4.2437 λ	9.777 λ	4.2438 λ
PSLL (dB)	< -13	< -13	< -20.5	< -19.1
HPBW (deg.)	6	13	6.6	13.2
Directivity (dB)	23.45		22.90	

3.3.4.2 PSLL Optimization in 8×16-element AW-NUSPA Array Using PSO

The effectiveness of the proposed technique is demonstrated by considering 8×16-element NUSPA array as optimization design problem. For this example swarm size and iterations were set to 1,000 and 200 respectively. The best inter-element spacings and amplitude excitation coefficients obtained for the NUSPA array along $\phi = 0^0$ and $\phi = 90^0$ planes are listed in Table 3-12. The variation of fitness value with number of iterations is shown in Fig. 3-96. The achieved radiation patterns at 9.5 GHz frequency for spacing amplitude (SA) syntheses of the array are demonstrated in Fig. 3-97 and 3-98 respectively for $\phi = 0^0$ and $\phi = 90^0$ planes. The 3D radiation pattern and intensity plot are shown in Figs. 3-99 and 3-100 respectively. The parameters derived from Figs. 3-97 - 3-100 are tabulated in Table 3-13 and compared with those corresponding to Taylor amplitude (TA)-tapered uniformly spaced array of similar size. It can be observed from Figs. 3-97 - 3-100 and Table 3-13 that there is slight improvement in HPBW and directivity of the proposed NUSPA array as compared with TA-tapered uniformly spaced array.

Table 3-12: Best inter-element spacings normalized to free space wavelength, and amplitude excitations for the one quadrant for the proposed NUSPA array.

Inter-element spacings across $\phi = 0^0$ plane	0.25 0.51 0.60 0.77
Amplitude excitation coefficients	1.00 0.98 0.89 0.44
Inter-element spacings across $\phi = 90^0$ plane	0.25 0.50 0.50 0.56 0.61 0.69 0.81 0.97
Amplitude excitation coefficients	1.0 1.0 1.0 0.92 0.88 0.73 0.48 0.22

It can also be seen from that side lobe levels in all the planes (inter-coordinal and principal) are better than ≤- 25 dB. The number of parameters to be optimized are 45% less than those reported in [Chen *et al.* (2006)], [Lin *et al.* (2010)], [Zhang *et al.* (2011)], and [Cen *et al.* (2012)] and hence relatively less computational cost is involved in the present study.

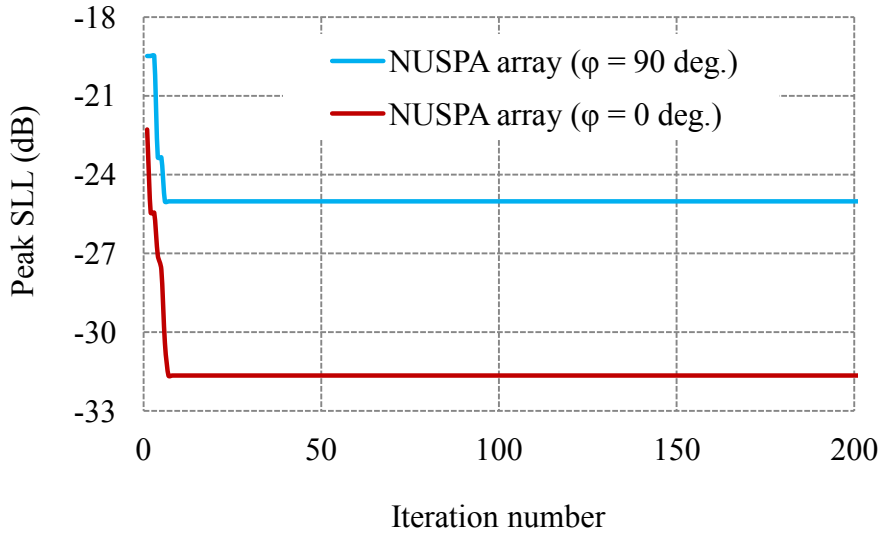

Fig. 3-96: Peak SLL vs. number of iterations for amplitude weighted NUSPA array.

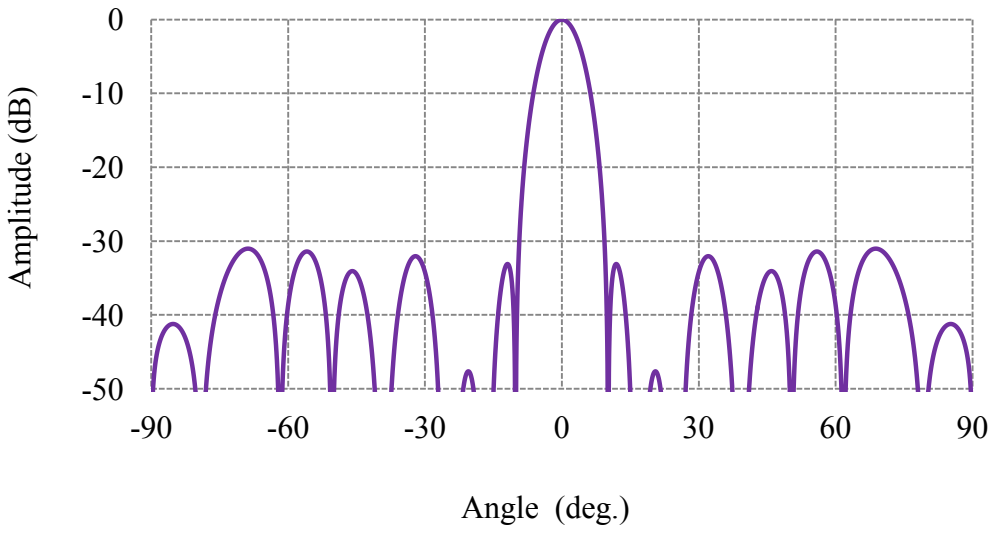

Fig. 3-97: Numerically evaluated radiation pattern of the proposed 8×16-element amplitude weighted NUSPA array in $\phi = 0^0$ plane.

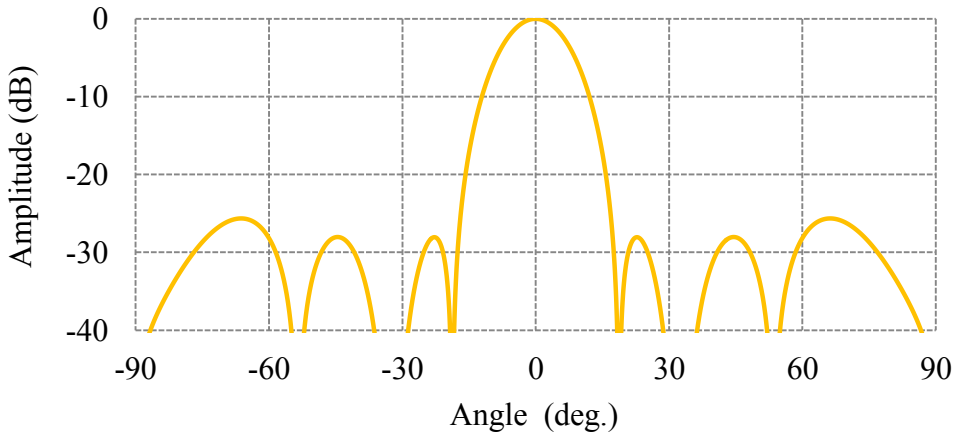

Fig. 3-98: Numerically evaluated radiation pattern of the proposed 8×16-element amplitude weighted NUSPA array in $\phi = 90^0$ plane.

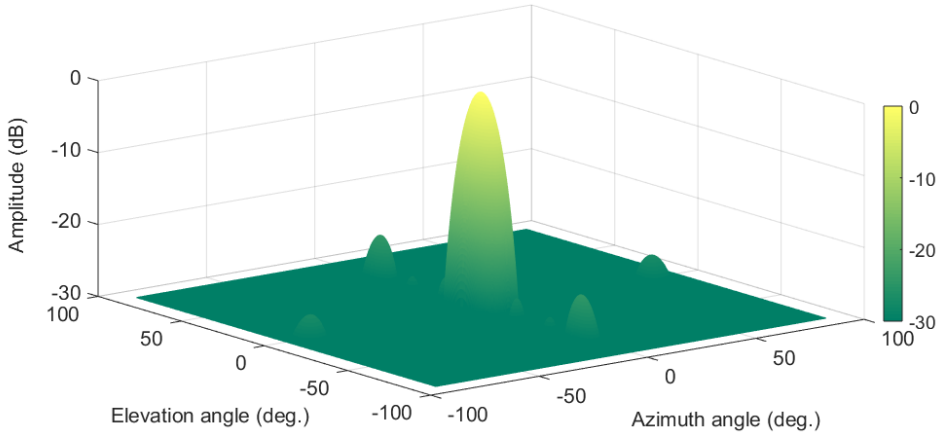

Fig. 3-99: 3D radiation pattern of the proposed 8×16-element amplitude weight NUSPA array.

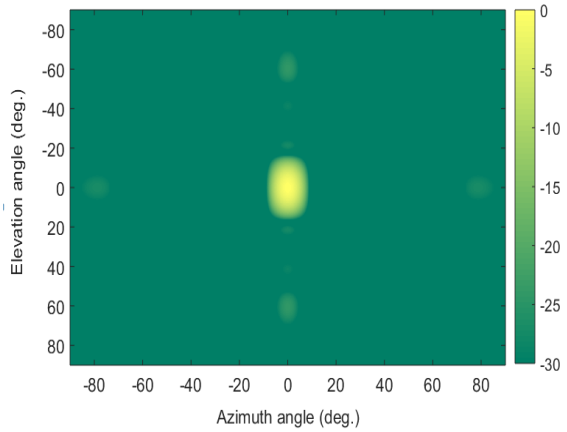

Fig. 3-100: Intensity plot of the proposed 8×16-element amplitude weighted NUSPA array.

Table 3-13: Comparison of numerical results for the proposed amplitude weighted NUSPA array with those for uniformly spaced Taylor tapered array

Design parameters	Uniformly spaced Taylor tapered array		Amplitude weighted NUSPA array	
	$\Phi = 0^0$ plane	$\Phi = 90^0$ plane	$\Phi = 0^0$ plane	$\Phi = 90^0$ plane
Size of array (λ)	9.776 λ	4.2437 λ	9.777 λ	4.2438 λ
PSLL (dB)	-30	- 25	-31.01	-25.02
HPBW (deg.)	6.8	14.4	6.6	13.2
Directivity (dB)	22.59		22.67	

3.4 Summary and Conclusion

This chapter has described the synthesis and design methods for sparse planar antenna (TPA and NUSPA) arrays, which are the extension of synthesis approaches developed for linear arrays in chapter 2. In this chapter, research work on numerical study has been divided into four parts on TPA arrays and two parts on NUSPA arrays. In addition, EM simulation and experimental validation have been performed on 8×8-element TPA array to further affirm the performance in practical applications.

From the numerical analysis of various examples, it is clear that the proposed synthesis methods for SPA arrays exhibit the following characteristics:

- Superior performance in suppression of PSLL at antenna boresight with minimum number of turn 'ON' elements
- Reduction of PSLL at antenna boresight as well as over the pre-specified scan volume
- Joint optimization of PSLL, HPBW and gain or directivity
- Reduction of PSLL by jointly optimizing thinned array configuration along with amplitude excitation coefficients

- The afore-mentioned characteristics have been achieved at less computational burden and great stability as compared to those associated with the existing state-of-the-art methods.

Additionally, it has been noticed from the synthesis approaches presented for NUSPA arrays that proposed methods offer more PSLL suppression as compared with the synthesis techniques reported in the literature.

The experimental results for 8×8-element AW-TPA array are also in agreement with the corresponding simulated and numerically computed ones. The results for the 8×8-element AW-TPA array presented in this chapter affirm the findings, implications and functioning of these types of synthesized arrays in practical scenarios.